

**Investigation of the impact of fibre
impairments and SOA-based devices
on 2D-WH/TS OCDMA codes**

By

Mohamed S K Abuhelala

A thesis submitted for the Degree
Of
Doctor of Philosophy

Centre for Intelligent Dynamic Communications
(CIDCOM)
Department of Electronic & Electrical Engineering
University Of Strathclyde
Glasgow G1 1XW
United Kingdom

November 2022

Declaration

This thesis is the result of the author's original research. It has been composed by the author and has not been previously submitted for examination, which has led to the award of a degree. The copyright of this thesis belongs to the author under the terms of the United Kingdom Copyright Acts as qualified by University of Strathclyde Regulation 3.50. Due acknowledgement must always be made of the use of any material contained in, or derived from, this thesis.

Signed: Mohamed Abuhelala

Date: 26/11/2022

Committee in-charge:

Convenor: Prof. Craig Michie

External Examiner: Prof. Milan Dado

Internal Examiner: Dr Vladimir Stankovic

Preface

This thesis is submitted to the University of Strathclyde for partial fulfilment of the requirements for the degree of Philosophies doctor.

This doctoral work has been performed at the Department of Electronic and Electrical Engineering, Centre for Intelligent Dynamic Communications (CIDCOM), with Prof Ivan Glesk as main supervisor and with co-supervisor Prof Ivan Andonovic.

Abstract

In seeking efficient last-mile solutions for high-capacity, optical code division multiple access (OCDMA) emerges as a promising alternative high-speed optical network that can securely support a multitude of simultaneous users without requiring extensive equipment. This multiplexing technique has recently been the subject of comprehensive research, highlighting its potential for facilitating high-bandwidth multi-access networking. When contrasted with techniques such as wavelength division multiplexing (WDM) and optical time division multiplexing (OTDM), OCDMA offers a more effective and equitable split of available fibre bandwidth among the users. This thesis presents my research focused on the incoherent OCDMA under the influence of optical fibre impairments that uses picosecond multi-wavelength pulses to form two-dimensional wavelength hopping time-spreading (2D-WH/TS) incoherent OCDMA codes. In particular, self-phase modulation, temperature induced fibre dispersion, chromatic dispersion, as well as the impact of semiconductor optical amplifier SOA devices deployment on 2D-WH/TS OCDMA code integrity were investigated. These aspects were investigated using a 17-km long bidirectional fibre link between Strathclyde and Glasgow University. In particular, I investigated the impact of temporal skewing among OCDMA code carriers and the importance of selecting small range of wavelengths as code carriers where wide range manifest high dependency on wavelength. This wavelength dependency is exploited furthermore to measure the induced temperature dispersion coefficient accurately and economically. I have conducted experiments to characterise the impact of SOA-device on 2D OCDMA code carries which is evaluated under different bias conditions. This evaluation addressed the potential challenges and ramifications of the gain recovery time of SOA and its wavelength dependency with respect to gain ratio and self-phase modulation (SPM). The OCDMA code was built using multiplexers and delay lines to create a 2D OCDMA code to allow studying the impact of deploying a SOA under different conditions on each wavelength. The concept described above is then extended to the investigation of the SOA's impact on a 2D-WH/TS OCDMA prime code under high bias current/gain conditions. The overall performance of two different 2D-WH/TS OCDMA systems deploying the SOA was also calculated. I have also investigated the possibility of manipulating chirp in 2D-WH/TS incoherent OCDMA to counteract the self-phase modulation-induced red shift by using single mode fibre and lithium crystals. I have investigated the performance of the picosecond code based optical signal when subjected to temperature variations similar to that experience by most buried fibre systems. I have proposed and demonstrated a novel technique, which I

examined analytically and experimentally, that utilises a SOA at the transmitter to create a new code with a new wavelength hopping and spreading time sequences to achieve a unique physical improved secure incoherent OCDMA communication method. A novel fully automated tuneable compensation testbed is also proposed of an autonomous dispersion management in a WH/TS incoherent OCDMA system. The system proposed manipulates the chirp of OCDMA code carriers to limit chromatic dispersion detrimental effect on transmission systems.

Acknowledgments

Without the assistance and support of the kind individuals in my life, only a few of whom may be specifically mentioned here, I would not have been able to complete this PhD thesis. I want to firstly express my deepest gratitude to my supervisor, Professor Ivan Glesk, for his unwavering support of my PhD studies and research, and his patience in correcting my manuscripts. He became to me like a big brother, uncle, and well-wisher, someone who has always stood with me. The fact that Prof. Ivan Glesk constantly leaves his office door open for his PhD students is what I find most amazing about him. In addition, I would like to express my profound gratitude to Professor Ivan Andonovic, my second supervisor, for giving me the drive to get through the challenging parts of this journey. A special thanks also goes out to Professor Anderson Sanches of Federal University of ABC for his professional direction, counsel, and work revising some of the publications I published during this project. Also, Md. Shakil Ahmed and Umair Ahmed Korai, my fellow labmates in the optics lab, for our fruitful conversations as we worked together. I also thank Mohsin Masood, Alan Davidson, and Stuart Hannah three of my friends from the University of Strathclyde, for their ongoing inspiration and zeal.

This PhD is in honour of Mr. Sadek Abuhelala, my father. Whatever I am today is solely a result of his unwavering encouragement, inspirational words, and treasured talks. He is the one who has always stood by me when I have faced challenges in my life. He often says, "You can always count on me to stand by your side and support you." I consider myself extremely fortunate to have my mother, Mrs. Nadia Ben Jabber, my brothers, Ahmed and Anas, and my sister, Omiana, who have all supported me, believed in my ability to complete the PhD study, prayed for my success, and have given me their best wishes for the rest of my life.

Moreover, I consider myself extremely fortunate to have such a loving and kind wife, Mrs. Rihanna Alhaj, who has been a constant source of inspiration in many spheres, particularly garnering a strong support and encouragement to pursue my academic journey. Throughout the course of my studies, I was able to depend completely on her patience and concern. Despite the fact that I had to put time and effort into my studies and be actively involved in the research, I am grateful to my child Awais Abuhelala for lifting my spirits. My brother and best friend, Anas Abuhelala (Takoma), who stayed with me through thick and thin, deserves a million thanks for his unwavering support and inspiration to carry on with my studies.

Table of content

Declaration	ii
Preface	iii
Abstract	iv
Acknowledgments	vi
Table of content	vii
List of Figures.....	x
List of Tables.....	xv
List of Abbreviations	xvi
List of Publications.....	xix
Chapter 1	1
Introduction.....	1
1.1 Motivation.....	1
1.2 Research Aims and Contributions.....	3
1.2.1 Summary of Contributions from Thesis	3
1.3 Organisation of the Thesis	4
Chapter 2	6
2.1 Overview of CDMA	6
2.2 CDMA Implementation in Optical Fibre Networks	6
2.3 Incoherent OCDMA.....	9
2.4 One-dimensional (1D) OCMDA Code.....	11
2.5 2D-Wavelength-hopping Time-spreading (2D-WH/TS) Codes.....	12
2.6 2D-WH/TS incoherent OCDMA and coding approaches.....	14
2.6.1. Arrayed Waveguide Gratings OCDMA Encoder	15
2.6.2 Thin-Film Filters OCDMA Encoder	16
2.6.3 Fibre Bragg Gratings based OCDMA Encoders.....	17
2.6.4. Holographic Bragg Reflector	19
Chapter 3	20
Optical Fibre Impairments on Transmission	20
3.1 Introduction.....	20
3.2 Chromatic dispersion in a single mode fibre	22
3.2.1 Material dispersion.....	24
3.2.2 Waveguide dispersion	26
3.2.3 Zero, Normal and Anomalous Dispersion	27

3.3 SOA induced Self-Phase Modulation	29
3.3.1 Chirp parameter in optical fibre communication	30
3.3.2 The Effect of Self-Phase Modulation on Group Velocity Dispersion.....	32
3.4 Chromatic Dispersion Compensation Techniques	33
3.4.1 Chromatic Dispersion Compensating Technique based on Optical Fibre	34
3.4.2 Tuneable Dispersion Compensation Techniques.....	37
Chapter 4	39
Ambient Temperature Fluctuations Effect on 2D-WH/TS OCDMA Code Integrity	39
4.1 Introduction	39
4.2 Temperature Dependence of Chromatic Dispersion in Optical Fiber	40
4.3 The Influence of Temperature Variations on Incoherent 2D-WH/TS OCDMA Codes.....	42
4.3.1 The scalability of the 2D-WH/TS OCDMA coding.....	45
4.4 Investigation on Temporal Skewing among OCDMA Code Carriers under Fiber Temperature Variations.....	45
4.4.1 Theoretical analysis	46
4.4.2 System Setup	48
4.4.3 Experimental Results and calculation	49
4.5 Simple method to accurately measure temperature dispersion coefficient.....	52
4.5.1 System setup	53
4.5.2 Results and analysis	54
4.6 Discussion	57
4.7 Summary chapter	58
Chapter 5	59
Investigation of 2D-WH/TS OCDMA Code Stability in Systems with SOA-based Device	59
5.1. Introduction	59
5.2. Impact of SOA-Based Devices Deployed in Fibre Link on Multi-Wavelength Picosecond Code Carriers	62
5.2.1 Description of Experimental Setup	62
5.2.2 Investigation of 2D-WH/TS OCDMA Code Carriers' Distortion under Different SOA Driving Conditions.....	64
5.2.3 Discussion	67
5.3 Impact of SOA High Bias Current on 2D-WH/TS OCDMA Prime Code Fidelity	72
5.4 Manipulation of chirp to mitigate SPM effect	75
5.4.1 Lithium-niobate crystal	76
5.4.2 Anomalous dispersive fibre	79
5.5. Chapter summary	82

Chapter 6	83
Applications of SOA based Devices for Improving 2D - WH/TS OCDMA Network Performance	83
6.1. Enhancing physical layer communication privacy by using SOAs in OCDMA networks	83
6.1.1. System setup	84
6.1.2. Obtained results and analysis	85
6.1.3. Summary	93
6.2. A Tuneable Automated System for Temperature Dispersions Mitigation using SOA	94
6.2.1. Description of Experimental Setup	95
6.2.2. Results and analyses	98
6.2.2.1. Calculation of the Full Width at Half Maximum	102
6.2.2.2. Automated system	104
6.2.3. Summary	108
Chapter 7	110
Conclusion & Future Work	110
7.1 Conclusion	110
7.2 Future work	112
References	114

List of Figures

Figure 2. 1. Basic characteristics of OTDM (a), OWDM (b) and OCDMA (c).

Figure 2. 2. Schematic of OCMDA System.

Figure 2. 3. A concept of 2D-Wavelength-Hopping Time-Spreading (2D-WH/TS) OCDMA code for different users in the network, where p_i is number of used time chips and w is number of used wavelengths (code weight). The various colours correspond to distinct wavelengths within the code sequence of each user.

Figure 2.4. Schematic of Arrayed Waveguide Gratings.

Figure 2. 5. 2D-WH/TS encoder Schematic diagram.

Figure 2. 6. Schematic diagram of a 2D-WH/TS encoder exploiting TFF where I is input port; T is transmitted port; R is reflected port.

Figure 2. 7. Schematic of a WHTS encoder utilising FBG, where OC is optical circulator; D_i is delays.

Figure 3. 1. Transmission impairments categories

Figure 3. 2. Illustration of refractive index depending on the wavelength induces the group velocity dispersion.

Figure 3. 3. Illustration of combination of D_w and D_m resulting in total dispersion D .

Figure 3. 4. Refractive index and group index as a function of wavelength, calculated from a three term Sellmeier's equation.

Figure 3. 5. SPM followed by negative and positive dispersion where in (a) $D < 0$, additional pulse broadening, (b) $D > 0$, pulse compression.

Figure 3. 6. Illustration of chromatic dispersion compensator rule.

Figure 4. 1. Where (a) The process of decoding a 2D-WH/TS OCDMA code after propagation in ideal conditions across a fully dispersion compensated fibre link resulting in undistorted autocorrelation function. (b) Illustration of distorted autocorrelation peak due to temporal skewing among code carriers in 2D-WH/TS OCDMA system.

Figure 4. 3. Illustration of the 2D-WH/TS incoherent OCDMA code.

Figure 4. 4. Illustrates the concept of delays selection.

Figure 4. 5. Experiment setup. EC -Environmental Chamber, DCF – Dispersion Compensating Fibre, Scope – Agilent Oscilloscope 86100C, FBG – Fibre Brag Grating, SCL – Supercontinuum source, MLL – Erbium doped fiber mode locked laser.

Figure 4. 6. Illustration of the impact of Δt ; blue squares define Δt_1 ; Δt_2 was calculated using equation 4.7. Red circles define Δt_1 ; Δt_2 was obtained from our measurements. The standard deviation for Δt_1 is 0.277 ps and for Δt_2 is 0.396 ps, respectively.

Figure 4. 7. The experimental set-up utilized to assess the skewing effect caused by temperature-induced dispersion in optical fibre among OCDMA code carriers

Figure 4. 8. The 2D-WH/TS OCDMA code carriers at the point a at the transmitter side. Used to measure the time shifting between λ_1 and λ_4 .

Figure 4. 9. The skewing effect is measured between λ_1 and λ_4 from the OCDMA code.

Figure 4. 10. Time shifting measurement in three temperature points; at 0°C, 20°C and 40°C.

Figure 4. 11. Time skewing between code carriers $\lambda_1 = 1551.72$ nm and $\lambda_4 = 1550.12$ nm spectrally separated by 1.6 nm as a function of different fiber temperatures.

Figure 5. 1. Schematic diagram of the experimental setup with illustration of two-dimensional wavelength-hopping time-spreading (2D-WH/TS) code carriers. FMLL –picosecond fiber mode locked laser, OS – optical supercontinuum, DMUX – de-multiplexer, MUX – multiplexer, SOA – semiconductor optical amplifier, DCF – chromatic dispersion compensating fiber.

Figure 5. 2. SOA's gain recovery time against the bias current.

Figure 5. 3. (a) Optical spectrum of the 2D-WH/TS OCDMA code based on four λ_1 to λ_4 multi-wavelength picosecond code carriers before entering the SOA biased at ~175 mA; **(b)** after passing the SOA followed by dispersion compensated fiber link (DCF) and λ_1 - λ_4 decoder. VOA—variable optical attenuator, OFL—optical fiber link.

Figure 5. 4. Experimental demonstration of code carriers' wavelength redshift observed on the optical spectrum analyzer: **(a)** code carriers at the input of the SOA; **(b)** effect of SOA on code carrier λ_1 at an SOA current of 7 mA/6dB gain, 80 mA/12 dB gain, and 250 mA/24 dB gain, respectively; **(c)** similarly for λ_2 ; **(d)** for λ_3 ; **(e)** for λ_4 ; **(f)** illustration of redshift on all four wavelength code carriers for an SOA current of 250 mA/24 dB gain.

Figure 5. 6. The measured amount of code carriers' wavelength redshift as a function of the SOA bias current.

Figure 5. 7. Simulation layout of 2D TS/WH OCDMA transmitter and receiver with SOA in the transmission link.

Figure 5. 8. Wavelength red shift for the SOA biased at 250 mA. The dashed line is simulations, and the dots are measured values for $\lambda_1 = 1550.12$ nm, $\lambda_2 = 1550.92$ nm, $\lambda_3 = 1551.72$ nm, and $\lambda_4 = 1552.52$ nm.

Figure 5. 9. Impact of SOA on 2D-WH/TS code based on four-wavelength code carriers as recorded by an optical spectrum analyzer: (a) without and (b) with the SOA present in the chromatic-dispersion (CD) compensated transmission link.

Figure 5. 10. Probability of error as a function of K simultaneous users for a (4, 53)/(3, 53) and (8, 53)/(7, 53) 2D-WH/TS OCDMA system without/with the deployment of an SOA, respectively, the latter causing a one channel code carriers' redshift.

Figure 5. 11. Experimental setup of 2D-WH/TS OCDMA using LiNbO₃ to mitigate SOA induced redshift. Where, MLL – mode locked laser, EDFA – erbium doped fibre amplifier, FBG – fibre Bragg grating, SOA – semiconductor optical amplifier, PC – polarisation controller, OSA – optical spectrum analyser, ESO - electrical sampling oscilloscope.

Figure 5. 12. (4, 53) 2D WH TS OCDMA autocorrelation peak as seen on the oscilloscope with back-to-back setup.

Figure 5. 13. Exhibit the effect of SOA redshift at bias current at 170 mA on (4, 53) 2D WH TS OCDMA autocorrelation peak.

Figure 5. 14. Illustrate how negative chirp is imposed on the code after deploying LiNbO₃ modulator mitigates the redshift caused by SOA with bias current of 170 mA.

Figure 5. 15. Schematic diagram of the experimental setup. MLL - mode lock laser. EDFA - Erbium dope fibre amplifier. VOA - variable optical attenuator. OSA - optical spectrum analyser. OAC - optical autocorrelator.

Figure 5. 16. Shows, in the right, the optical pulse of $\lambda_1 = 1550.12$ nm with FWM of 7.6 ps. In the left is the input optical spectral with linewidth of 0.6 nm.

Figure 5. 17. Shows, on the right, the redshift of 0.84 nm from the original wavelength $\lambda_1 = 1550.035$ nm. On the left, the optical pulse of 9.4 ps. This figure was captured without the additional 1300 m SMF 28 to the setup.

Figure 5. 18. On the right, is the measured optical pulse in time domain using optical autocorrelator. The optical pulse at FWM is fully retrieved to 7.6 ps. On the left, the optical spectrum of the output pulse after passing through the EDFA at the receiver side.

Figure 6. 1. Experimental setup of physical-enhanced secure communication system in 2D WH TS OCDMA system; PS ML – picosecond mode locked laser, EDFA – Erbium doped fibre amplifier, 2D-WH TS OCDMA – wavelength hopping time spreading optical code division multiple access, CDC –chromatic dispersion compensation, SOA – semiconductor optical amplifier, OSC – optical oscilloscope, OSA- Optical spectrum analyser, SC – supercontinuum.

Figure 6. 2. Depicts the 2D WH TS OCDMA code measured by oscilloscope after the encoder.

Figure 6. 3. Illustration of the structure of the 2D WH TS OCDMA encoder.

Figure 6. 4. Illustration of the structure of the decoder to retrieve the autocorrelation peak.

Figure 6. 5. Illustrates the newly formatted 2D WH TS OCDMA code in time and frequency domains imposed by tuning the SOA at the transmitter. Where FD is the frequency domain and TD is the time domain. SOA is the semiconductor amplifier, DDF dispersion compensated fibre

Figure 6. 6. shows the newly formatted 2D-WH/TS OCDMA at point B before the decoder using tuneable filter.

Figure 6. 7. Autocorrelation peak of two perfectly aligned wavelengths with one mismatched wavelength.

Figure 6. 8. Illustration of the two WH TS code sequences generated by the same OCDMA encoder.

Figure 6. 9. Experimental setup of an automated system to compensate for chromatic dispersion effect on OCDMA system; MLL -mode locked laser, EDFA – Erbium doped fibre amplifier, FBG – fibre Bragg grating, CDC –chromatic dispersion compensation, SOA – semiconductor optical amplifier, DAQ – data acquisition.

Figure 6. 10. Picture of the components of the automated tuneable system setup

Figure 6. 11. Picture of 3D printed mechanical device to control the SOA bias current.

Figure 6. 12. Autocorrelation peak at the receiver before and after adding and removing 66 m of SMF: (A) shrinking of 2 ps from the original autocorrelation width,(B) back-to-back autocorrelation width, (C) broadening of 4 ps from the original autocorrelation width.

Figure 6. 13. Screenshot of selecting the waveform source for VI in LabVIEW.

Figure 6. 14. Screenshot of the transfer of waveform parameters in VI (VISA).

Figure 6. 15. Screenshot of extraction of waveform information from the instrument response (Oscilloscope 86100C).

Figure 6. 16. Capture of clearing of the instrument buffer.

Figure 6. 17. Capture of the calculation of the FWHM (Full Width at Half Maximum).

Figure 6. 18. Virtual scope VI displays the autocorrelation peak with two cursors denoting the FWHM.

Figure 6. 19. Illustrates the ratio ($\tau\tau_0$) of the autocorrelation width (Y axis) and the corresponding change on the rotation direction of the DC motor (X axis) by adjusting the bias current of the SOA.

Figure 6. 20. Illustration of the VI in the motor controller when the system exhibits under-compensation.

List of Tables

Table 2. 1. Comparisons of OWDM, OCDM, and OTDM techniques [20] [21]

Table 3. 1. Typical dispersion and slope values in various types of fibres [91].

Table 5. 1. Geometrical and material parameters used in the simulation.

Table 6. 1. Calculation of the autocorrelation peak of the original decoder designed.

Table 6. 2. Calculation of the 0.5nm redshift induced on all code carriers and its effect on the autocorrelation peak.

Table 6. 3. Calculation of the autocorrelation peak of a new decoder designed considering additional delay lines and new filter for λ_5 .

List of Abbreviations

1D	One-dimensional
2D	Two-dimensional
2D-OOC	Two-dimensional optical orthogonal codes
2D-WH/TS	Two-dimensional wavelength-hopping/time-spreading
ASE	Amplified spontaneous emission
Att	Optical attenuator
AWG	Array Waveguide Gratings
BER	Bit error rate
BPF	Band-pass filter
CD	Chromatic dispersion
CDC	Chromatic dispersion compensation
CDMA	Code division multiple access
CFBG	Chirped fibre Bragg gratings
CFG	Chirped fibre grating
CHPC	Carrier-hopping prime code
CMG	Chirped Moiré gratings
CW	Continuous wave
CW/HB	Continuous-wave holding beam
DCF	Dispersion compensation fibre
DDF	Dispersion decreasing fibre
DWDM	Dense wavelength division multiplexing
EDFA	Erbium-doped fiber amplifier
FBG	Fibre Bragg gratings
FBG-DCM	FBG based dispersion compensation modules
FEC	Forward error correction
FWHM	Full-width at half-maximum
GTE	Gires-Tournois etalons
GVD	Group velocity dispersion
HD-FEC	Hard-decision forward error correction
HNLF	Highly non-linear fibre
IL	Insertion loss
IOR	Index of refraction

ITU	International telecommunication unit
LAN	Local area network
LiNbO ₃	Lithium niobate
MAI	Multi-access interference
MLL	Mode locked laser
MPC	Modified prime codes
MZI	Mach–Zehnder interferometer
NC-FBGs	Nonlinearly chirped fibre gratings
NLSE	Nonlinear Schrodinger equations
OA	Optical attenuator
OAC	Optical auto-correlator
OBN	Optical beat noise
OCDM	Optical code division multiplexing
OCDMA	Optical code division multiple access
ODL	Optical delay line
OHL	Optical hard limiting
ONU	Optical network unit
OOC	Optical orthogonal code
OOK	On-off keying
OSA	Optical spectrum analyser
OSC	Oscilloscope
OSG	Optical supercontinuum generator
OSNR	Optical signal to noise ratio
OTDM	Optical time division multiplexing
PC	Polarization controllers
PC	Prime codes
PCF	Photonic crystal fibre
PD	Photodetector
PLC	Polarisation loop controller
PMD	Polarization mode dispersion
RF	Radio frequency
RZ	Return to zero
SC	Supercontinuum
SLM	spatial light modulator

SMF	Single mode fibre
SNR	Signal-to-noise ratio
SOA	Semiconductor optical amplifier
SOA-MZI	Semiconductor optical amplifier based – Mach-Zehnder Interferometer
SPM	Self-phase modulation
SSMF	Standard single mode fibre
SWG	Sub-wavelength waveguide gratings
T/W	Time/wavelength
TD	Temperature-induced dispersion
TDM	Time division multiplexing
TF	Tuneable optical filter
TFF	Thin-film filter
VIPA	virtually imaged phase arrays
WDM	Wavelength division multiplexing
WH/TS	Wavelength hopping time spreading
XPM	Cross-phase modulation

List of Publications

Journal papers:

1. **M. S. K. Abuhelala**, U. A. Korai, A. L. Sanches, W. C. Kwong, and I. Glesk, “Investigation of 2D-WH/TS OCDMA code stability in systems with SOA-based device,” In *Applied Sciences*, vol. 10, no. 21, Nov. 2020. DOI: 10.3390/app10217943.

2. M. S. Ahmed, **M. S. K. Abuhelala**, and I. Glesk, “Managing dispersion affected OCDMA autocorrelation based on PS multi-wavelength code carriers using SOA,” *IEEE/OSA Journal of Optical Communications and Networking*, vol. 9, no. 8, pp. 693-698, Jul. 2017. DOI: 10.1364/jocn.9.000693.

3. N. Mathur, G. Paul, J. Irvine, **M. S. K. Abuhelala**, A. Buis, and I. Glesk, “A practical design and implementation of a low cost platform for remote monitoring of lower limb health of amputees in the developing world,” In *IEEE Access*, vol. 4, pp. 7440 – 7451, May. 2016. DOI: 10.1109/ACCESS.2016.2622163

4. M. Masood, **M. S. K. Abuhelala**, and Ivan Glesk, “A comprehensive study of routing protocols performance with topological changes in standard networks,” In *International Journal of Electronics, Electrical and Computational System*, vol. 5, no. 8, pp. 31-40, Aug. 2016.

Conference papers:

1. A. L. Sanches, **M. S. K. Abuhelala**, T. R. Raddo, S. Haxha, and I. Glesk, “Rate-flexible optical CDMA networks based on coherent modulation formats,” In Proc. *22nd International Conference on Transparent Optical Networks, ICTON, 2020*. Bari, Italy, N.J.: IEEE.

2. **M. S. K. Abuhelala**, M. S. Ahmed, M. Ibrahim, and I. Glesk, “Investigation temporal skewing among O-CDMA code carriers under fibre temperature variations,” In *Proc. 25th Telecommunications Forum TELFOR, 2017*. DOI:10.1109/telfor.2017.8249490.

3. M. S. Ahmed, **M. S. K. Abuhelala**, and I. Glesk, “Management of OCDMA autocorrelation function distorted by dispersion effects,” In *Proc. 19th International Conference on Transparent Optical Networks, ICTON*, 2017. Piscataway, N.J.: IEEE. DOI: 10.1109/ICTON.2017.8024789.

4. M. Masood, **M. S. K. Abu Helala**, and I. Glesk, “Detailed analysis of routing protocols with different network limitations,” In *Proceedings of the 20th Slovak-Czech-Polish Optical Conference on Wave and Quantum Aspects of Contemporary Optics*, vol. 10142, 2016. DOI: 10.1117/12.2256834

Chapter 1

Introduction

1.1 Motivation

Information and communication technology has seen a remarkable rise in demand over the last ten years, such that almost every element of modern life has been impacted by information technology. Applications that require a lot of bandwidth are constantly being developed for an ever-ready pool of consumers, the majority of whom are eager to try out the newest information access methods [1]. The rise of the internet has completely changed how we interact, play, and communicate. On-demand television, which delivers information utilising a broadband connection to the home, is replacing more outdated traditional television access methods like terrestrial broadcasting. Moreover, by using cutting-edge multimedia communication technology to connect headquarters with other branch offices that may be dispersed all over the world, businesses are reducing the cost of travel while increasing productivity and profitability [2].

With the development of several large-capacity datacentres where data can be stored and retrieved at any time, cloud computing, text-, audio-, and video-based social media, internet-based radio, and television, as well as the necessity to store a lot of data, computing has undergone a revolution.

All the technologies discussed above depends on effective internet accessibility to both homes and businesses. As a result, telecom companies are continuously developing efficient ways to supply greater broadband speeds. The majority of service providers currently use digital subscriber line (DSL), which offers a bandwidth of roughly 1.5 Mbps, as their primary access network technology. As part of the entire service provider network, this causes a significant bottleneck in the access network. It will be difficult to guarantee that the end users will receive broadband-based services such as video-on-demand (VoD) if the main distribution infrastructure is not able to deliver the same capacity, regardless of how much money is invested in high-capacity backbones in the core of the service provider network infrastructure. As a consequence, efficient technologies have now been rolled out in order to maximise the

number of bits of information that can be pushed down to each consumer as fast as possible [3]. This entails redesigning the transport, distribution, and access networks of the telecommunications provider and substituting fibre optic-based technologies such as fibre to the cabinet (FTTC), fibre to the building (FTTB), and fibre to the home (FTTH) for the legacy copper-based digital subscriber lines to the consumer premises.

Service providers need to utilise the capacity of the current fibre infrastructure in order to offer dependable, effective, and cost-effective access options. Several access approaches, which allow multiple users to share the same physical infrastructure without sacrificing security and speed, have made this viable [4].

Due to the success of the Code Division Multiplexing (CDMA) technology in the wireless industry, various ideas have been put forward and investigated in an effort to replicate the successful deployment of the CDMA technology using optical fibre. As potential advantages of implementing OCDMA, scalability and security have been highlighted in particular. However, the majority of the findings previously published in the literature have mostly been based on theoretical calculations that do not account for the unique physical properties and constraints of the optical fibre medium. The simplest OCDMA implementation is the incoherent method [5] [6], which has been the focus of numerous studies since the 1980s. It merely needs direct detection (power summation) of the optical signal pulses and intensity modulation. However, in contrast with coherent OCDMA bipolar codes cannot be obtained, because incoherent OCDMA techniques can only employ the intensity of the optical pulse, which could reduce the number of concurrent users [7].

For usage in fibre optic networks, optical time division multiplexing (OTDM) [8] and OCDMA [9] have been developed. Researchers have become interested in the incoherent OCDMA family of codes based on two-dimensional wavelength hopping time spreading (2D-WH/TS) in recent years [9]. The 2D-WH/TS OCDMA utilises multi-wavelength picosecond code carriers in order to support and achieve superior cardinality and a large number of simultaneous users [10]. Nonetheless, OCDMA is not yet standardised since research is currently being done to establish the optimum way to implement it, and employing picosecond code carriers could have unfavourable dispersion effects [11] during data transmission if the issue is not adequately addressed. The goal of this PhD study is to analyse the impact of dispersion on 2D-WH/TS OCDMA fibre transmission and to identify strategies for reducing it.

The traditional approach to compensating for chromatic dispersion (CD) frequently involves employing Dispersion compensating fibre (DCF) modules with matched lengths.

When dealing with multi-wavelength picosecond incoherent OCDMA systems, this method can be time-consuming, complex, and challenging to execute if the fibre lengths are unknown beforehand or the dispersion is changing as a result of environmental changes. The dispersion correction mechanisms may need to be tuneable in nature due to a number of troublesome problems. For instance, dispersion management with great accuracy is required in practically all 40+ Gb/s systems, preferably employing tuneable dispersion compensators as detailed in [12]. OCDMA codes are created in OCDMA systems by distributing the multi-wavelength picosecond pulses over a data bit-width. These brief multi-wavelength pulses travelling in the optical fibre would be widened and impacted by a phenomenon known as time-skewing due to CD or temperature-induced dispersion (TD). As a result, the recovered OCDMA autocorrelation function varies in shape, particularly in width, at the receiver side. The bit error rate (BER) and overall number of concurrent users of the OCDMA system may be significantly impacted by this [13], [14]. Dispersion management is therefore essential to preserving system performance. This motivated this research to explore these behaviours of the 2D-WH/TS OCDMA systems with an emphasis on codes produced utilising picosecond optical pulses.

1.2 Research Aims and Contributions

In order to better understand how optically encoded data behaves during transmission in the optical fibre while being affected by optical fibre impairments, the practical elements of incoherent 2D WH/TS OCDMA implementations are studied in this thesis. The entire thesis is only focused on incoherent 2D-WH/TS OCDMA.

1.2.1 Summary of Contributions from Thesis

1. Evaluate a common used equation to anticipate the impact of temporal skewing on OCDMA code carriers and the effect of temperature induced fibre dispersion on OCDMA prime code. Additionally, an adjustment is proposed to the equation to make it applicable to a broader spectral range.

2. The measurement of skewing among OCDMA codes is the first demonstration of a straightforward and economically advantageous way for precisely measuring the temperature dispersion coefficient in 2D-WH/TS incoherent OCDMA.

3. To achieve best utility and understanding of any challenges underlying deploying SOA in incoherent OCDMA, stimulating the SOA effect in various derived current in the OCDMA system is examined and system's performance is assessed using bit error rate.

4. Investigation of the possibility to manipulate chirp in 2D WH/Ts incoherent OCDMA to counteract the self-phase modulation-induced red shift by using single mode fibre and lithium crystals.

5. The use of SOA at the transmitter to generate a new code with a new wavelength hopping and spreading time sequence is proposed, tested, and studied in a unique physical improved secure incoherent OCDMA communication method.

6. The temperature variation-induced dispersion effect on the OCDMA autocorrelation peak is proposed to be eliminated using a unique completely automated tuneable compensation mechanism.

1.3 Organisation of the Thesis

The motivation, the goals and aims of the thesis, and an overview of the major contributions of this research are all summarised in **Chapter 1**. Following that, **Chapter 2** provides an overview of optical code division multiple access systems. It also provides a detailed analysis of current OCDMA implementations, with a special emphasis on incoherent 2D-WH/Ts OCDMA. Also reviewed are a number of background subjects that are important to the discussions in later chapters.

The transmission impairment is covered in **Chapter 3**. Subsequently, the dispersion in the fibre optic system is focused on. The theory and impact of chromatic dispersion are highlighted, as well as how it affects the multi-wavelength OCDMA system. Here, a number of methods of compensation are also covered. Additionally, dispersion and nonlinearity are treated separately in the derivation of the nonlinear Schrodinger equation. Also highlighted is the analysis of the dispersion effect on 2D-WH/Ts OCDMA based on multi-wavelength picosecond carriers.

In **Chapter 4**, it is shown that the temperature-induced dispersion coefficient is wavelength dependent, and it examines the impact of temperature on OCDMA prime codes and the effects of temporal skewing on OCDMA code carriers. A simple and cost-efficient

novel configuration to accurately measure the temperature dispersion coefficient in 2D-WH/TS OCDMA by the measurement of skewing among OCDMA codes is proposed and analysed.

In **Chapter 5**, it is for the first time investigated how the use of semiconductor optical amplifier-based devices in photonic networks may affect the performance of multi-wavelength picosecond code carriers of 2D-WH/TS incoherent OCDMA systems. It also shows how these impacts can be minimised by using pre-compensation methods at the transmitter.

Chapter 6 proposes, demonstrates, and analyses a novel physical enhanced secure incoherent OCDMA communication system using SOA. A novel fully automated tuneable compensation system is also proposed in this chapter to eliminate the temperature variation induced dispersion effect on the OCDMA autocorrelation peak.

Chapter 7 discusses the results and the future directions for the project.

It is important to note how this thesis is structured, with background research and theories pertinent to the research issue being covered in the first section of each chapter (4-6) and a summary given at the end of each chapter, followed by the experiments.

Chapter 2

2.1 Overview of CDMA

One kind of multiplexed communication methods is called CDMA, or Code Division Multiple Access, which offers a way to "simultaneously multiple access to the network." One such network "medium" may be a radio channel that is used concurrently by a number of users using various and distinctive orthogonal code sequences. Numerous CDMA-based technologies have been developed to aid in wireless networks and radio transmission [15]. Spread Spectrum Multiple Access, sometimes known as SSMA, is another name for CDMA. Time-Division Multiple-Access (TDMA), in contrast to CDMA, requires time synchronization for every user. Similarly, Frequency-Division Multiple-Access (FDMA) requires the allocation of bandwidth, whereas CDMA does not. In radio frequency communication systems like 2G and 3G cellular telephone networks, the CDMA technology is widely employed [16].

2.2 CDMA Implementation in Optical Fibre Networks

The usage of optical fibre has fundamentally changed the world of telecommunication. Optical OCDMA (OCDMA) can be referred to as a "next generation CDMA" technique that makes use of fibre optics [17], where data is transferred by light pulse streams through optical fibres. Optical signals have a higher bandwidth. The conversion of low information rate electrical data into high-data rate optical signals is made possible by the extra bandwidth provided by optical fibre for use by "fibre-optic" CDMA [18]. Other communication technologies use a technique called WDM, or Wavelength Division Multiplexing, to separate data channels (users) from each other. Each user in WDM uses a different light wavelength. OCDMA, on the other hand, employs a different strategy, in which every piece of information is encoded and spread over a number of time slots and wavelengths. By using OCMA based systems it is possible to establish a rapid and secure link to the network backbone [19].

OCDMA is also able to send data asynchronously without experiencing packet collisions or loss. OCDMA systems utilise the current fibre-optic backbones, therefore their implementation is less complicated than that of other technologies [16]. OTDM (Optical Time-Division Multiplexing), OWDM (Optical Wavelength-Division Multiplexing), and OCDMA technologies are thoroughly compared in Table 2.1.

Table 2. 1. Comparisons of OWDM, OCDM, and OTDM techniques [20] [21]

Multiplexing Techniques	Main Advantages	Disadvantages	Applications	Operational Cost
OWDM	<ol style="list-style-type: none"> 1. More advanced methods. 2. Extremely high bandwidth effectiveness. 3. High system capacity. 4. 10 Tbit/s rate can be attained, according to experiments, with a single fibre. 	<ol style="list-style-type: none"> 1. Precise laser source is required; 2. Laser source synchronisation is strictly enforced; 3. Low-rate multiplexing sites are lacking. 	<p>Backbone networks and the primary multiplexing method currently employed in optical communications</p>	<ol style="list-style-type: none"> 1. Expensive equipment overall. 2. Yet very cost-effective due to significant bandwidth expansion.
OCDMA	<ol style="list-style-type: none"> 1. Fewer conversions between optical, electronic, and optical. 2. Extremely private and secure transmissions. 3. Access that is asynchronous. 4. Strong interference resistance 5. No precise synchronisation is required. 	<ol style="list-style-type: none"> 1. There are currently just a few effective coding sequences and encoder/decoders in use. 2. The realisation advancement has made few ground-breaking improvements. 	<p>Hardly ever actual applications at this time.</p>	<ol style="list-style-type: none"> 1. Less expensive than an OWDM system in terms of equipment and system support costs.
OTDM	<ol style="list-style-type: none"> 1. Large bitrate to bandwidth ratio. 	<ol style="list-style-type: none"> 1. Synchronisation in high-rate transmissions that 	<p>Practical applications are</p>	<ol style="list-style-type: none"> 1. Low overall equipment costs.

	2. Minimal nonlinear impact on optical equipment during transmission.	is extremely precise. 2. Limited system capacity.	only partially achieved.	2. But poor system capacity results in low cost-effectiveness.
--	---	--	--------------------------	--

Figure 2.1 illustrates the fundamental properties of OTDM, OWDM, and OCDMA with respect to various time slots and wavelengths. OCDMA can be seen of as a hybrid of OWDM and OTDM, however instead of allocating each user their own set of OWDM and OTDM channels, OCDMA encrypts the data bit of each user employing sets of various time slots and wavelengths. Importantly, binary data streams made up of +1 and -1 signals cannot be transmitted via an optically based communication system; instead, binary data in the form of 0 and 1 is required. The reason for this is that an optical system cannot distinguish between different light or optical signal phases.

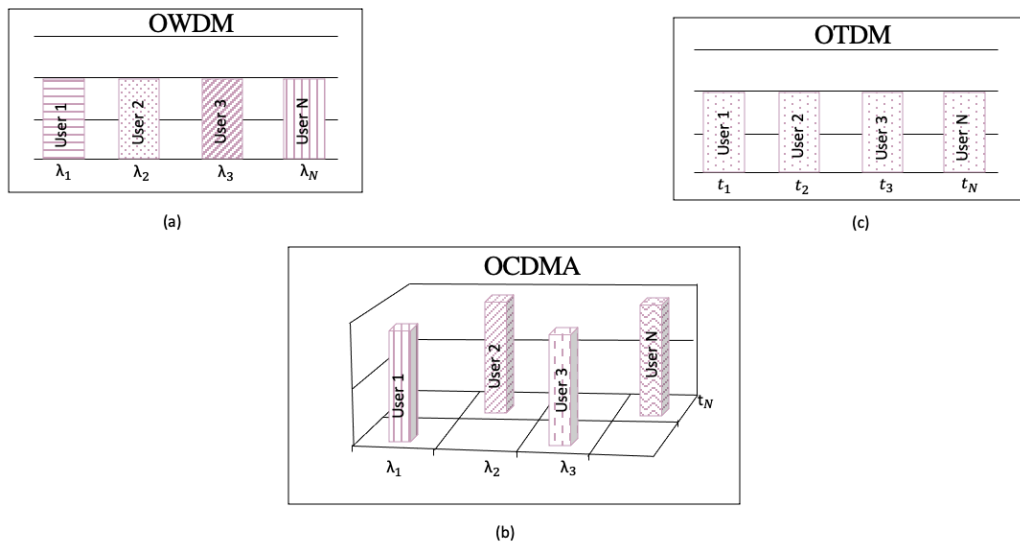


Figure 2. 1. Basic characteristics of OTDM (a), OWDM (b) and OCDMA (c).

As a result, an optical system can only detect signals by determining how much power or energy the light signals have. The use of several repeaters on the optical trunk line is required to compensate for the significant attenuation loss over long distances, which is a downside. Given that fibre-optic cables are commonly installed across long distances, sometimes even beneath the ocean, this drawback is rather inevitable [17]. OCDMA makes it possible for several users to connect to the network at once and asynchronously. Due to its nearly delay-

free operation and minimal need for optical signal processing, it has become increasingly popular in recent years. OCDMA employs asynchronous data transfer, which can simplify network management and control. OCDMA is hence suitable for LANs (Local Area Networks) and other network applications. Every node can run in an asynchronous manner without the need for a global clock owing to OOC (Optical Orthogonal Code). There is no need for a central node to arbitrate disputes between channels because the number of network nodes and the number of codes is equal. If additional codes are available, adding new users is also straightforward. If additional codes are not readily available, a system upgrade to add more time slots and wavelengths can be performed. OCDMA provides dynamic coding, which greatly increases the security of the network connection [17] [22] [23]. That makes it extremely difficult for listeners to intercept a communication without having access to the key [19] because optical codes can be changed at any time, and the frequencies employed change frequently and quickly. For instance, it would take an eavesdropper more than a thousand years to check every possible combination of 961 chips or time slots and 41 wavelengths at the rate of codes per second, reducing the likelihood of a security breach to a minimum. Since distinct categories of multimedia may be categorised using multi-rate OOC, where the data rate is the quantity of delivered data bits within a specific amount of time. Moreover, OCDMA also offers service differentiation, where for example low-rate codes can be used for file transfer and e-mail communication, while high-rate codes can be used for video or audio data [24]

2.3 Incoherent OCDMA

An incoherent OCDMA is a sub-set of OCDMA systems that can be summed up as follows: each user is given a special code sequence (unique in time and wavelength) to represent the user data bit. The receiving end obtains and recognises this specific code sequence, which is then used to demodulate the data that has been received.

- The most crucial component for accurate detection is that these code sequences are completely orthogonal thus there is no crosstalk with any code sequences of other users.

- Each of this code sequence in the wavelength domain encoding contain a set of wavelengths received from, for example, a "single broadband optical source" with its output spectrally sliced into numerous narrow optical wavelengths bands.

- Each of this code sequence in the time domain for time-spreading coding represents a sequence of time slots (chips) positions allocated within the data bit.

When the unique combination of the above is accomplished a generation of orthogonal code sequences is guaranteed.

- All network users can be then connected via a star coupler featuring a bi-directional data stream, as is shown in Figure 2.2. This bi-directionality makes it simple and affordable way to add more users.
- At the receiving end the signal intended for a given user can be decoded and removed from the network traffic by a ‘matched to the transmitter, data receiver [16].

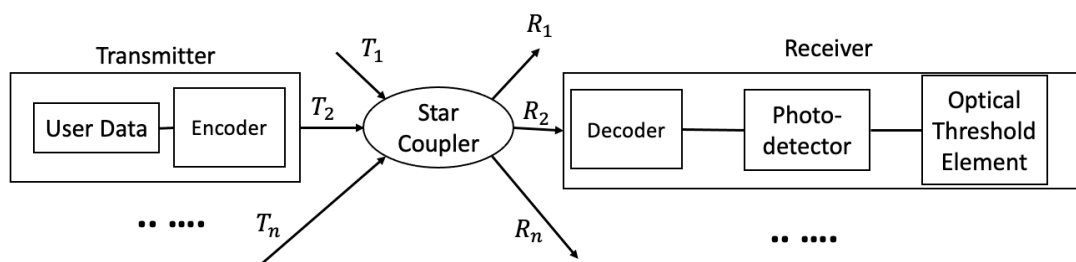


Figure 2. 2. Schematic of OCMDA System.

In conclusion, by following these above steps every data stream is encoded as follows:

- (a) Data bit is time-spread and spectrally-hopped encoded by a different (unique) code sequence;
- (b) Encoded signals can all be fed into a star coupler simultaneously and asynchronously;
- (c) Mixed signals travel through the star coupler over a variable distance to its destinations;
- (d) Encoded signals are decoded at the receiving ends a matched decoder [25].

Some wideband incoherent OCDMA systems use broadband Amplified Spontaneous Emission (ASE), whilst other incoherent OCDMA systems use coherent laser sources [9].

Due to its potential to offer a flexible bandwidth provisioning, phase insensitivity, asynchronous network access, and resilient performance, the incoherent OCDMA has attracted a lot of attention. It is anticipated that incoherent OCDMA will be the technology to be used to meet the enormous bandwidth requirements of fibre-to-the-home (FTTH) services. In particular, as we will see later, the more advanced Wavelength-Hopping Time-Spreading (WH/TS) 2D incoherent OCDMA systems, has proven to have a number of advantages over other incoherent approaches. [26].

2.4 One-dimensional (1D) OCMDA Code

As already mentioned, the one-dimensional (1D) OCDMA coding can be carried out in either the time or frequency domain. Due to its simplicity, 1D coding is frequently employed in both coherent and incoherent systems, where it is implemented using various algorithms. Each data bit is spread into multiple brief time intervals, called chips, in OCDMA systems with temporal coding, and the intensities or phases of these chips are modified in accordance with a pre-designed code sequence. Similarly, spectral coding involves slicing the spectrum of each data bit into a number of small bandwidths, known as frequency bins, and manipulating the intensities of these frequency bins. Although the structures of the algebraic congruence codes in 1D incoherent OCDMA codes are straightforward and easily implemented in hardware, they have weak correlation characteristics and cardinalities, which are limited to prime integers. Significant developments with regards to their performance have been made, but they still fall short of practical expectations. The drawback of 1D incoherent OCDMA codes is that the cardinality of the code is inversely correlated with the spreading length [27]. Additionally, from a practical standpoint, it is challenging to make optical pulse widths less than the order of picoseconds in optical fibre communication systems.

The 1D incoherent OCDMA codes are single carrier codes (code weight of 1) in which a particular sequence of prime numbers uniquely describes the spreading pattern. In 1983, the initial set of prime codes for OCDMA applications was released [7]. The extended Reed-Solomon code and the prime code have a close relationship [28]. Later, the finite field arithmetic algorithm, often known as the Galois field, was used to create the first prime code [29]. In its basic form, to construct a prime sequence, $S_i = (s_{i,0}, s_{i,1}, s_{i,2}, \dots, s_{i,j}, \dots, s_{i,p-1})$, each element $s_{i,j}$ can be obtained by the relationship

$$s_{i,j} = i, j \pmod{p} \quad (2.1)$$

where p is a prime number, and $s_{i,j}$, i , j are all elements of the Galois field GF (p). The maximum cross-correlation value of 2 for prime codes is a result of their unique construction [30] [31]. The unique properties of prime codes that contribute to their low cross-correlation values include:

1. Balanced code: A prime code has an equal number of 1s and -1s, which ensures that its mean value is zero. This balance helps to reduce cross-correlation values [32] [33] [34].

2. No consecutive 1s or -1s: In a prime code, there are no two consecutive 1s or -1s, which reduces the chances of high cross-correlation values [32].
3. Unique phase shifts: Prime codes use unique phase shifts to differentiate between users, which results in low cross-correlation values [32].

This low cross-correlation value is desirable because it reduces the interference between different users' signals.

This and other practical factors have led to certain tight restrictions being placed on the original prime code. For instance, the code weight, length, and cardinality restrictions for a prime number p are as follows: p , p^2 , and p , respectively [35] [7]. Extended prime code, synchronised prime code, generalised prime code, and modified prime code are variations of prime codes [7]. To reach a maximum cross correlation value of 1, which is a 50% reduction from the cross-correlation value of the original prime code, the extended prime code [36] was developed. The generalised prime code [37] is built in a way that allows for more flexibility in terms of code weight, code length, and cardinality without compromising the correlation features.

2.5 2D-Wavelength-hopping Time-spreading (2D-WH/TS) Codes

Due to its superior correlation capabilities when compared to 1D coding, the hybrid Wavelength-Hopping/Time-Spreading (WHTS) 2D coding has recently garnered increasing attention. A well-designed 2D code can reduce user interference to the absolute minimum and significantly increase BER. Although it has not been thoroughly studied yet, the hybrid 2D system is still a contender for the OCDMA system of the future. In the following, the idea of an overview of 2D codes is provided.

The data bit is encoded in the wavelength domain in addition to the time domain in the 2D OCDMA system. This results in separate optical pulses being coloured with various time slots and wavelengths, as shown in Figure 2.3 [15].

The 2D OCDMA technology is a combination of time-spreading and wavelength-hopping communications. As a result, 2D codes are created by combining two different 1D codes that originate from both OOC and prime sequence codes. One of these 1D codes is used as a spreading code, while the other is used as a hopping code to tint the optical pulses within a code sequence so that they are centred at various wavelengths. Since research studies of the 2D OCDMA are lacking, the majority of 2D codes are derived from 1D codes that already exist.

Although different combinations of 1D coding schemes, such as spatial/time-spreading, spatial/wavelength-hopping, and wavelength-hopping/time-spreading (WHTS) coding, can be used in 2D OCDMA systems, the WHTS coding scheme has received the most attention due to its high feasibility, high security, and low cost. Compared to one-dimensional codes, this coding is capable to support a significantly higher number of codes [39]. An example wavelength hopping time spreading OCDMA code produced using a 2D algebraic method is shown in Figure 2.3.

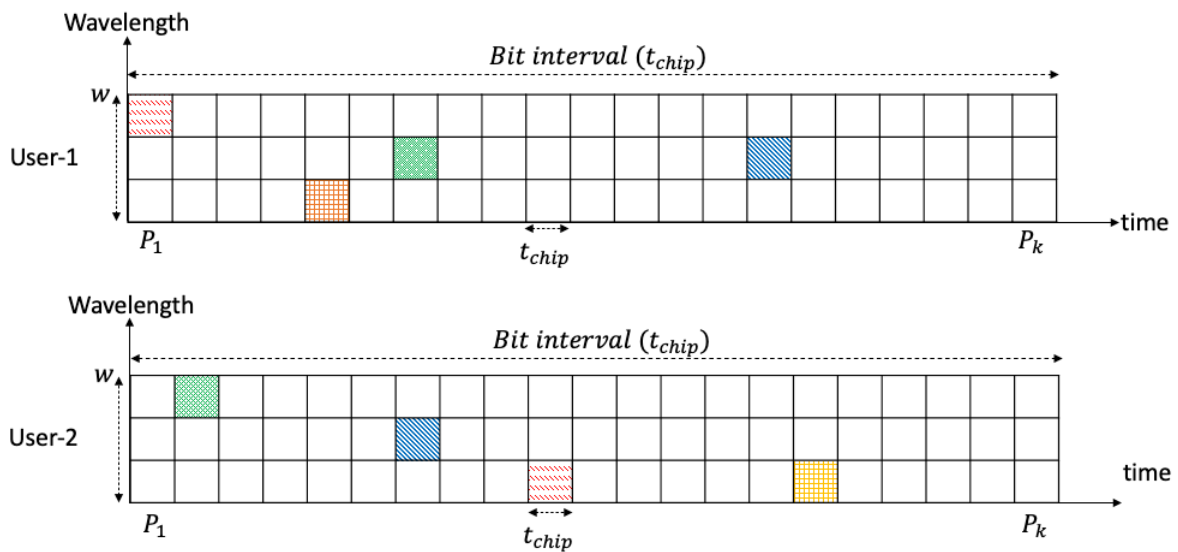


Figure 2. 3. A concept of 2D-Wavelength-Hopping Time-Spreading (2D-WH/TS) OCDMA code for different users in the network, where p_i is number of used time chips and w is number of used wavelengths (code weight). The various colours correspond to distinct wavelengths within the code sequence of each user.

The binary (0, 1) matrices of length $p_1 p_2 \dots p_k$, weight w , with k being a collection of prime numbers $\{p_1 p_2 \dots p_k\}$ are used to represent the code sequences $(p_1 p_2 \dots p_k)$. It is worth noting that $p_1 p_2 \dots p_k$ is the number of columns, which corresponds to the length of the matrices, and w is the number of rows, which corresponds to the quantity of accessible wavelengths [31, 33]. One pulse (i.e., a binary one) appears in each row of each matrix, and each pulse in a matrix is connected to a unique carrier wavelength. Further, the code has zero autocorrelation side lobes ($\lambda_a = 0$) and a cross-correlation function of at most one ($\lambda_c = 1$). Each pulse in a matrix is connected with a unique carrier wavelength. Any 2D-WH/TS code

matrix can therefore be thought of as a collection of ordered pairs, where an ordered pair (w, pk) records the vertical and horizontal position of a binary one from the bottom-left corner of the matrix, where w stands for wavelength, and t displays the position of the binary one in the matrix (time or chip) [40]. This makes the wavelength hopping time spreading code a class of $(w, p, 0, 1)$, where w is the number of wavelengths and p is the number of chips.

Correlation qualities, the maximum supported user number, and BER are the three key criteria used in the OCDMA system to evaluate a signature code. These three characteristics are mutually exclusive and directly related. For a certain code-length sufficient correlation qualities, or good code designs are required, in order to retain as many users as feasible within a reasonable BER. While a large code-length (CL) will increase security and correlation qualities as well as BER performance, it will also limit system throughput and complicate the transceiver architecture. When the CL is large enough, the correlation qualities will be worsened while the SNR is increased at the receiving end, lowering the BER. Because one of these attributes affects the others, all of them are taken into account to enable the signature code to support as many users as possible with the least amount of interference (MAI, etc.) between users. Since it is difficult to create a signature code with entirely perfect characteristics, a trade-off between these elements must be identified. Improving one component would either improve or deteriorate the others. In other words, all of them need to be evaluated in conjunction and an optimised signature code has to be developed, that can serve as many users as possible with the least amount of disturbance, also taking cost and security into consideration.

2.6 2D-WH/TS incoherent OCDMA and coding approaches

OCDMA networks provide high speed data communications for multiusers. The key elements for that are laying in the construction of OCDMA encoders and decoders. The complexity and expense of optical transmitters and receivers, power loss, the number of users in a network, and the reproducibility of the encoder and decoder can all be strongly impacted by their architectures and implementations [38]. The optical source and the encoder are the two primary components of the transmitter, whereas the decoder and the photo receiver make up the receiver. There are numerous encoding techniques that explore various technologies and methodologies that have been demonstrated for usage with incoherent OCDMA encoders. These consist of the employment of holographic Bragg reflectors (HBR) [39], fibre Bragg gratings (FBG) [40], and thin-film filters (TFF) in combination with optical delay lines (ODL)

[41]. A wavelength-hopping pattern is initially produced using a WH/TS encoder based on array waveguide gratings (AWG) and TFFs before a time-spreading pattern is produced. The constituent wavelengths of a code sequence are each individually delayed, enabling the employment of a quickly tuneable timeslot tuner for dynamic code modification. However, an HBR-based encoder inhibits independent control and delay of each wavelength by tightly combining the generation of the wavelength-hopping and time spreading patterns. Encoders built on a linear array of FBGs enable independent wavelength control, whereas independent wavelength delay necessitates a complicated system [9].

2.6.1. Arrayed Waveguide Gratings OCDMA Encoder

Due to their potential for low insertion loss, arrayed waveguide gratings (AWGs) on silicon and lithium niobate technologies have received a lot of attention since the early 1990s [42] [43] [44]. A phased array of optical waveguides that serves as a grating is depicted in Figure 2.4. An assortment of planar waveguides receives the input signal via coupling. The waveguides are at various lengths to provide the signal in each waveguide with various phase shifts. Due to the frequency dependence of the mode-propagation constant, these phase changes are likewise wavelength-dependent [45].

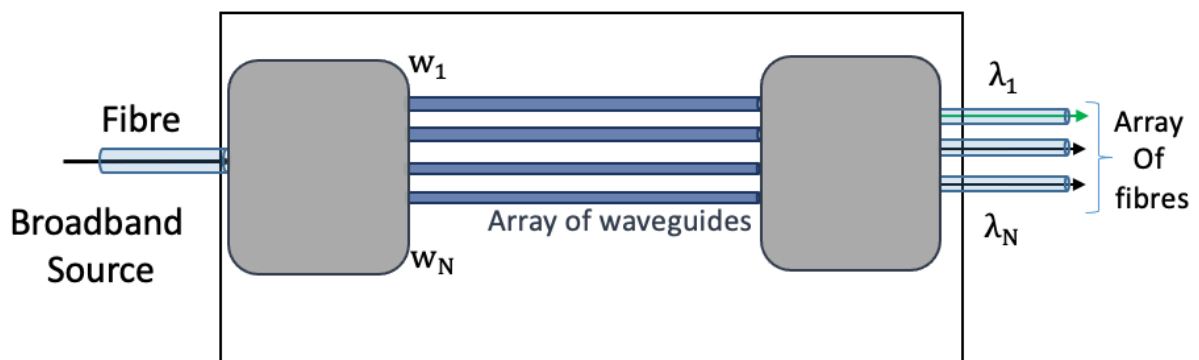


Figure 2.4. Schematic of Arrayed Waveguide Gratings.

Polarisation dependency, temperature sensitivity, a good flat spectrum response, and insertion loss less than 3 dB are typical features of AWGs [9]. They are simple to combine with a photodetector and offer a cross talk threshold which is better than -35 dB. AWGs have a variety of uses, including WH/TS encoders and decoders [46]. The complete WH/TS encoder/decoder can be included into the AWG, which is a mature technology today and has

the benefit of having a smaller footprint [9]. Fig. 2.5 illustrates the use of two AWGs in a 2D-WH/TS encoder together with the delay length $DL_1 - DL_N$.

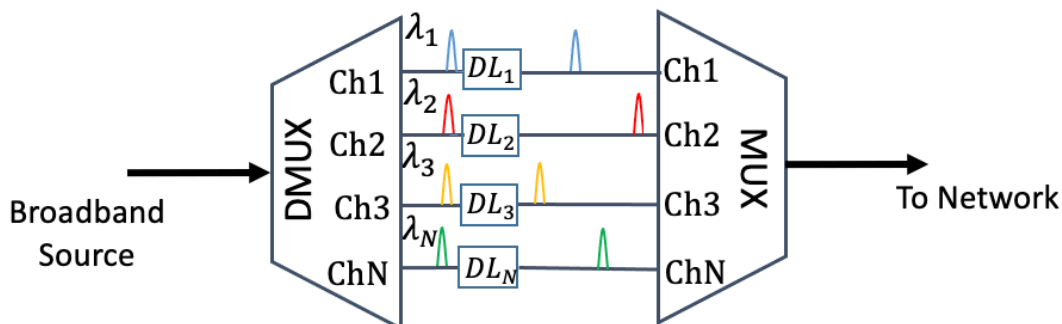


Figure 2. 5. 2D-WH/TS encoder Schematic diagram.

2.6.2 Thin-Film Filters OCDMA Encoder

Fabry-Perot (FP) etalons with several reflecting dielectric thin-film layers that are utilised to create the mirrors encircling the etalon cavity can be thought of as thin-film filters (TFF). TFFs can function as bandpass filters in a manner akin to an FP etalon. TFF performance is governed by the principles of thin-film optics [47], which have been investigated for a number of applications, including edge filters, anti-reflection coatings, and high-reflectance coatings [48]. By cascading a number of these filters and adjusting delay duration D_i , a 2D-WH/TS encoder/decoder can be created using a TFF-based WDM multiplexer and demultiplexer, as shown in Fig. 2. 6. The wavelength λ_0 is passed through the first filter in the cascade, while all other wavelengths $\lambda_1, \lambda_2, \dots, \lambda_i$ are reflected into the second filter. The following filters pass some wavelengths while reflecting others. After that exposure to various delays D_i , the filters on the right-side multiplex λ_i again.

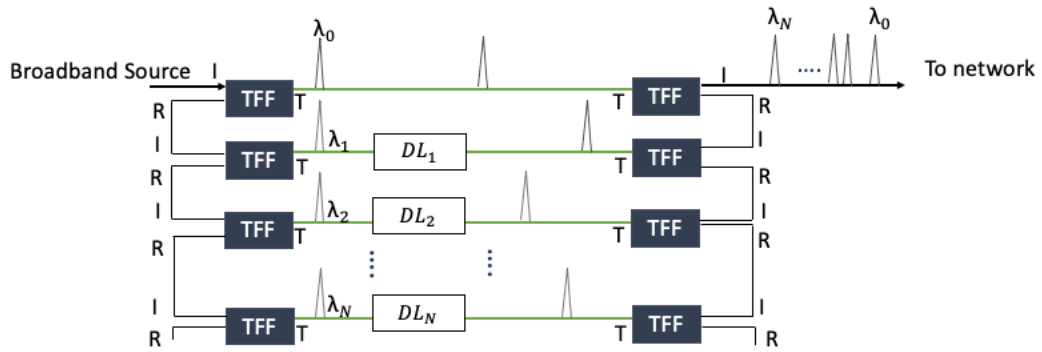


Figure 2. 6. Schematic diagram of a 2D-WH/TS encoder exploiting TFF where I is input port; T is transmitted port; R is reflected port.

Due to their adaptability, low loss and cost, as well as passive temperature correction, TFFs have become a dominating filter technology in commercial sectors. At low channel counts, they offer the lowest loss option, whereas at high channel counts, they offer loss that is comparable to AWG. The device is also exceptionally stable to temperature changes and insensitive to the polarisation of the signal. TFFs have been used in a variety of optical networking applications, including switchable add-drop filters and optical switches [49] [50]. The usage of TFFs in a WH/TS system suggests that the optical pulse width is the only factor limiting chip size. In contrast, the distance between neighbouring gratings introduces an extra limitation in FBG-based encoders and decoders. Thus, the larger code matrix that results can be leveraged to improve system performance, which has been shown in recent trials, where TFFs have been used for WH/TS encoders and decoders [21] [51].

2.6.3 Fibre Bragg Gratings based OCDMA Encoders

Fibre Bragg gratings (FBGs) have recently been used in optical networks for a variety of purposes [52] [53]. Applications include wavelength routing and add/drop multiplexing in WDM networks, as well as techniques for dispersion compensation and wavelength stabilisation in fibre lasers. A number of OCDMA encoding techniques, including spectral amplitude coding [54], spectral phase coding [55], temporal phase coding [56], and WH/TS [57] [58], have also been implemented using FBGs. The benefits of the usage of FBG-based techniques in OCDMA are the all-fibre encoding and decoding, greater efficiency and the ability to allow reconfigurable systems using tuneable devices. It is a well-known method to employ FBGs for WH/TS optical code encoding and decoding in OCDMA systems by

spreading multiple wavelengths across a bit period, storing them in time chips at the transmitter end, and finally reciprocally de-spreading them to create an autocorrelation peak at the reception end [40]. There are two categories of fibre gratings: those that couple co-propagating waves (usually working in transmission mode and referred to as long-period gratings) or those that couple counter-propagating waves (often operating in reflection mode) [59].

Consider FBG written into an optical fibre with the Bragg condition given by equation 2.2.

$$\lambda = 2n_{eff}\Lambda \quad (2.2)$$

where λ is the wavelength of the incident light, n_{eff} is the effective refractive index of the propagating mode, and Λ is the grating period. If the wavelength of the incident light satisfies this condition, the input light will be reflected by the refractive index perturbation [52] and the reflected waves will add coherently. Otherwise, it will cancel out with each reflection and go out of phase over time. This means that coherent reflection of the incoming light happens when the Bragg condition is met (otherwise it is mostly transmitted). Utilising strain, it is possible to tune the FBG centre wavelength to some extent.

Implementations of FBGs for WH/TS code generation are based on two structures: the linear array of FBGs or chirped Moiré gratings (CMGs) [60] [58] [61] [62].

The utilisation of a single passive grating structure to accomplish WH/TS encoding/decoding is made possible by CMGs structures, which are made up of superposed linearly chirped FBGs [63]. The number of codes that can be used, however, is constrained by the linear relationship between wavelengths and time as well as the intrinsic coupling between the wavelength-hopping and time-spreading patterns in CMGs. The function of wavelength filtering is integrated with appropriate time delays in a single fibre device, making FBG, considering its low cost, a very promising approach to miniaturisation and complexity [64]. A schematic of an FBG-based WH/TS encoder is shown in Fig 2.7. Here an optical pulse from the broadband source such as a supercontinuum (SC) source is sent to four consecutive Bragg gratings written into optical fibre via an optical circulator (OC) to generate a 2D-WH/TS OCDMA code.

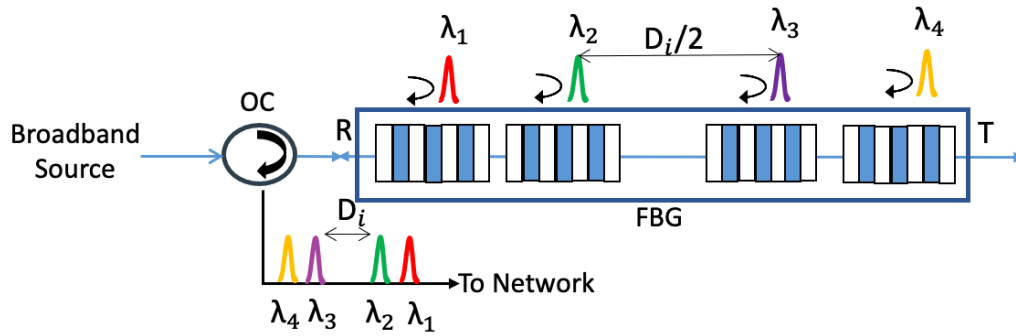


Figure 2. 7. Schematic of a WHTS encoder utilising FBG, where OC is optical circulator; D_i is delays.

2.6.4. Holographic Bragg Reflector

Recently, a new platform for an integration technology was created using the volume holography principle. Holography is a technique that uses coherent light (laser light) to record the phase and amplitude characteristics of a three-dimensional (3D) object on a 2D photographic plate [45]. The end product is a hologram, which is an opaque representation of intricate whorls and stripes on the plate. In order to interact with certain signal beams and provide signal routine and wave-front transformations with strong spectral control, practically flawless 2D volume holograms can therefore be built. A subset of these volume holograms is represented by photonic crystals [65]. Utilising silica as the substrate, the technique has been demonstrated for use in coarse and dense WDM systems as well as for spectrum comparison [66]. The HBR [26] [67] serves as the fundamental building piece of the platform. An HBR applies a specific spectral filtering function while imaging the signal from an input to an output port. Like TFFs and FBGs, it offers good channel-specific pass-band control, and the spatial separation of the input and output ports eliminates the need for large circulators or lossy power splitters. The fact that HBRs can simultaneously provide spectrum slicing and temporal delay suggests that HBR-based WH/TS encoders/decoders can have very tiny physical footprints. Multiple HBRs can be superimposed, interleaved, or overlaid to design multiport devices [68].

Chapter 3

Optical Fibre Impairments on Transmission

3.1 Introduction

At larger information rates, extending the range of optical transmissions becomes a significant difficulty. The quality of the optical signal throughout the propagation path will generally be reduced by transmission impairments, which will also degrade optical transmission. Linear and nonlinear impairments are two types of physical or transmission issues that affect optical communications [69] [70] [71]. In the context of fibre optics, the phrases linear and nonlinear refer to intensity independent and dependent phenomena, respectively. When the impairment of an optical element is linear and independent of the optical strength of the signals it transmits, the impairment is said to be caused by the optical element. Contrarily, nonlinear flaws are dependent on the optical power of the signals being transmitted, and as a result, the degree of degradation is greatly influenced by the strength of the optical signals [69] [70] [71]. Nonlinear impairments are dynamic in nature, whereas linear impairments are static.

Attenuation, chromatic dispersion (CD), polarisation mode dispersion (PMD), insertion loss (IL), and others are some significant linear impairments. The main nonlinear impairments are stimulated Raman scattering (SRS), stimulated Brillouin scattering (SBS), and nonlinear crosstalk [69] [72], which is caused by the Kerr effect and includes four-wave mixing (FWM), self-phase modulation (SPM) and cross-phase modulation (XPM). While attenuation primarily impacts the optical signal-to-noise ratio (OSNR), polarisation mode dispersion (PMD) and chromatic dispersion among these impairments generate temporal dispersion [70]. In actual use, optical fibre amplifiers such as an EDFA can typically compensate for the OSNR-affecting deficiencies [69]. The summary of transmission impairments based on linear and nonlinear effects is shown in Figure 3.1 [69].

Modal, chromatic, and polarisation mode dispersion are the three types of dispersion. Further, material and waveguide dispersion are the two components that make up chromatic

dispersion [73]. Intra-modal dispersion refers to the combined effect of material and waveguide dispersions for a single mode. Modal dispersion, also known as inter-mode dispersion, is brought on by differences in propagation constants between various modes [74].

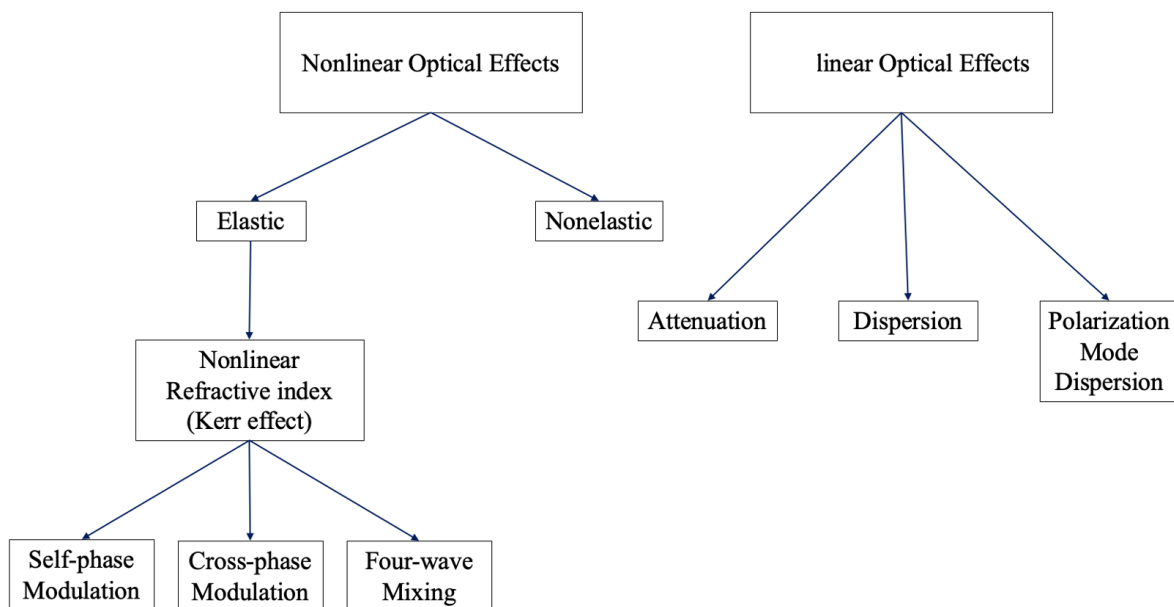


Figure 3. 1. Transmission impairments categories

When there are numerous modes of the same signal, multimode optical fibre exhibits modal dispersion. Pulse broadening results from the propagation of pulses along the optical fibre at various speeds. However, because there is only one fundamental mode propagating in a single-mode fibre, modal dispersion typically does not happen [42] [72]. Even if chromatic dispersion no longer exists, modal dispersion still does [74]. Contrarily, even if a multimode optical fibre has just a single mode excited, only intramodal chromatic dispersion needs to be taken into account [74].

Imperfections in the cross-sectional circularity of optical fibres are what lead to PMD. PMD may be caused by abnormalities, heating, or external pressures acting on the fibre. The dispersion caused by PMD does not depend on wavelength like chromatic dispersion does. Additionally, PMD has a smaller magnitude than chromatic dispersion [70]. In terms of linear impairments, chromatic dispersion is regarded as one of the most detrimental effects on system performance [69] [70].

Chromatic dispersion and self-phase modulation are two optical fibre impairments that will be discussed in greater detail in this chapter because they are pertinent to the chapters that follow.

3.2 Chromatic dispersion in a single mode fibre

The aperture, core diameter, wavelength, refractive index profile, laser linewidth parameters, etc. all contribute to the optical pulse broadening as a pulse of light travels through a fibre optic cable [75]. One of the primary limitations on the performance of optical fibre systems is this well-known issue. The operation of optical fibres is tailored to a specific wavelength. The spreading of the optical pulse is a result of the longer wavelengths travelling down the fibre more quickly than those with shorter wavelengths.

The intermodal dispersion in multimode fibres causes short optical pulses (10 ns/km) to be significantly broadened. In comparison to single mode, the signal is significantly worsened by dispersion in multimode optical fibres. For long-distance communication, single mode optical fibre is used as a result [42], although dispersion also affects optical pulses in single-mode optical fibre.

It has to do with the various mode indices (or group velocities) connected to various modes in the modal description. Because the energy of the injected pulse is only transmitted via a single mode, intermodal dispersion does not exist, which is the fundamental benefit of single mode fibres. However, pulse enlargement does not completely disappear. Due to chromatic dispersion, the group velocity connected to the fundamental mode depends on frequency. GVD, intramodal dispersion, or simply fibre dispersion is the phenomenon when various spectral components of the pulse move at marginally different group velocities. After travelling a distance through the fibre, this will cause the optical pulse to expand as illustrated in Figure 3.2.

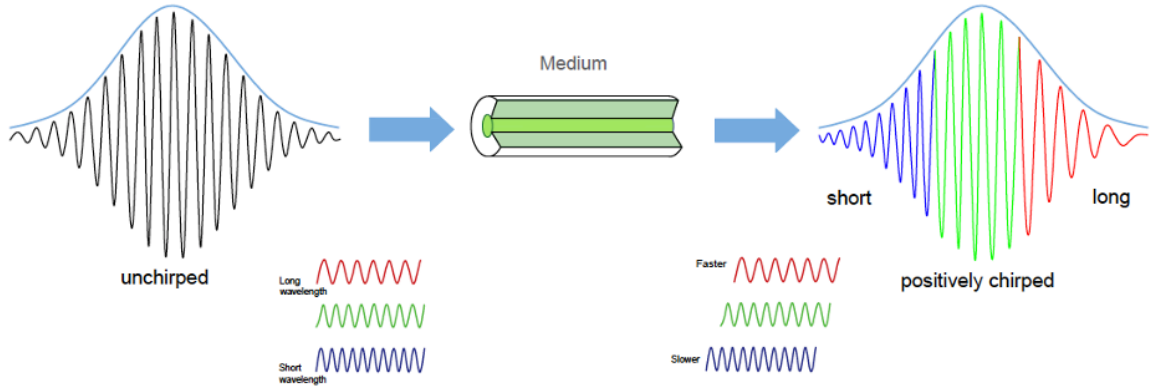


Figure 3. 2. Illustration of refractive index depending on the wavelength induces the group velocity dispersion.

Material dispersion and waveguide dispersion are the two sources of group velocity dispersion. We take into account both of these and go through how GVD reduces the effectiveness of systems using single-mode fibres [42].

To characterise chromatic dispersion, one normally specifies the size of the effect per distance [76]. One can express the dispersion parameter as follows by including the two dispersions of material and waveguide:

$$D = \frac{1}{L} \frac{d\tau}{d\lambda} \quad (3.1)$$

where the total of two terms D can be written

$$D = D_m + D_w \quad (3.2)$$

Units of ps/(nm km) are frequently used since the dispersion parameter D represents the propagation time difference per distance and per wavelength difference.

Material dispersion, denoted by D_m' , is a wavelength-dependent contribution resulting from the index's dependence on the wavelength, and is a phenomenon present in all bulk glasses, not just fibers. The material itself is independent of geometry, but when it comes to waveguides, dispersion (D_w) is influenced by the specific optical fiber geometry. The core and cladding indices in fibers differ slightly [72]. When the wavelength changes, there is a

transition from predominantly core index to predominantly cladding index. As a result, the effective index exhibits a wavelength dependence [72].

3.2.1 Material dispersion

Consider a plane monochromatic wave with wave number ω and angular frequency β . One starts from a series expansion of the propagation constant β where $\beta(\omega)$ can be expanded using Taylor series at the central frequency of ω_0 as:

$$\beta(\omega) = n(\omega) \frac{\omega}{c} = \beta_0 + \beta_1(\omega - \omega_0) + \frac{1}{2}\beta_2(\omega - \omega_0)^2 + \dots \quad (3.3)$$

With

$$\beta_m = \left. \frac{d^m \beta}{d\omega^m} \right|_{\omega=\omega_0} \quad (3.4)$$

Let us evaluate what β_m here means.

$$\beta_0 = \beta(\omega = \omega_0) = kn \quad (3.5)$$

Where n is the normal phase index

$$\begin{aligned} \beta_1 &= \left. \frac{d\beta}{d\omega} \right|_{\omega=\omega_0} \\ &= \left. \frac{d}{d\omega} \left(n(\omega) \frac{\omega}{c} \right) \right|_{\omega=\omega_0} \end{aligned} \quad (3.6)$$

$$= \frac{1}{c} \left(n(\omega_0) + \omega \left. \frac{dn(\omega)}{d\omega} \right|_{\omega=\omega_0} \right) \quad (3.7)$$

When $\omega = 2\pi c/\lambda$ is inserted here it becomes

$$\beta_1 = \frac{1}{c} \left(n(\lambda_0) - \lambda \left. \frac{dn(\lambda)}{d\lambda} \right|_{\lambda=\lambda_0} \right) \quad (3.8)$$

The group index, n_{gr} , is written in the bracketed expression.

$$n_{gr} = n - \lambda \frac{dn}{d\lambda} \quad (3.9)$$

The equation for β_1 has the following form:

$$\beta_1 L = \frac{L}{c} n_{gr} = \tau \quad (3.10)$$

And we obtain β_2 as

$$\beta_2 = \frac{d\beta_1}{d\omega} = \frac{1}{c} \left(2 \frac{dn}{d\omega} + \omega \frac{d^2 n}{d\omega^2} \right) \quad (3.11)$$

Group velocity dispersion parameter [42] [76], or GVD parameter, is the name of this quantity and it is frequently expressed in units of ps^2/km . The dispersion coefficient D , which is frequently utilised by technicians, is not preferred by theorists as much as the GVD parameter is. The conversion is performed through

$$D_m = \frac{d\beta_1}{d\lambda} = \frac{d\beta_1}{d\omega} \frac{d\omega}{d\lambda} = \beta_2 \frac{d}{d\lambda} \left(\frac{2\pi c}{\lambda} \right) \quad (3.12)$$

So that,

$$D_m = -\beta_2 \left(\frac{2\pi c}{\lambda^2} \right) = -\frac{\omega}{\lambda} \beta_2 \quad (3.13)$$

3.2.2 Waveguide dispersion

In fibres, there is waveguide dispersion D_w in addition to material dispersion D_m . For step index fibres, we indicate that the result can be computed from [76] [77] without providing an explicit derivation.

$$D_w = -\frac{Vn_K\Delta}{\lambda c} \frac{d^2}{dV^2}(Vb) \quad (3.14)$$

Where V is the normalized frequency, also known as the V-number, which is a dimensionless parameter that characterizes mode propagation in the optical fiber. n_K is the effective refractive index of the guided mode in the optical fiber. Δ is the relative index difference between the core and cladding in the optical fiber, which is given by $(\Delta n / n_1)$, where n_1 is the refractive index of the core. λc is the wavelength of light in the optical fiber, typically expressed in nanometers. $\frac{d^2}{dV^2}(Vb)$ represents the second derivative of the normalized mode field distribution with respect to the normalized frequency V , evaluated at the V-number corresponding to the desired wavelength, Vb .

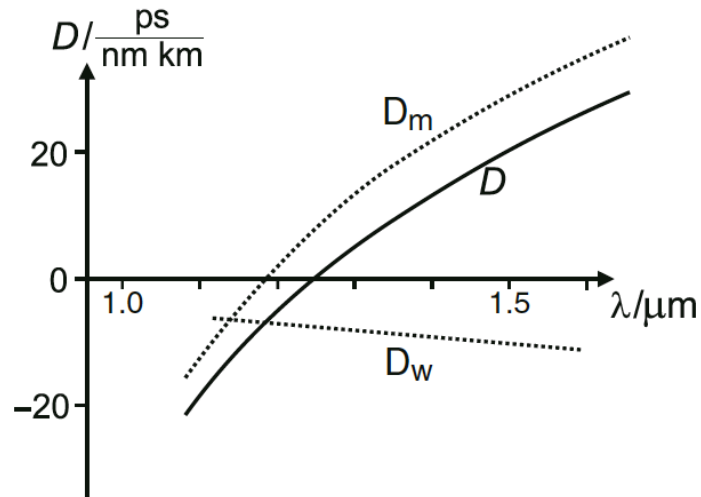


Figure 3. 3. Illustration of combination of D_w and D_m resulting in total dispersion D .

As shown in Figure 3.3., the total dispersion D results from the material contribution of the core D_m and the waveguide contribution D_w .

3.2.3 Zero, Normal and Anomalous Dispersion

The refractive index for fused silica as determined by Sellmeier's equation is shown in Figure 3.4. we can note the following things:

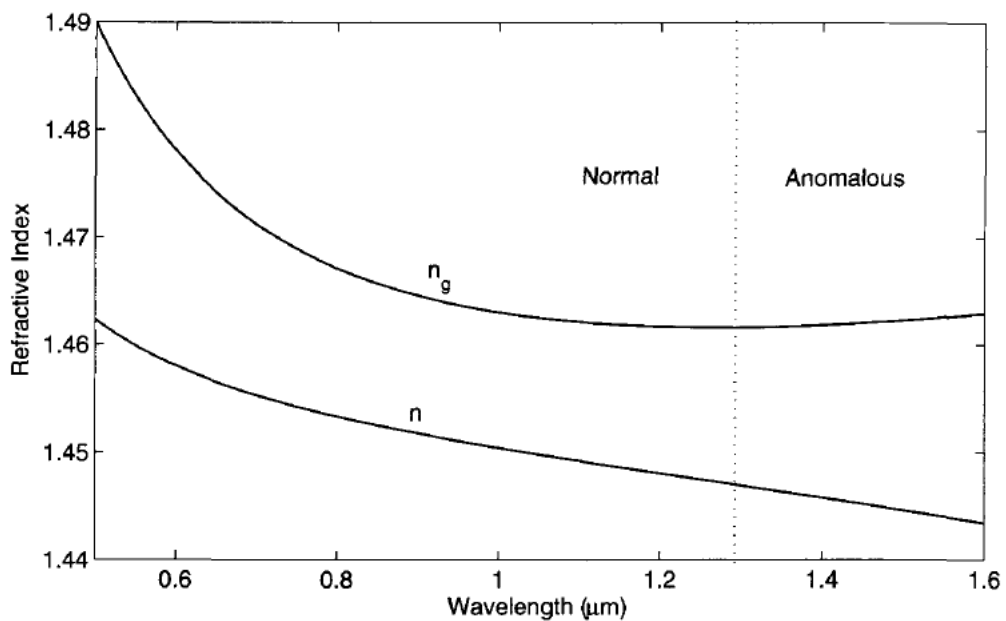


Figure 3. 4.Refractive index and group index as a function of wavelength, calculated from a three term Sellmeier's equation.

First, $dn/d\lambda < 0$ in the visible and near infrared light, from which it is inferred that $n_{gr} = n - \lambda(dn/d\lambda) > n$, implying that the group index is larger than the phase index. The group index n_{gr} is almost constant in the near infrared region, hovering about $n_{gr} = 1.46$. The point of inflexion for the refractive index, $n(\lambda)$, is at $\lambda \approx 1.27\mu m$. The wavelength at which there is no dispersion is said to have zero group delay at this point, when $D_m = \beta_2 = 0$ and group delay is small [42] [76]. This phrase is technically erroneous because only the first order in the series expansion of the dispersion vanishes in this situation, even though higher-order terms all nevertheless make a contribution. Hereafter, in this thesis, this specific wavelength will be referred to as λ_0 .

The parameter $D = (\lambda/c)(d^2n/d\lambda^2)$ is negative for $\lambda < \lambda_0$ and in the visible light, in particular, when $d^2n/d\lambda^2$ is positive, while D is positive for $\lambda > \lambda_0$. The pattern found there was historically thought to be "normal" because the visible range was examined first. Then, "normal dispersion" is the case where $D < 0$. As depicted in Figure 3.5, the opposite scenario, where $D > 0$, is referred to as "anomalous dispersion". If the fibre is employed in the second window, close to $1.3\mu m$, there is a minimum of dispersion ($D \approx 0$), but there is anomalous dispersion in the third window, close to $1.5\mu m$.

It is worth reiterating that the group velocity dispersion is the only type of dispersion that is being discussed in this thesis. Similar nomenclature is employed for the refractive index dispersion in that both "normal" and "anomalous" dispersion exist there. The term "normal" refers to the scenario in which the index declines toward longer wavelengths, which is the norm for the majority of transparent range of the material. Only the reverse, known as anomalous dispersion, occurs at atomic resonance frequencies of the index.

In the visible and near infrared light, the waveguide contributes negatively to the overall dispersion, with $17\text{ ps}/(\text{nm km})$ being a typical number for ordinary fibres. It behaves in opposition to the material dispersion at long wavelengths [76]. As a result, the zero-dispersion wavelength in standard fibres is somewhat skewed toward longer wavelengths when compared to bulk fused silica, typically by about 20–30 nm. Next, we will consider the second important effect, self-phase modulation.

3.3 SOA induced Self-Phase Modulation

Different names for the same kind of device are used in the literature, including Semiconductor Optical Amplifier (SOA), Laser Diode Amplifier (LDA), Semiconductor Laser Amplifier (SLA), Travelling Wave Amplifier (TWA), and Fabry-Perot Amplifier (FPA). Moreover, a semiconductor laser without (or with only very little) optical facet feedback and a SOA are very similar. The SOA amplifies an input signal by stimulating emission as it travels along its optical waveguide. By electrically pumping the carrier population in the active zone, the optical gain is produced. A semiconductor pn double heterojunction, which provides carrier confinement and optical guiding, is the foundation of all the many SOA structures that are currently accessible [78]. The SOA can be deployed in two regions based on the applications (linear or non-linear). When SOA is used for the purpose of amplifying the signal then SOA must operate in the linear region. This region provides stability of SOA output gain to -3 dB on maximum level of amplification [42]. In the nonlinear region, SOA gain level is sacrificed for enabling patterns such SPM, XPM and FWM. In practical, nonlinear region begins from -3dB of the maximum level of amplification.

Self-phase modulation is one of the primary nonlinear phenomena that result in the spectral broadening of an optical pulse. Gain saturation, which causes an intensity-dependent shift in the refractive index in response to changes in carrier density, was discovered to be the fundamental mechanism underlying SPM in SOAs. The nonlinear reaction time of a SOA is dependent on its carrier life time (τ_{eff}) [9] which determines how quickly the SOA gain recovers and is often longer than 0.1 ns [10], whereas the Kerr-based nonlinear response of an optical fibre is almost instantaneous [8]. This is due to the fact that the pulse width is only a minor portion of the τ_{eff} gain-recovery time. As the leading edge of the pulse saturates the SOA gain, the nonlinear phase increases quickly, and the mode index rises as the carrier density falls. The nonlinear phase saturates with just a minor drop in the trailing part of the pulse because the gain cannot recover significantly over the pulse duration. To shorten the gain recovery time of the SOA, this thesis will also take into account the amplified spontaneous emission (ASE) in the saturation region.

The frequency chirp imposed by the SPM on an amplifying pulse will change depending on how the chirp profiles of an optical pulse change as it passes through an SOA. It has a slight blue chirp imposed on its trailing edge but a red shift over its leading edge [79]

This (chirp) shift in phase $\Delta\varphi$ at the SOA output is dependent on a variety of variables, including: (1) confinement factor Γ , (2) the net power gain change Δg , (3) the device length L , and (4) the *alpha-factor* α of SOA. This can be expressed mathematically as follows [80]:

$$\Delta\varphi(N) = \alpha\Gamma\Delta gL/2 \quad (3.15)$$

A high confinement factor Γ and α values of 2–8 are seen for bulk or QW structures. Whenever an optical signal is injected into a medium or an electrical bias is applied to a diode, the *alpha-factor* links the "change in refractive index" with the "change in gain." The *alpha-factor* connects the two values with a straightforward constant, whereas the refractive index and the material gain, or absorption are related via the more complicated Kramers-Kronig (KK) integral formula [81]. The relationship between the change in gain and the change in refractive index with regard to a change in carrier density N is used to create the formula for the *alpha-factor* in an SOA [82].

$$\alpha = \frac{-4\pi}{\lambda} \frac{\partial n_r / \partial N}{\partial g / \partial N} \approx -\frac{4\pi}{\lambda} \frac{\Delta n_r}{\Delta g} \quad (3.16)$$

Here, Δn_r is the change of the real part of effective refractive index n , Δg is the change of the modal gain g in the medium of the SOA, and λ is the wavelength in vacuum. In the sections that follow, a more detailed explanation of the causes of optical pulse chirp and the related chirp parameter will be covered.

3.3.1 Chirp parameter in optical fibre communication

When the frequency of a signal changes over time, it is said to be chirping. The time dependency of the instantaneous frequency of the pulse allows the identification of the presence of chirp in an optical pulse. When an optical pulse is unchirped and is travelling through a single mode fibre, the medium of the fibre will cause the pulse to chirp based on the kind of medium, as seen in Figure 3.5.

An optical pulse that has been chirped experiences a change in carrier frequency over time, and this "frequency change" is connected to the phase derivative. The linear frequency chirp that is applied to an optical pulse is controlled by the parameter C . The frequency chirp that is applied

to an optical pulse greatly broadens its spectrum. The performance of a fibre optic communication system may be constrained by frequency chirp. It depends on whether the immediate frequency of the optical pulse is rising or falling with time [83]. The GVD parameter β_2 and the chirp are both positive in the region of normal dispersion. In this situation, the speed of the higher frequency components is slower than the speed of the lower frequency components near the leading edge of the pulse. On the other hand, the GVD parameter β_2 and the chirp, $C < 0$, are both negative in the region of anomalous dispersion. The higher frequency components' speed towards the pulse's leading edge is faster than the lower frequency components' speed at the trailing edge.

A Ti:LiNbO₃ based optical modulator was used in [84] to assess the fibre CD penalty as a function of the modulation chirp value for a high bit-rate transmission system. Dispersion-related impairments were reduced for the specified transmission lines by properly optimising or adjusting the frequency chirp. Additionally, it was noted that a positive value of the chirp C resulted in an increased dispersion penalty. On the other hand, C could limit the pulse broadening, leading to lower dispersion penalties, with regulated implementations of negative chirp [84]. Chirp C can have an impact on an optical pulse with a temporal Gaussian form and can be characterised as [78]:

$$P_I(t) = P_0 \exp \left[-2.77(1 + iC) \left(\frac{t}{\tau} \right)^2 \right] \quad (3.17)$$

Where P_0 is the maximum amplitude and the half-width at the 1/e intensity point is represented by the parameter τ . The relation relates it to the full-width at half-maximum (FWHM) of the pulse.

$$T_{FWHM} = 2(\ln 2)^{1/2} T_0 \approx 1.665 T_0 \quad (3.18)$$

The frequency chirp applied to the pulse is controlled by the parameter C . If the carrier frequency of a pulse varies over time, that pulse is said to be chirped. The phase derivative and frequency change are connected, and they are represented by:

$$\delta\omega(t) = -\frac{\partial\phi}{\partial t} - \frac{C}{T_0^2} t \quad (3.19)$$

The Fourier domain makes it simple to express the pulse as

$$P_L(f) = \text{ifft}\{P_L(t)\} \times \{\exp(-j\omega^2 \times \beta_2/2) \times L\} \quad (3.20)$$

Where β_2 is the group velocity dispersion parameter for the fibre connection in ps^2/km , ω is an angular frequency, and $\{\exp(-j\omega^2 \times \frac{\beta_2}{2}) \times L\}$ takes into account the GVD effects brought on by fibre propagation.

3.3.2 The Effect of Self-Phase Modulation on Group Velocity Dispersion

The dispersion length L_D and nonlinear length L_{NL} are key to understand the trade-off between GVD and SPM in fibres, as demonstrated by the two formulas

$$L_D = \frac{T_0^2}{|\beta_2|}, \quad L_{NL} = \frac{1}{\gamma P_0} \quad (3.21)$$

The propagation will be dominated by GVD if the dispersion length is significantly less than the nonlinear length, $L_D \ll L_{NL}$, in which case dispersion happens on a length scale considerably shorter than that of SPM. In this case, SPM can be roughly neglected. This circumstance, also referred to as the group velocity limited (GVD) regime, occurs most frequently in optical communication. The low power of the optical pulse and pulse width are also taken into account in this section. On the other hand, if the nonlinear length is significantly less than the dispersion length, $L_{NL} \ll L_D$, then SPM happens on a much lower propagation length scale than GVD, and we may dismiss GVD to an approximation because the propagation will be dominated by SPM [85]. On the other hand, temporal optical solitons are said to exist when the dispersion and nonlinear lengths are comparable and must maintain equality between GVD and SPM. Soliton transmission makes use of this characteristic of the interaction of SPM with anomalous dispersion. The pulse width decreases as a result of the "red" frequencies in the rising edge of the pulse being delayed and the "blue" frequencies in the falling edge being accelerated. The pulse begins to widen again as the blue frequencies overtake and catch up to the red ones. Figure 3.5 summarises the interaction of SPM with fibre dispersion.

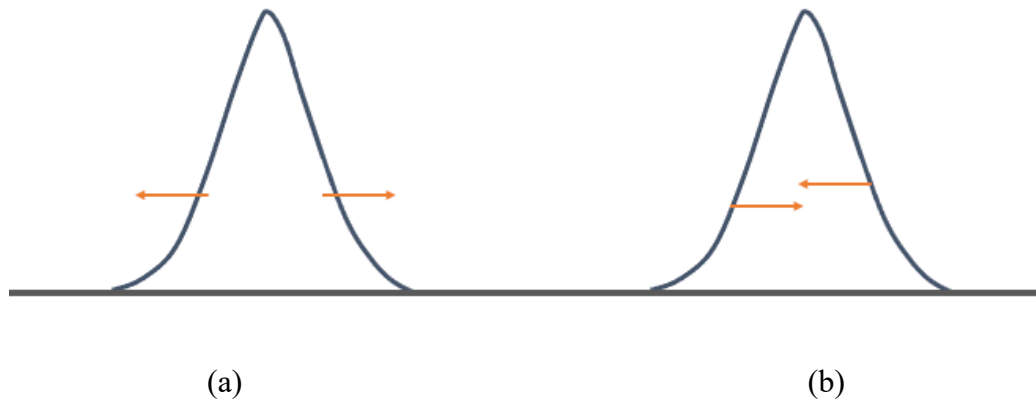


Figure 3. 5. SPM followed by negative and positive dispersion where in (a) $D < 0$, additional pulse broadening, (b) $D > 0$, pulse compression.

3.4 Chromatic Dispersion Compensation Techniques

The temporal breadth of the pulse will eventually depend on the outcome of chromatic dispersion in optical fibre, whether it is positive or negative. In optical communications systems based on picosecond pulses, dispersion management is crucial, because if the dispersion is too large, a group of pulses representing an OCDMA bit can spread in time and merge/overlap, making the bit-stream incomprehensible. This restricts the amount of time a signal can be transmitted before requiring regeneration.

Sending a signal at a wavelength where chromatic dispersion is zero (for example, approximately 1.3 mm in silica fibres) could be one method to reduce the amount of spreading caused by dispersion in pulses. Zero chromatic dispersion accidentally provides circumstances for other nonlinear effects like four-wave mixing, which in reality leads to more issues than it resolves [86].

In spectrally encoded OCDMA systems, dispersion correction techniques [87] [88], and [89] have been developed. Techniques that employ compensating elements, such as dispersion compensating fibre (DCF) [90], optical phase conjugation (OPC) [91], or chirped fibre grating (CFG) [57], can be used to compensate for chromatic dispersion. The idea of compensating for chromatic dispersion is shown schematically in Figure 3.6.

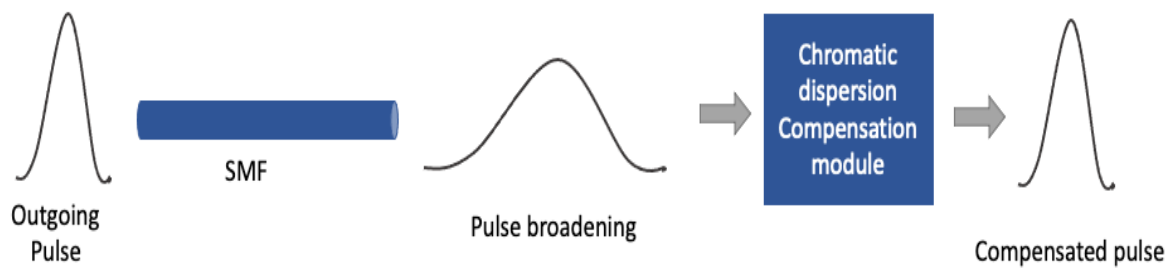


Figure 3. 6. Illustration of chromatic dispersion compensator rule.

It is noteworthy to point out the significance of dispersion control in EDFAs and short pulse lasers. The length of the laser pulses is mostly influenced by the total dispersion of the optical resonator. The net negative dispersion created by a pair of prisms can be used to counteract the laser gain medium's typically positive dispersion. Dispersive effects can also be created by diffraction gratings, which are frequently utilised in high-power laser systems. Recently, chirped mirrors have been created as an alternative to prisms and gratings. Various wavelengths have varied penetration lengths, and hence different group delays, due to the coating on these dielectric mirrors. A net negative dispersion can be achieved by adjusting the coating layers.

3.4.1 Chromatic Dispersion Compensating Technique based on Optical Fibre

Fibre-based chromatic dispersion is naturally reliable and offers certain benefits technically by keeping unwanted nonlinear effects, such as SPM and FWM, under control. Utilising unique tools is another way to get rid of chromatic dispersion [92]. Dispersion correcting modules (DCM) are frequently employed in fibre optic transmission systems to compensate for chromatic dispersion. A predetermined amount of compensating dispersion value is offered by these modules. Between two fibre amplifiers (EDFA), DCM is frequently positioned [42] [93]. Chromatic DCM can make use of dispersion compensating fibre (DCF), fibre Bragg grating (FBG), and optical phase conjugation (OPC). Standard SMF length (in km) or the total adjusted value of dispersion (given in ps/nm) [93] are the usual ways to specify the DCM length. For several kinds of nonzero dispersion shift fibres (NZDSF) and SMF that can be utilised for dispersion compensation, Table 3.1 displays typical dispersion and slope values.

Typically, DCM including DCF has large insertion and attenuation losses in the fibre. Optical amplification can be used to make up for this loss [94]. Due to nonlinear optical effects (NOE), DCF may face some optical signal distortions because its effective core area A_{eff} is substantially lower than the typical ITU-T G.652 SMF [93]. An efficient core section of a typical DCF is $A_{eff} = 12 \mu m^2$ whereas A_{eff} is present in the standard SMF. = $80 \mu m^2$. Compared to normal SMF, DCF has an attenuation coefficient of $\alpha = 0.6$ dB/km as opposed to $\alpha = 0.2$ dB/km. In fibres with lower values for A_{eff} the nonlinear effects are more pronounced, while lowering optical power can reduce the influence of nonlinear optical phenomena [73].

Table 3. 1. Typical dispersion and slope values in various types of fibres [95].

Type of Fibre		Typical slope at 1550nm (ps/nm ² .km)	C-Band dispersion range (1530 to 1565nm) (ps/nm.km)	L-Band dispersion range (1570 to 1620nm) (ps/nm.km)
Conventional SMF-28		0.057	15.9–17.8	18.1–21.0
NZDSF (early)	Type-1	0.067	1.3–8.6	3.9–7.3
	Type-2	0.067	2.2–4.6	4.8–8.2
NZDSF (large effective area)		0.1	1.8–5.3	5.8–10.8
NZDSF (reduced slope)		0.045	3.5–5.1	5.3–7.5
NZDSF (new large eff. Area)		0.085	2.6–5.5	5.9–10.1
NZDSF (new light fibre)		0.057	6.8–8.9	9.1–12.0

Negative dispersion of a DCF, with $D = -80$ ps/(nm.km), is present and it should be mentioned that DCF increases polarisation mode dispersion (PMD), with a typical value of 0.1

ps/ \sqrt{km} [93]. The origin of PMD is a result of the pulse broadening that occurs when distinct frequency components of pulses with various polarisation states propagate at various speeds. For high-speed optical communication systems, PMD becomes a major limiting factor [42].

It is also possible to use DCM with chirped FBG to compensate for chromatic dispersion. It has a grating period that is not constant but changes linearly across the length of the grating, with the shortest grating period found at the beginning [93]. However, these periods gradually lengthen as the grating gets longer. Shorter signal wavelengths are reflected more frequently and have less propagation delay via the FBG as a result, but longer signal wavelengths must penetrate the fibre grating deeper before being reflected back, incurring greater propagation delay through the FBG. The length of a fibre grating is typically between 10 and 100 cm [93]. An important benefit of employing an FBG-based chromatic dispersion compensation module over a DCF fibre module is its very short length and relatively low insertion loss.

An FBG-based chromatic dispersion compensation module can compensate the same fibre span length with an insertion loss of only up to 4 dB, in contrast to commercial DCF, which is used to compensate accumulated chromatic dispersion of a 100 to 120 km standard SMF span and has about 10 dB of insertion loss [94]. An FBG-based chromatic dispersion compensation module can be employed at greater optical powers without causing any nonlinear optical effects, in contrast to a DCF-based chromatic dispersion compensation module [42].

In addition to DCF-DCM and FBG-DCM, optical phase conjugation (OPC), which achieves an inversion of the optical signal phase, can also be used to compensate for the accumulated chromatic dispersion. OPC, also known as spectral inversion, is a potential technology that can mitigate the impacts of nonlinear optical phenomena like Kerr nonlinearities (FWM) and SPM and compensate for cumulative chromatic dispersion in long-haul fibre transmission systems [96]. Due to the fact that dispersion builds up linearly throughout fibre optic transmission links, OPC-DCM placement must be perfect in order to receive full dispersion compensation. This is done to make sure that the distortion in the second half of the link, which occurs after the OPC-DCM, cancels out the distortion in the first part of the link, which occurred before the OPC-DCM. OPC-DCM cannot always be positioned precisely in the centre of the fibre transmission link. In order to accomplish complete chromatic dispersion adjustment, an additional DCF module might be used [42] [96]. With parameters that have low dispersion fluctuations, low insertion loss, low nonlinearity, low cost, and good temperature stability, high-quality dispersion compensation modules are available [97].

3.4.2 Tuneable Dispersion Compensation Techniques

When a short length of SMF-28 needs to be added, the standard method, DCF, of dispersion management is not a particularly practical solution, necessitating compensation by matching the length of the DCF fibres. When using ultra-short optical carriers, a high dispersion compensation accuracy (sub-picosecond) is required [98]. The bulkiness of DCF for fine CD tuning in this case is its biggest drawback. Therefore, the requirement for tuneable dispersion correction systems is generally acknowledged. Tuneable dispersion compensators [99] are required in DWDM systems, because the channels at the outermost transmission bands exhibit over- or under-compensation. However, the central channel of the band employs a set CD compensation. When considering reconfigurable networks, the residual CD is always subject to change because of rerouting or for optical add/drop multiplexing. Therefore, the upgrade from a 10 Gb/s link to a 40 Gb/s link requires very fine CD correction as the acceptable dispersion threshold gets smaller.

There are many different types of tuneable dispersion compensators that have been demonstrated, including chirped fibre Bragg gratings (CFBG), adaptive tuneable dispersion control, dispersion equalisation by monitoring extracted-clock power level, virtually imaged phase arrays (VIPA), microelectromechanical systems (MEMS), tuning (thermal) of free space or FBG coupled-cavities Gires-Tournois etalons (GTEs), and others [100] [101] [102]. According to [100], the tuneable chirp and dispersion compensation are obtained using devices such as fibre Bragg gratings with on-fibre integrated heaters. The drawbacks of this method include its suitability for single-channel operation and the need for optical circulators to recover reflected signals. In [102], it was demonstrated that the virtually imaged phase array (VIPA) may be used as a variable dispersion correction approach to reduce the dispersion tolerances in a 40 Gb/s DWDM system. The periodic properties of VIPA-based compensators were found to be advantageous over FBG and PLC devices since just a small number of modules were needed to span the whole C or L band. In [103], the nonlinearly chirped fibre gratings (NC-FBGs) were employed to demonstrate tuneable dispersion compensation for single and multichannel 40 Gb/s systems. Wide tuning ranges, little intra-channel third-order dispersion, and obtaining both positive and negative dispersion values are benefits of the technique. The equalisation was appropriate for both positive and negative values of dispersion by adjusting the phase-shift differences of the interferometric arms in [104], which used a planar light-wave circuit (PLC) based dispersion equaliser made of a number of asymmetric Mach-Zehnder interferometers in cascade. A tuneable dispersion compensator was used to achieve dispersion

compensation in [101] using an adaptive tuneable dispersion compensation technique, where an error was first calculated from the time-domain waveform of the output signal. The errors were then minimised using the steepest-descent method. A tuneable dispersion compensator based on a virtually imaged phased-array (VIPA) and spatial light modulator (SLM) was demonstrated in [105].

Chapter 4

Ambient Temperature Fluctuations

Effect on 2D-WH/TS OCDMA Code Integrity

4.1 Introduction

In recent years, there has been a steady rise in traffic demand. The optical links between the major cities, which are typically terrestrial lines of hundreds of kilometres operating at 10 Gbit/s per channel, must be upgraded in order to meet this growing traffic demand. Increasing the amount of data transmitted over each channel to 40, 80, or even 160 Gbit/s is one possible answer to the problem of upgrading these links. It is not unexpected that the principal operators aim to support these high-speed systems by leveraging the cables that have already been laid. Typically, the most cost-effective strategy will involve upgrading terminal equipment while using the same previously installed links. On the other hand, the bulk of cables currently in use are made with G.652 fibres. Within the average spectral window, these fibres exhibit a significant amount of chromatic dispersion. In this particular window, the optical gain is adjoined by erbium-doped fibre amplifiers. High data rate systems must integrate dispersion compensation techniques since this is the only method to overcome the severe limitations imposed by chromatic dispersion [106]. Diverse technologies and strategies have been developed in an effort to meet the demand for precise compensation of chromatic dispersion. Using dispersion-compensating fibre (DCF) modules is one of the most prevalent and effective solutions for dispersion management. However, because of the imperfect nature manufacturing process, the value of chromatic dispersion varies from transmission fibre to another. It is important to stress on the fact that the temperature of the environment surrounding an optical fibre highly affects its chromatic dispersion. As a result, employing simply DCF modules

would make it incredibly difficult to meet the demanding dispersion requirements of such high-speed signals [107].

The optical fiber lines are buried at a depth of roughly 1.5 meters under the ground. At this depth, seasonal temperature variations of approximately 20 degrees Celsius are discernible. It has been determined that SMF-28's temperature-induced dispersion (TD) is -0.0015 in ps/nm/km/°C [108] [109]. Comparing this number to SMF-28's CD value of +17 ps / nm / km, it appears to be insignificant.

Nonetheless, considering the fibre CD is fully compensated, this small value of TD can have an impact on OCDMA systems based on multi-wavelength picosecond code carriers.

This fluctuation of the temperature caused by ambient temperature produce instability of behaviour of chromatic dispersion and induced time-skewing among OCDMA code pulses which will then lead to the OCDMA auto-correlation function distortion [14]. This will be explained in more depth during this chapter.

This chapter investigates the temperature induced dispersion coefficient on 2D WH/TS incoherent OCDMA system as a function of different wavelengths. The contributions in this chapter are extracted from two papers I co-authored [110] and [111]. A thorough background and literature review are covered in sections 4.2 and 4.3. The ramification of thermal skewing on OCDMA code carriers is experimentally investigated in section 4.4 accompanied by evaluation of the conventional equation that was predominantly used to predict the impact of the temperature induced dispersion. Additionally, an adjustment is proposed to the equation to make it applicable to a broader spectral range. In section 4.5, a novel straightforward and cost-effective design for precise measurement of the temperature dispersion coefficient is proposed. The results obtained in this chapter are discussed in section 4.6 and then summarized in the Conclusion.

4.2 Temperature Dependence of Chromatic Dispersion in Optical Fiber

The following expression is typically used to represent the total chromatic dispersion, which is determined by the material and waveguide contributions [112].

$$D = \frac{S_o}{4} \left(\lambda - \frac{\lambda_o^4}{\lambda^3} \right) \quad (4.1)$$

where S_0 is the dispersion slope at wavelength λ_0 when dispersion is zero wavelength. When assuming that both S_0 and λ_0 are temperature-dependent, and then compute the temperature-dependent derivative of (4.1), we obtain the following:

$$\frac{dD}{dT} = \frac{1}{4} \left(\lambda - \frac{\lambda_0^4}{\lambda^3} \right) \frac{dS_0}{dT} - \frac{S_0 \lambda_0^3}{\lambda^3} \frac{d\lambda_0}{dT} \quad (4.2)$$

This expression describes the relationship between temperature and chromatic dispersion of the optical fibre over the C and L bands. The two main terms contribute in $\frac{dD}{dT}$ are $\frac{dS_0}{dT}$ and $\frac{d\lambda_0}{dT}$. Even though the former term, $\frac{dS_0}{dT}$, is relatively low, the first term in equation 4.2 is necessary to obtain an accurate value of $\frac{dD}{dT}$. To find out the temperature dependency of dispersion around λ_0 , both λ and λ_0 set to be identical to obtain the following equation.

$$\left. \frac{dD}{dT} \right|_{\lambda=\lambda_0} = -S_0 \frac{d\lambda_0}{dT} \quad (4.3)$$

The equation 4.2 is essential for determining the significance of temperature in optical communication systems. For high-speed systems, however, the slope of the chromatic dispersion around the central wavelength is just as significant as the chromatic dispersion itself. Using equation 4.1, the slope of the chromatic dispersion can be computed by first taking the derivative to obtain the wavelength, which leads in the expression 4.4.

$$\frac{dD}{d\lambda} = \frac{S_0}{4} \left(1 + 3 \frac{\lambda_0^4}{\lambda^4} \right) \quad (4.4)$$

It is possible to get an expression for the variation of the dispersion slope with temperature beginning with equation 4.4 and again assuming that λ_0 and S_0 are functions of temperature. As obtained in equation 4.5.

$$\frac{d}{dT} \frac{dD}{d\lambda} = \frac{S_0}{4} \left(1 + 3 \frac{\lambda_0^4}{\lambda^4} \right) \frac{dS_0}{dT} + 3S_0 \frac{\lambda_0^3}{\lambda^4} \frac{d\lambda_0}{dT} \quad (4.5)$$

To apply formulas 4.2 and 4.5, one must be aware of four values: the zero-dispersion wavelength, the zero-dispersion dispersion slope, and their temperature-dependency. Before going any further, just to demonstrate the accuracy of equation 4.2 in two different wavelengths. I started by evaluating equation 4.2 with wavelength 1550 nm and 1545 with spectral separation of 6.12 nm. All parameter values were obtained from [112]. The temperature dispersion for operation wavelength 1550 nm is:

$$\frac{dD}{dT} = \frac{1}{4} \left(1550 - \frac{1319.15^3}{1550^3} \right) (-0.7 \times 10^{-6}) - \frac{(9.352 \times 10^{-2})(1319.15)^3}{1550^3} \times 0.024$$

$$\frac{dD}{dT} = -0.00152 \text{ ps/nm/km/C}$$

The temperature dispersion for operation wavelength 1545 nm is

$$\frac{dD}{dT} = \frac{1}{4} \left(1545 - \frac{1319.15^3}{1545^3} \right) (-0.7 \times 10^{-6}) - \frac{(9.352 \times 10^{-2})(1319.15)^3}{1545^3} \times 0.024$$

$$\frac{dD}{dT} = -0.00153 \text{ ps/nm/km/C}$$

$\frac{dS_0}{dT}$, $\frac{d\lambda_0}{dT}$ the two terms can be found from [112]. From the equation above the temperature induced dispersion is the same for both wavelengths with fraction of change of 0.00001. Further in this chapter we will find out if this value can be deployed for all C band or require some adjustments.

4.3 The Influence of Temperature Variations on Incoherent 2D-WH/TS OCDMA Codes

A wavelength-time matrix that represents a logical 1 in a bit sequence makes up the 2D-WH/TS codes. The number of wavelengths available defines the number of rows in the matrix (also known as the code weight (w)), while the number of columns in the matrix determines the code length. The formula for establishing the relationship between the bit period (T_b) and the chip width (T_c) is as follows:

$$T_c = \frac{T_b}{N_c} \quad (4.6)$$

Where N_c represents the number of chips (columns) in the code matrix. The design of 2D-WH/TS codes with a variety of code properties, including cardinality and correlation values, is covered in depth in the literature [7] [113]. The study described in this chapter is applicable to any incoherent 2D-WH/TS code without restriction.

The process of decoding the 2D-WH/TS code under ideal circumstances is depicted in figure 4.1a. To achieve the perfect conditions, it must be assumed that the codes has been transmitted across a fully dispersion-compensated link. In addition, it is assumed that any losses caused by the fiber's attenuation have been compensated. Ideal conditions also involve the presumption that even after propagating in a fully dispersion compensated fiber link, the wavelength pulses contained in the code will still be in their time chips and spaced (in time) as originally intended. It is evident that all of the wavelength pulses that were initially spread out in time have completely been dispreads after the code has passed through the decoder. The wavelength pulses' de-spreading has thus resulted in a single autocorrelation peak. The combined power of all the individual wavelength pulses (code weight (w)) that made up the autocorrelation peak, as depicted in the figure, determines the height of the autocorrelation peak.

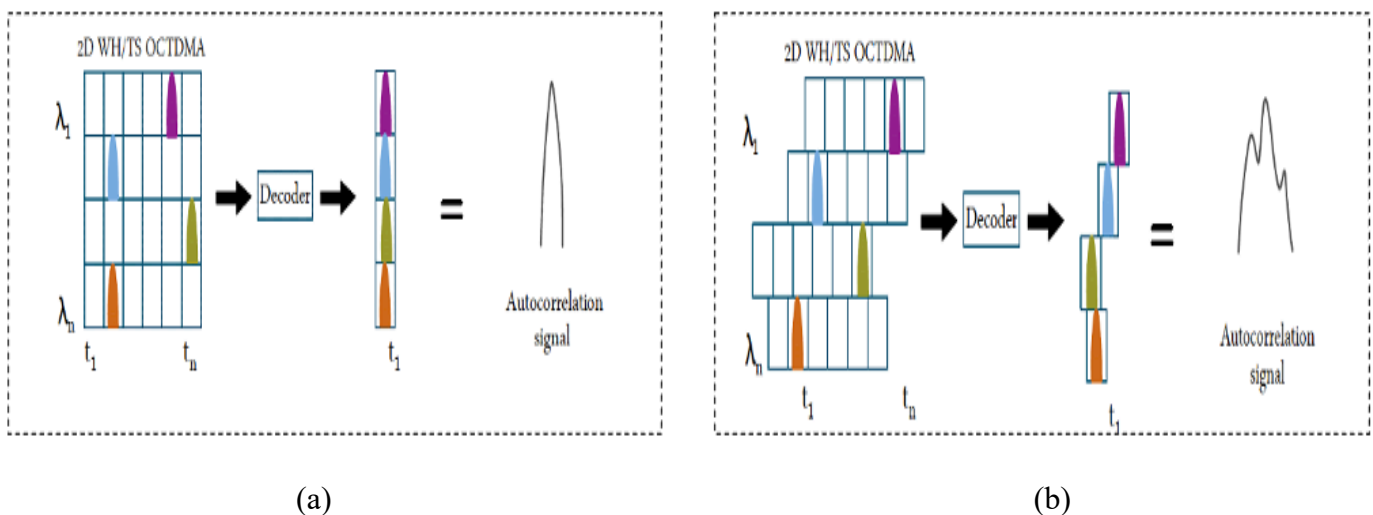


Figure 4. 1. Where (a) The process of decoding a 2D-WH/TS OCDMA code after propagation in ideal conditions across a fully dispersion compensated fibre link resulting in

undistorted autocorrelation function. (b) Illustration of distorted autocorrelation peak due to temporal skewing among code carriers in 2D-WH/TS OCDMA system.

Nevertheless, when the surrounding ambient temperature fluctuates, it alters the thermal coefficient of the fibre. This in turn changes the overall dispersion and results in under compensated link. Overall, all the optical pulses skewed and arrived in different time window. Hence: the OCDMA code will be temporally shifted, and the decoder will output a distorted autocorrelation function (see figure 4.1b for illustration). The effect is proportional to the average of the temperature change (ΔT) and the distance the signal has travelled (L).

The severity of the misalignment of code carriers detected by the photo detector at the receiver is influenced by temperature-induced skewing which govern the thresholding process. An elevated bit error rate will be the result of improper thresholding of the distorted autocorrelation signal [114] [115]. It is feasible to mitigate this effect by employing delay lines that are calibrated to the skewed-chip duration after a predetermined distance; but, doing so will complicate the system, particularly when considering the real-world settings of the temperature changes. It is important to keep in mind that fluctuations in temperature have an effect on both synchronous and non-synchronous OCDMA systems due to the misalignment of the pulses during the decoding process. It is important to quantify the temperature variation effect on autocorrelation peak for each user. Consequently, I will now analyse the influence that varying temperature has on the autocorrelation peak. Considering the pulses which form the incoherent 2DWH/ TS OCDMA code to have a pulse width (τ) equal to or less than the chip width (t_c), $\tau \leq t_c$; the temperature-driven temporal skew (Δt) can be expressed as:

$$\Delta t = D_{temp} * \Delta T * \Delta \lambda * L \quad (4.7)$$

And the pulse shrinking ($\Delta \tau$) as;

$$\Delta \tau = D_{temp} \times \Delta T \times \Delta \lambda \times L \quad (4.8)$$

Where, D is the fibre temperature coefficient in ps/nm/km/°C, ΔT (°C) is the average of thermal changes of the fibre transmission line with length L measured in km, $\Delta \lambda$ is the overall spectral spacing of the 2D-WH/TS OCDMA wavelengths in nm, $\Delta \lambda$ is the linewidth of each wavelength in the code measured in nm. For the purposes of the computations of the autocorrelation peak, all code carriers are algebraically summed to form the envelope of the

autocorrelation function S_t as described in equation 4.9. Considering all wavelengths in the code have Gaussian shape with constant power level among all wavelengths P_p .

$$S_t(L) = \sum_{k=0}^{w-1} P_p e^{\left[-2.77 \left(\frac{t-(k\Delta t)}{\tau-\Delta\tau}\right)^2\right]} \quad (4.9)$$

Where the constant -2.77 reflects its FWHM values and w is a number of wavelength code carriers (also known as a codes weight). P_p is the transmitter power; Dt is the time skewing in picoseconds, and $\Delta\tau$ is the amount of the pulse width change also in picoseconds.

4.3.1 The scalability of the 2D-WH/TS OCDMA coding

When employing multi-wavelength OCDMA code carriers, it is necessary to choose a wavelength spectrum for the OCDMA system. The system's chromatic dispersion management is vulnerable to temperature fluctuations. It is well known that more N_c chips allow for the development of bigger code sets. This rise in code cardinality will result in more concurrent OCDMA users, which will improve scalability [7]. In order to increase the number of chips contained within the 2D-WH/TS OCDMA code, it is necessary, according to equation 4.6 to reduce the chip width T_c if the data rate remains unchanged. In order to accomplish this in a practical manner, the duration of each pulse included in the 2D-WH/TS OCDMA code must be reduced. Therefore, the need of ultra-optical pulses to generate the 2D-WH/TS codes is one of the most crucial requirements to attain a large code set for the OCDMA system.

To ensure effective and dependable data transmission during the practical deployment of these 2D-WH/TS code-based incoherent OCDMA systems, environmental considerations impacting the transmission medium must be taken into account. This will be proven in the section that follows.

4.4 Investigation on Temporal Skewing among OCDMA Code Carriers under Fiber Temperature Variations

4.4.1 Theoretical analysis

To understand the effect of temperature induced fluctuations on the optical pulse position during the transmission, Osadola in [14] has studied temporal skewing D_t of code carriers (see equation (4.7)) in 2D-WH/TS incoherent OCDMA system. From the experimental study [111], which agrees with our results for SMF-28 fiber, time skewing D_t decreases with the increase of the fiber temperature. Equation 4.7 holds for cases when the spectral interval for selecting code wavelength carriers is considered to be small (only a few nm).

In order to be more general, equation 4.7 needs to be modified in the following way:

$$\Delta t_n = D(\lambda_n)_{temp} \times L \times \Delta\lambda \times \Delta T \quad (4.10)$$

where, $n = 1, 2, 3, \dots, w$. Here, w is the code weight [14]. $D(\lambda_n)_{temp}$ is the temperature induced dispersion coefficient in ps/nm·km·°C, L is the fiber length in km. $\Delta\lambda$ is the spectral spacing between adjacent wavelengths code carriers. The temperature induced dispersion can be re-written as:

$$D(\lambda_n)_{temp} = \frac{\Delta t_n}{L \times \Delta\lambda \times \Delta T} \quad (4.11)$$

$\Delta\lambda$ is the spectral spacing between adjacent wavelengths code carriers and defined as:

$$\Delta\lambda = \lambda_{ref} - \lambda_n \quad (4.12)$$

Where, λ_{ref} is the longest wavelength and will be called a reference wavelength. ΔT is the rate of change of fiber temperature is defined as

$$\Delta T = |T_{initial} - T_{final}| \quad (4.13)$$

To find out the values of $D(\lambda_n)_{temp}$ from equation 4.11, an experimental result was obtained. The recovered auto-correlation function for 2D-WH/TS OCDMA affected by the skewing and

dispersion due to the fibre temperature changes can be calculated by equation 4.9. The k factor and Δt_n in equation 4.10 are pictorially described where $k = w-1$. For the illustration, see figure. 4.2. I will explain the use of the factor k in depth in the discussion section.

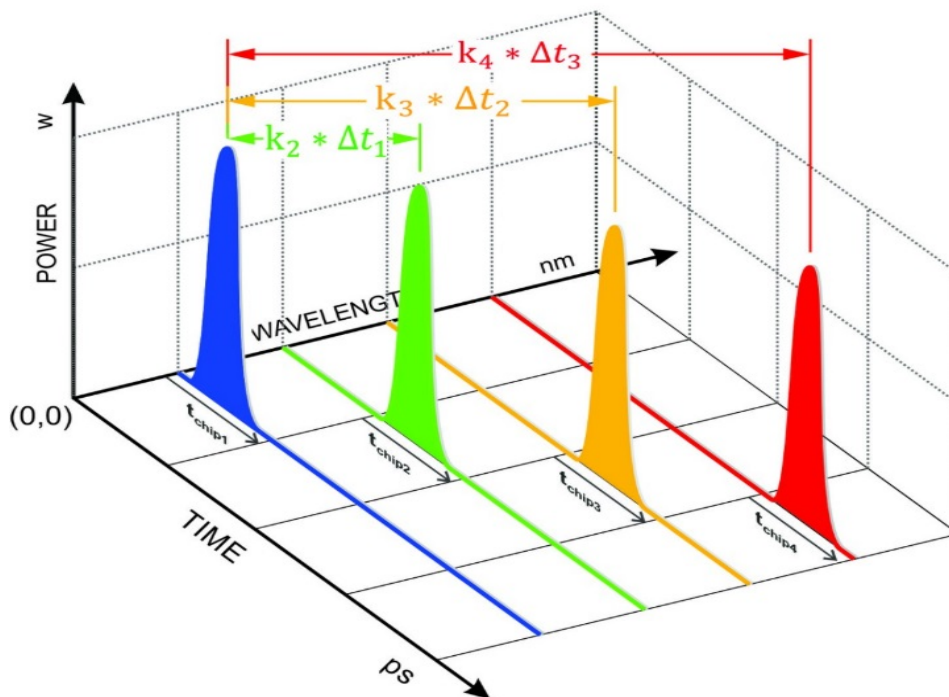


Figure 4. 2. Illustration of the 2D-WH/TS incoherent OCDMA code.

The main goal of this investigation was to examine the accuracy of equation 4.7 and then determine if using constant (i.e., wavelength independent) value of D_{temp} for the temperature induced dispersion coefficient in optical fiber, would be suitable also for a broader range of wavelengths if they are used as the optical code carriers in 2D-WH/TS incoherent OCDMA system. The approach we followed in this work was using three wavelengths ($\lambda_1=1545$ nm, $\lambda_2=1550.12$ nm, $\lambda_{ref}=1551.72$ nm). Wavelength λ_{ref} was used as the reference for calculating relative delays Δt between the individual wavelength pulses' positions.

Initially, the delay was fixed, for $Dt_1 = 27$ ps and for $Dt_2 = 36$ ps respectively. The fiber temperature was $T= 0$ °C. This can be seen in figure. 4.4.

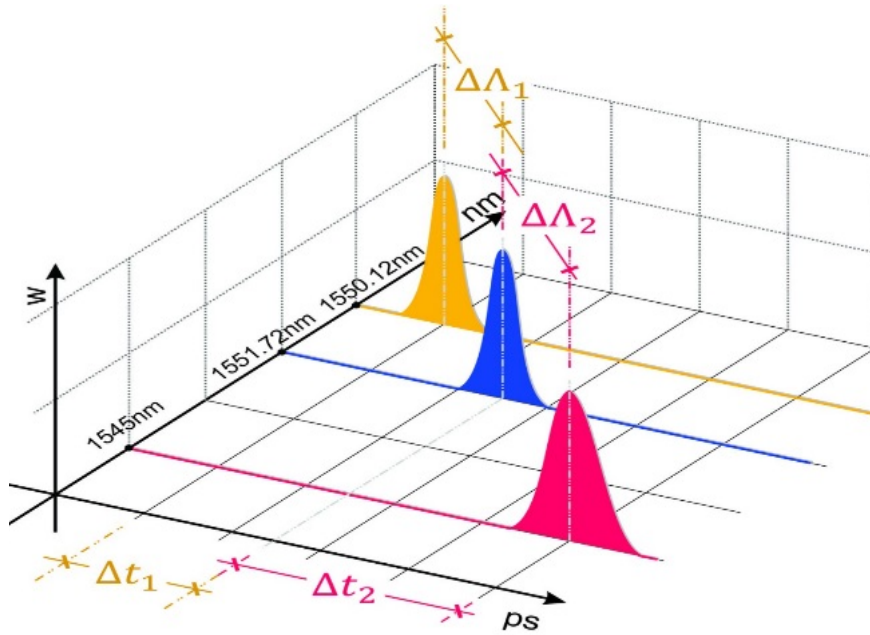


Figure 4. 3. Illustrates the concept of delays selection.

To investigate the limitations of equation 4.7, we used two different values for spectral spacing, a ‘narrow spectral spacing’ of 1.6 nm in case of Δt_1 delay and a ‘wide spectral spacing’ of 6.72 nm for Δt_2 delay. In this investigation, the temperature induced coefficient of the dispersion compensated fibre (DDCF) was neglected because it has a very small impact in the calculation $DDCF = 0.0009 \text{ ps}/(\text{km}\cdot\text{nm}\cdot^\circ\text{C})$ [116].

4.4.2 System Setup

As it is shown in Figure 4.5, a Mode-Locked Laser (MLL) generates optical pulses with a central wavelength of 1545 nm having a linewidth of 2.6 nm. Supercontinuum Generator (SCL) is then used to produce an optical supercontinuum with its central wavelength of 1550 nm and the linewidth of 3.2 nm. By using a Fiber Bragg Grating (FBG) OCDMA encoder (OKI Industries, Japan) four optical pulses are produced (carved from the supercontinuum) $\lambda_1 = 1550.92 \text{ nm}$, $\lambda_2 = 1550.12 \text{ nm}$, $\lambda_3 = 1551.72 \text{ nm}$, and $\lambda_4 = 1552.52 \text{ nm}$. Each wavelength pulse has a 0.8 nm linewidth. The optical pulse at 1545 nm is then delayed in time by an optical delay line and injected along with all four wavelengths λ_1 to λ_4 by using a 2×1 optical fiber coupler. This arrangement would allow us to study the individual relative position changes Δt of the pulses while being propagated in an optical fiber spool made of 19.5 km long Standard Single Mode Fiber (SMF-28) made by Corning, Inc. The spool is housed in an environmental

chamber (EC) SM-32C from Thermatron Industries (see figure 4.5 to introduce the desired temperature changes to SMF-28. The fiber link is fully compensated for chromatic dispersion by using a commercial Dispersion Compensated Fiber (DCF). The temporal skewing due to the influence of fiber temperature changes was observed using an Agilent Oscilloscope (86100C) with an optical sampling head of a limited bandwidth of 65 GHz.

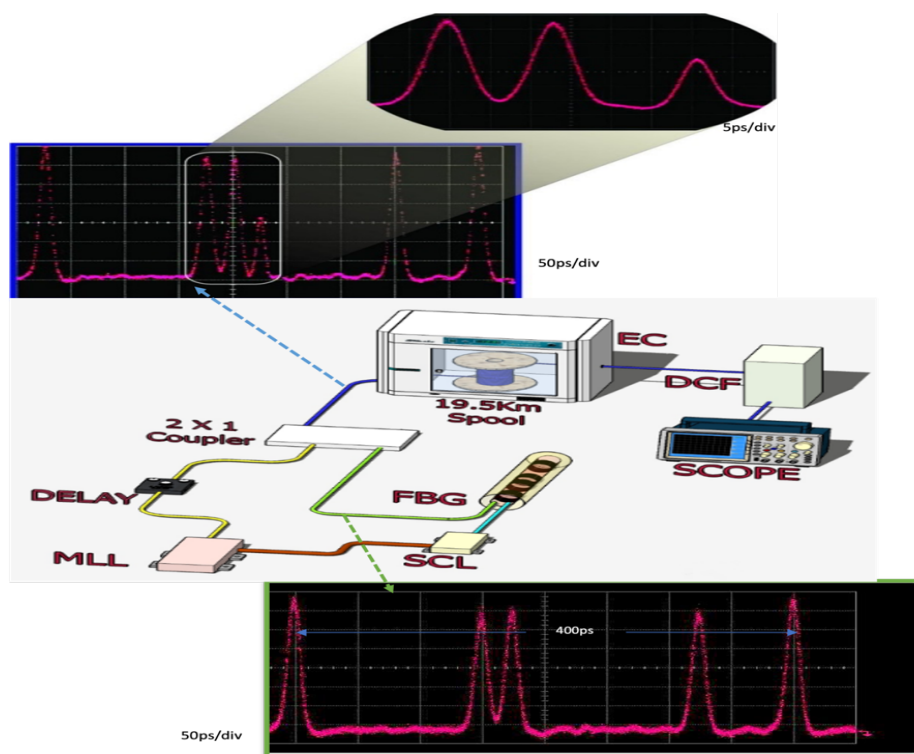


Figure 4. 4. Experiment setup. EC -Environmental Chamber, DCF – Dispersion Compensating Fibre, Scope – Agilent Oscilloscope 86100C, FBG – Fibre Brag Grating, SCL – Supercontinuum source, MLL – Erbium doped fiber mode locked laser.

4.4.3 Experimental Results and calculation

To ensure the experimental setup can support obtaining accurate results, we take in to account the following:

- In each measurement for obtaining Δt_1 and Δt_2 MLL and SCL settings were always rechecked by an optical Spectral Analyzer to ensure the same linewidth is maintain across all measurements.

- Measurements were taken for temperatures from 0°C to 40°C with steps of 10°C in each data taking, the temperature in the Environmental Chamber was let to stabilize for three and half hours before changing the temperature settings.
- Each measurement was repeated 5 times for the same temperature. We used average values for obtaining Δt_1 and Δt_2 .
- All wavelengths are in (nm). $\lambda_1 < \lambda_4$
- the frequency spectrum of $\lambda_1 = \lambda_4 = 0.8 \text{ nm}$
- The spacing between λ_1 and λ_4 is $1551.72 - 1550.12 = 1.6 \text{ nm}$

$$\Delta t = D_{temp} * \Delta T * \Delta \Lambda * L$$

Set 1

$$\Delta t_1 = 27 - 24.7 = 2.3 \text{ ps}$$

Set 2

$$\Delta t_1 = 26.8 - 24.3 = 2.5 \text{ ps}$$

Set 3

$$\Delta t_1 = 27 - 24.6 = 2.8 \text{ ps}$$

Set 4

$$\Delta t_1 = 26 - 24.4 = 1.6 \text{ ps}$$

Set 5

$$\Delta t_1 = 26 - 24.8 = 1.2 \text{ ps}$$

$$\Delta t_{ave1} = \frac{2.3 + 2.5 + 2.8 + 1.6 + 1.2}{5} = 2.08 \text{ ps}$$

$$\Delta t = D_{temp} * \Delta T * \Delta \Lambda * L$$

$$D_{temp} = -Dt_{ave1}/(L * \Delta\lambda * \Delta T) = 2.08/(19.5 * 1.6 * 40) = -0.0016 \text{ ps / nm.km.C}$$

Set1

$$\Delta t_2 = 36 - 22 = 14 \text{ ps}$$

Set2

$$\Delta t_2 = 36 - 21 = 4 \text{ ps}$$

Set3

$$\Delta t_2 = 36 - 21.5 = 14.5 \text{ ps}$$

Set4

$$\Delta t_2 = 36 - 21 = 15 \text{ ps}$$

Set5

$$\Delta t_2 = 36 - 20.5 = 15.5 \text{ ps}$$

$$\Delta t_{ave2} = \frac{13.5 + 15.2 + 14.8 + 13.8 + 15.1}{5} = 14.48 \text{ ps}$$

$$D_{temp} = -\frac{Dt_{ave2}}{L * \Delta\lambda * \Delta T} = \frac{14.48}{19.5 * 1.6 * 40} = -0.0028 \text{ ps / nm.km.C}$$

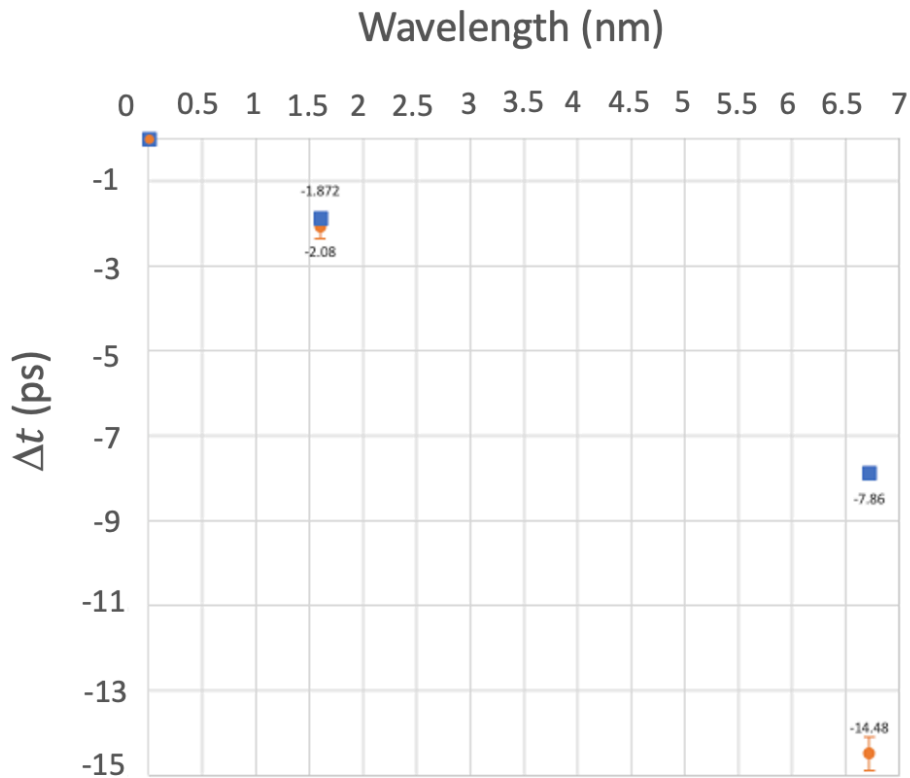


Figure 4. 5. Illustration of the impact of Δt ; blue squares define Δt_1 ; Δt_2 was calculated using equation 4.7. Red circles define Δt_1 ; Δt_2 was obtained from our measurements. The standard deviation for Δt_1 is 0.277 ps and for Δt_2 is 0.396 ps, respectively.

4.5 Simple method to accurately measure temperature dispersion coefficient

Temperature-induced dispersion necessitates the use of high precision equipment due to its small alterations on each optical pulse. Due to the fact that the temperature coefficient is so small (0.0015 ps/nm/°C) for small spectrum spacing [14], measuring the temperature dispersion on optical pulses-width can be a tough and time-consuming endeavour. However, changes are noticeable if one of the parameters in equation 4.2 is altered, such as the transmission line length, the optical spectrum, the temperature rate, or all of the aforementioned variables. In actuality, this process is not flawless since the addition of extra length brings a new variable into the equation. This additional parameter is chromatic dispersion, which is caused by an incompatibility between the transmission link and the dispersion compensating link. Also, adjusting the optical laser line width will inevitably change the pulse width [117]. And thirdly, accelerating the rate of temperature increase exposes the fiber links to higher temperatures,

which raises the danger of fibre damage. Moreover, calculating the temperature coefficient based on zero dispersion wavelength necessitates knowledge of parameters that are not always readily available [108].

The following section examines a common approach (pulse broadening) for measuring the temperature-induced dispersion and introduces a straightforward and cost-effective design for precise measurement of the temperature dispersion coefficient.

4.5.1 System setup

Measuring the TD using pulse-width spreading rate requires equipment with high-speed optical sampler. For example, a digital communication analyser with optical sampling head of 64 GHz can only provide accurate measurement of an optical pulse with not less than 15.6 ps pulse duration. In 2D-WH/TS OCDMA pulse duration is one of the key elements which govern the number of simultaneous users and interference – the shorter the pulse duration the more simultaneous users can be added in the network [118]. The skewing effect among code carriers in OCDMA can be used as an alternative method to determine TD.

In order to solely investigate the effects of temperature-induced dispersion on OCDMA systems employing 2D-WH/TS codes based on multi-color picosecond pulses, the FWHM of all code carriers was set to 8 picoseconds. As part of the experiment, a spool of 19.5 km of SMF-28 was placed inside of the environmental chamber to mimic the transmission link. The DCM module used to fully compensate for the link CD was kept at the room temperature outside of the chamber. These measurements were performed with an oscilloscope (Agilent Infiniium DCA-J 86100C with a 64 GHz optical sampling head) for temperatures changes between 0 and 42 °C. The environmental chamber was utilized in order to gather data in increments of 4 °C. In order to verify that the temperature measurements we took were accurate, we made sure to wait a minimum 2.5 hours between readings.

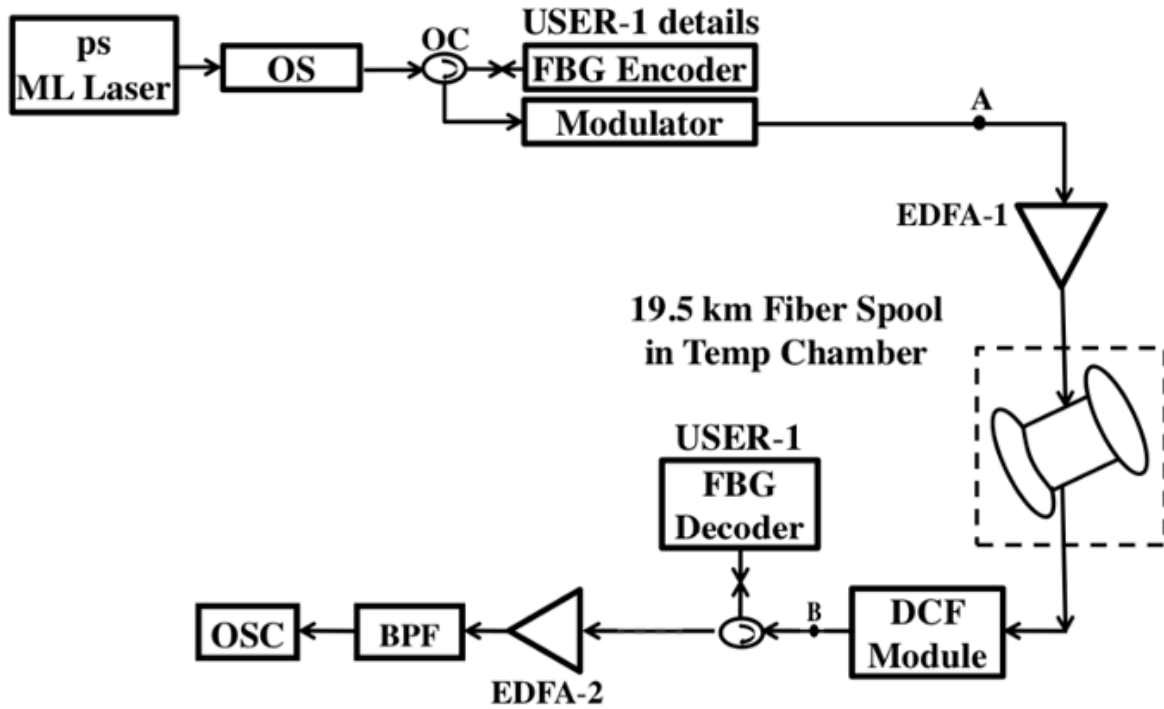


Figure 4. 6. The experimental set-up utilized to assess the skewing effect caused by temperature-induced dispersion in optical fibre among OCDMA code carriers. Ps ML Laser – picosecond mode locked laser, OS – optical supercontinuum, OC – optical coupler, EDFA – erbium-doped fiber amplifier , DCF – dispersion compensating fibre, BPF – bandpass filter, OSC – optical oscilloscope.

The primary focus of attention is on the two optical pluses λ_1 and λ_4 . They are separated in time by 25ps, with λ_1 is 1550.12 nm and λ_4 is 1551.72 nm. This arrangement of λ_1 and λ_4 in conjunction with the use of a 65 GHz optical sampling header enables me to accurately measure the individual relative position changes between the code carriers in the code illustrated in figure 4.7.

4.5.2 Results and analysis

In figure 4.8, OCDMA code using prime time spread sequence and orthogonal optical code of four wavelengths $\lambda_1 - \lambda_4$ for bit duration (T) of 400 ps is illustration.

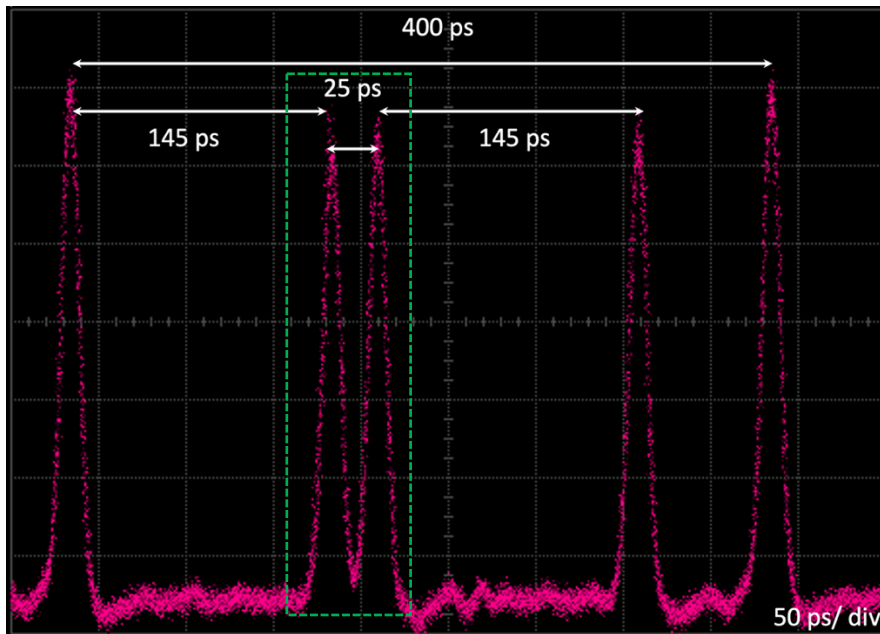


Figure 4. 7. The 2D-WH/TS OCDMA code carriers at the point a at the transmitter side.
Used to measure the time shifting between λ_1 and λ_4 .

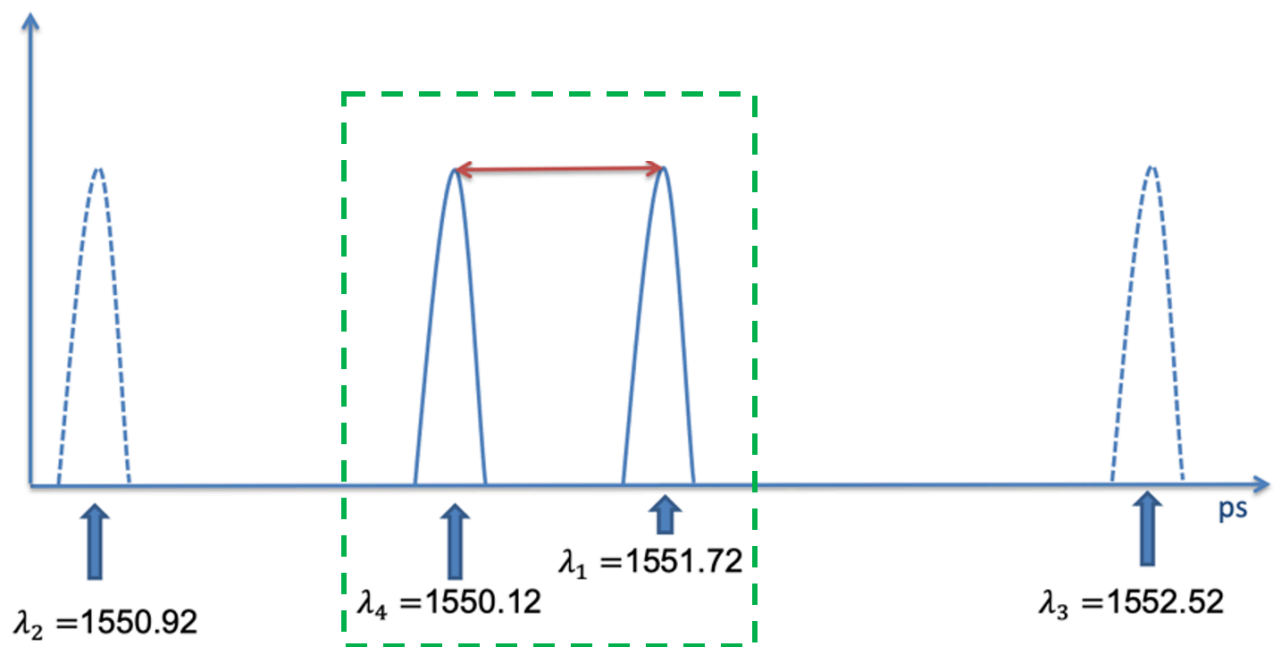


Figure 4. 8. The skewing effect is measured between λ_1 and λ_4 from the OCMDA code.

In OCDMA, the temperature dispersion effect differs between the skewing and dispersion equations in one important way: while the skewing effect can be expressed as

$$\Delta t = D_{\text{temp}} \times L \times \Delta\Lambda \times \Delta T$$

$$\Delta t = -0.0015 \times 19.5 \times 1.6 \times 20$$

$$\Delta t = -0.98 \text{ ps skewing}$$

the dispersion equation has a distinct difference and can be expressed as

$$\Delta\tau = D_{\text{temp}} \times L \times \Delta\lambda \times \Delta T$$

$$\Delta\tau = -0.0015 \times 20 \times 0.8 \times 19.5$$

$$\Delta\tau = -0.47 \text{ ps pulse spreading}$$

From the calculation the temporal coefficient is the same in both equations. However, skewing equation takes into consideration channel spacing ($\Delta\Lambda$) among code carriers not the linewidth of wavelength $\Delta\lambda$. Meaning, we can double the effect of temperature in order to measure the temperature coefficient more accurately. The recovered OCDMA code carriers on the receiver side were observed by an oscilloscope, at point B as shown in figure (4.6).

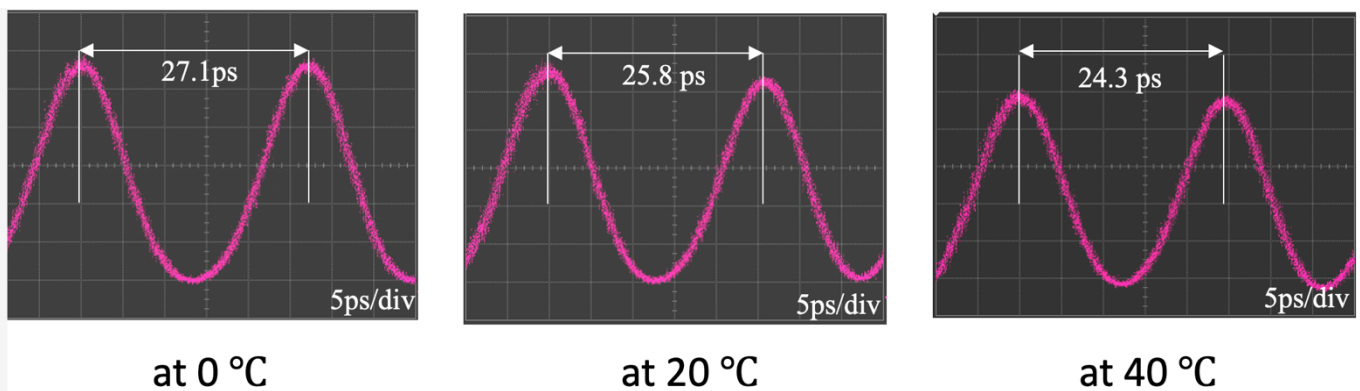


Figure 4. 9. Time shifting measurement in three temperature points; at 0°C, 20°C and 40°C.

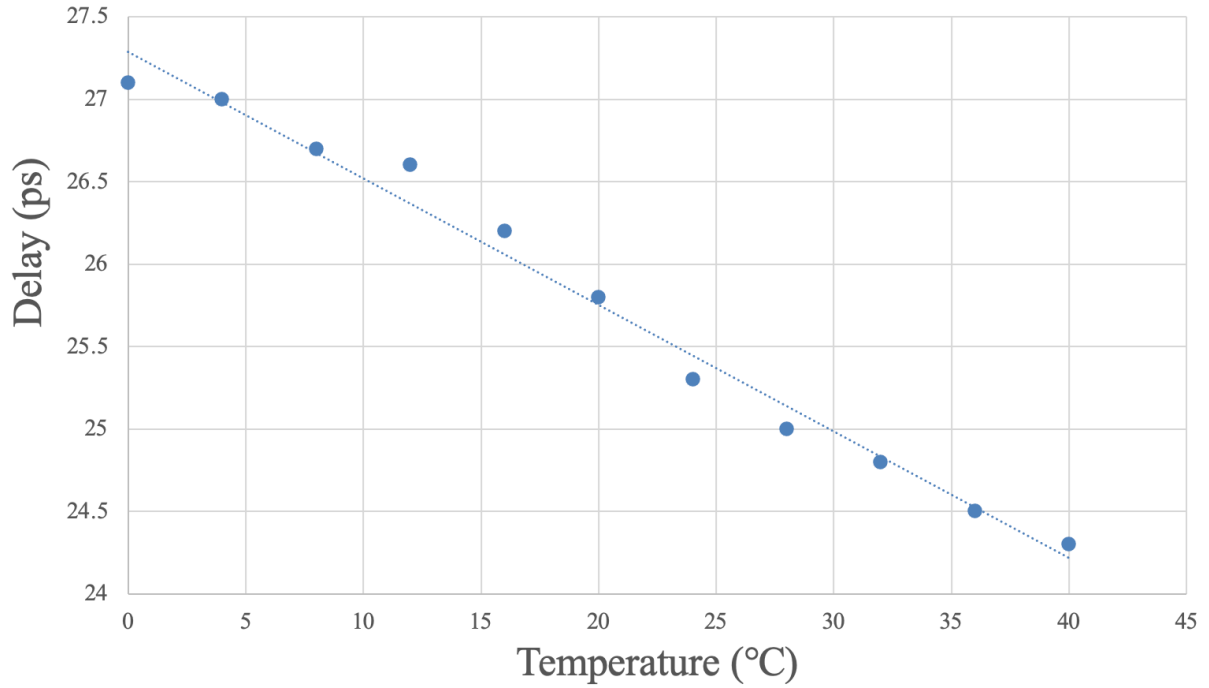


Figure 4. 10. Time skewing between code carriers $\lambda_1 = 1551.72$ nm and $\lambda_4 = 1550.12$ nm spectrally separated by 1.6 nm as a function of different fiber temperatures.

4.6 Discussion

It is important to realize that the chromatic dispersion is mostly depends on the fibre material [119]. Although, there are several types of SMF on the market, the temperature variation dependence of D_{tmp} for SMFs does not ‘hugely’ change from fibre to fibre [116] and is known to be -0.0015 ps/nm \times km \times °C [111]. We have experimentally tested the equation by considering two spectral spacing, 1.6 nm and 6.72 nm, respectively. When using the narrower spectral spacing of 1.6 nm our measurements for D_{tmp1} perfectly agree with the literature [120] [108]. However, for the large spectral spacing between wavelengths, the measurement data related to D_{tmp2} do not agree with the former. From Figure 4.6, the calculated Δt_2 if based on the temperature induced dispersion coefficient known from the literature would be $\Delta t_1 = -7.86$ ps. Our measurements indicate that Δt_2 is equal to -14.48 ps, which can be used to determine the temperature-induced dispersion coefficient (D_{temp}) using equation 4.8. This coefficient is wavelength-dependent and has a value of -0.0027 ps/nm \times km \times °C. Therefore, it is necessary to modify the expression of skewing provided in equation 4.7 as $\Delta t_n = D(\lambda_n)_{temp} \times L \times \Delta\lambda \times$

ΔT where, $n = 1, 2, 3, \dots, w$.

The K factor shown in figure 4.2 are represented by $w-1$, indicating that the autocorrelation function is calculated for four wavelengths with wavelength one always being idle. For the other wavelengths in the code, wavelength two is multiplied by the skewing factor Δt and a factor of 1, wavelength three by Δt and a factor of 2, and so on.

In the second part of this chapter, I used the walk-off between two pulses in the OCDMA code carriers to determine the temperature-dependent dispersion coefficient. The two pulses are temporally positioned equal to or above 15.6 ps from each other gives us way out of having to have an oscilloscope with an optical high sampling head to accurately measure the ultrafast optical pulse-width.

The effect of temperature can likely be double noticed by using skewing rather than measuring the pulse width. a 2D-WH/TS OCMDA code with four wavelengths spread in time as shown in figure 4.7 and figure 4.8. I use the λ_1 and λ_4 which have 1.6 nm channel spacing.

4.7 Summary chapter

In this chapter, we have experimentally investigated the temperature induced dispersion coefficient for SMF-28 as a function of different wavelengths. Our results showed good agreement with the value found in the literature for a narrow spectral spacing between wavelengths. In contrast, if using a wider spectral region of wavelengths (namely from 1545 nm to 1551 nm), we found changing dispersion slope for D_{tmp} . This clearly indicates D_{tmp} wavelength dependency, i.e. $D_{tmp} = D(\lambda n)temp$. Hence, we proposed to modify the conventional expression and applying equation 4.8 for finding the temporal width of the recovered 2D-WH/TS incoherent OCDMA auto-correlation function by the receiver. This to suite wider spectrum enabling the prediction of the temporal coefficient of multi-wavelength picosecond code carriers from a wider than a few nanometres spectral range.

In addition, we have developed a strategy to determine the temperature dispersion coefficient by measuring the skewing between two optical pulses. This skewing effect was measured as a function of fiber link temperature.

Chapter 5

Investigation of 2D-WH/TS OCDMA Code Stability in Systems with SOA- based Device

5.1. Introduction

With the increasing demand of spectral and transmission rate, all optical networks has become a topic of interest for many researches. Promoting deploying SOAs in the networks to implement varies applications. Unlike its counterpart fibre-based amplifiers, advantages from its easy integration due to its small size (micrometres), ultra-fast dynamic response and strong, wide net gain spectrum (~ 1530 nm to ~ 1560 nm) and strong nonlinearities patterns [121]. SOA can amplify ultra-short optical pulses of the order of picoseconds [122] as they possess very large bandwidth (few THz).

In the field of optics, SOAs offer several advantages over Erbium-Doped Fiber Amplifiers (EDFAs) in certain applications [42]. These advantages include a more compact size greater wavelength flexibility, the ability to generate nonlinear optical effects [78], faster response times, and cost-effectiveness [78]. However, the choice between SOAs and EDFAs depends on the specific requirements of the application, as EDFAs still have advantages in terms of lower noise figure and higher gain [123], making them suitable for long-haul optical communication systems, while SOAs are generally more suitable for short-haul systems and applications requiring fast response times or nonlinear optical effects [42].

The challenges faced in deploying SOA is primarily lay in the application. There are two regions of operation linear and non-linear. When SOA is used for the purpose of amplifying the signal then SOA must operate in the linear region. SOAs could be the most favourable

preamplifier in medium haul application (~ 20 km) when set up properly. This region provides stability of SOA output gain to -3 dB on maximum level of amplification [42].

In addition, the gain recovery time of the SOA, which refers to the time required for the SOA to return to its initial gain level after amplifying a passing pulse, is an important parameter to consider. This factor is critical in determining the SOA's performance, as it directly impacts the quality and reliability of the system's signal.

Equally important, polarisation sensitivity of the SOA. Since the polarization state of any in-line component in the optical communication system is unknown, as optical fibre does not preserve the state of polarisation, it is very important that SOA is polarisation insensitive to maintain best polarisation dependent [124]. An undesired drawback of SOAs in this region of operation is that the SOA low input saturation power which also determining the boundary between linear and nonlinear regions. Thus, maintaining the input peak power lower than the SOA input saturation power is crucial. In the nonlinear region, SOA gain level is sacrificed for enabling patterns such as SPM, XPM and FWM. This region of operation also comes with its challenges. In practical, nonlinear region begins from -3dB of the maximum level of amplification (SOA is saturated). Two main parameters can influence the saturation depth, the input power and the SOA bias current [42].

In any amplifier, nonlinearities due to gain saturation leading to pulse distortion because the leading edge of the pulse saturates the amplifier which reduces the gain available for the trailing edge of the pulse [125]. Under different operating conditions, both pulse compression and pulse broadening can be obtained in the saturation region but no such cases arise if pulse energy is a small fraction of the saturation energy and hence the input pulse can be amplified without significant distortion. Sometimes pulse shape may remain unchanged, but spectrum can be distorted considerably which is particularly important where the changes in the carrier density occurring as a result of gain saturation and leading to large change in refractive index [78].

In WDM, a great deal of switching architectures utilizing SOAs in different configurations such as 2×2 multi-cascaded switch fabrics, cross-point matrices, for broadcast and select, wavelength selection [126], and DeMux operation [127] have already been successfully demonstrated and commercially available. Also, in 1D incoherent OCDMA systems SOA has proved that it is a powerful tool for systems for high frequency to remarkably suppresses the intensity noise, which is helpful for reducing the beat noise in spectrum-sliced incoherent light [121] [128]. Here SOA operates in the nonlinear region in a simple configuration and saturated

by CW. Nevertheless, as 2D WH/TS OCDMA system is in both time and frequency domains, there might be challenges encounter of deploying SOA. In [79], for the first time, 2D OCDMA utilized SOA as a tuneable compensation tool for induced temperature dispersion. The SOA was used in the linear region at the receiver after the decoder to manipulate induced temperature dispersion by the induced chirp on the autocorrelation peak. Notably, to prevent the challenge of the gain recovery time of the SOA, the authors manipulated the induced chirp in all code carriers after the decoder. Having said that, this increases the necessity of investigating the implementation of SOA in OCDMA systems for all optical processing networks [42].

The severity of gain recovery time on 2D-WH/TS OCDMA systems using SOAs is evident even at low data [129]. This is because of the nature of the code carriers' time-spreading. The code carriers are spread with different time delays when forming a unique code signature for each user. The SOA's response time to incoming code is related to carrier lifetime, which in turn determines the SOA gain recovery [42]. A slow SOA gain recovery time poses a stringent limitation on the choices of the 2D-WH/TS code spreading, thus limiting the overall system scalability, including the number of simultaneous users. For the sake of illustration, even a 2.5 Gbit/s OCDMA system, if using a temporal code carriers' separation of 25 ps (i.e., 40 OCDMA GHz/s chip rate), will experience the equivalent SOA limitations of a 40 Gbit/s on-off keying (OOK) system.

Many techniques have been developed and demonstrated to address and improve the gain recovery time of SOAs [42] [130] and these techniques fall into three categories. In the first category, a continuous wave beam is utilized to saturate the SOA at the operating wavelength, which lies in the SOA's spectral gain region or near the transparency point. The second method comprises the use of quantum wells or quantum dots semiconductors [42]. The third technique utilizes the SOA's amplified spontaneous emission (ASE) when driving the SOA with a high bias current into saturation. In [130], this method was used to reduce the gain recovery time from 200 ps down to 10 ps with the caveat that signal quality margins were somewhat sacrificed in situations where the SOA was followed by spectral slicing [131]. As the 2D-WH/TS systems can deploy both SOAs and spectral slicing, more investigations are required.

This chapter investigates for the first time how the implementation of semiconductor optical amplifier (SOA)-based devices in photonic networks can negatively impact the integrity of two-dimensional wavelength-hopping time-spreading (2D-WH/TS) optical code-division multiple access (OCDMA) codes based on multi-wavelength picosecond code carriers. The background and literature review of 2D-WH/TS OCDMA code stability in systems with SOA-based device are covered in section 5.1. In section 5.2, the distortion of 2D-WH/TS OCDMA

code carriers was examined for various SOA bias currents. The SOA's impact on individual wavelength code carriers under three distinct SOA driving conditions was then investigated. Additionally, SOA effects were simulated at different currents in the OCDMA system to optimize performance and understand deployment challenges. In section 2.3, the experiment explores the effects of high SOA bias current on OCDMA code fidelity, using a commercial FBG-based encoder and decoder with an optimized 2D-WH/TS CHPC. In section 5.4, several methods are proposed to reverse the ramifications of the redshift among code carriers caused by SOA. It is important to note that the results obtained in each experiment are discussed in the relevant section (5.2, 5.3 and 5.4) and then summarized in the Conclusion in section 5.5.

5.2. Impact of SOA-Based Devices Deployed in Fibre Link on Multi-Wavelength Picosecond Code Carriers

In a 2D-WH/TS OCDMA system, each user's data are carried by a unique code. Each code requires a unique time-spreading of wavelengths (i.e., code carriers) over a bit period. The temporal separation of code carriers can be anywhere from a few to several hundreds of picoseconds and depends on the design parameters and the targeted number of simultaneous users [7]. SOA-based optical devices can be implemented in OCDMA systems to play an important role [132] [131] [133]. However incorrect implementation may have undesirable effects on the system performance. The subsequent investigation will demonstrate how the use of an SOA under different driving conditions influences 2D WH/TS OCDMA code carriers and affects the code integrity.

5.2.1 Description of Experimental Setup

The experimental setup for the above investigation is shown in figure 5.1. Here, an optical clock of wavelength of 1547 nm, generated by an erbium doped fiber mode locked laser (FMLL) manufactured by PriTel, Inc. (Naperville, IL, USA), has a linewidth of 1.4 nm. The optical clock is driven by an RF synthesizer (Agilent E8257D) at 2.5 GHz. The optical clock pulses then enter an optical supercontinuum (OS) generator, which consists of a 25 dBm erbium doped fiber amplifier (EDFA) and an approximately 1 km long dispersion decreasing fiber, thus producing a 3.2 nm wide optical supercontinuum in the spectral region from 1550 to 1553.2 nm. The 2D-WH/TS code is then generated by an encoder comprising of a 1×4 DWDM

de-multiplexer (DMUX), four adjustable fiber optical delay lines, and a 4×1 DWDM multiplexer (MUX). Both MUX and DMUX have a channel spacing of 100 GHz (i.e., 0.8 nm). The resulting pulse-width at the MUX output is 7 ps at Full Width at Half Maximum (FWHM). The DMUX spectrally slices the optical supercontinuum into four wavelengths (to be used as code carriers), $\lambda_1 = 1550.12$ nm, $\lambda_2 = 1550.92$ nm, $\lambda_3 = 1551.72$ nm, and $\lambda_4 = 1552.52$ nm. The wavelength separation corresponds to a 100 GHz channel spacing (ITU channels CH34 to CH31). After being appropriately delayed by optical delay lines, the individual code carriers are then recombined by a MUX to form the desired 2D-WH/Ts code. The generated code then passes through a 16 km long SMF-28 optical fiber followed by a 2.5 km long matched chromatic dispersion compensating fiber (DCF) module, thus forming an 18.5 km chromatic-dispersion compensated (CDC) fiber link. The SMF-28 fiber has its group velocity dispersion parameter (GVD) $\beta_2 = -20$ ps²/km. The 2D-WH/Ts OCDMA encoder's delay lines, D1, D2, D3, and D4 (see figure 5.1), were set to generate 1, 6, 11, and 16 chip delays, respectively. An optical spectrum analyzer (OSA) (Agilent 86146B) with 0.06 nm resolution was used in all measurements.

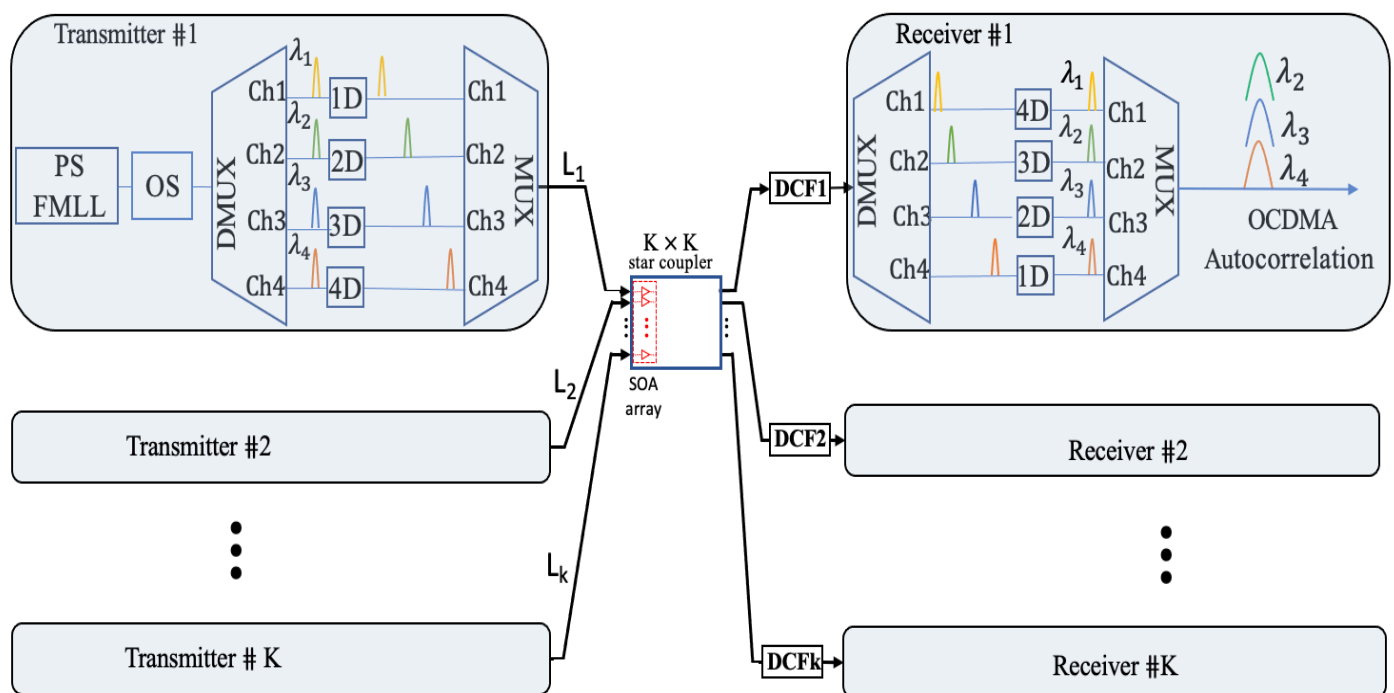


Figure 5. 1. Schematic diagram of the experimental setup with illustration of two-dimensional wavelength-hopping time-spreading (2D-WH/Ts) code carriers. FMLL – picosecond fiber mode locked laser, OS – optical supercontinuum, DMUX – de-multiplexer,

MUX – multiplexer, SOA – semiconductor optical amplifier, DCF – chromatic dispersion compensating fiber.

It should be noted that a 1 chip delay is defined as T_{bit}/N , where T_{bit} is a bit period and N is the number of chips. Here, $T_{\text{bit}}/N = 400/53$, i.e., ~ 7.5 ps/chip (~ 133 GHz chip rate). The encoder thus generates a 2D-WH/TS code $(1-\lambda_1, 6-\lambda_2, 11-\lambda_3, 16-\lambda_4)$. Similarly, a matched decoder was set to $(16-\lambda_1, 11-\lambda_2, 6-\lambda_3, 1-\lambda_4)$. These settings will guarantee the arrival of all four wavelengths code carriers to arrive at the OCDMA decoder's output at the same time. This enables the formation of an OCDMA autocorrelation peak of the code weight $w = 4$.

5.2.2 Investigation of 2D-WH/TS OCDMA Code Carriers' Distortion under Different SOA Driving Conditions

The 2D-WH/TS OCDMA code carriers' distortion was explored for SOA bias currents of 7 mA, 80 mA, and 250 mA, which provide a gain of 6 dB, 12 dB, and 24 dB, respectively. For this investigation, we used a Kamelian small gain SOA (OPA-20-N-C-FA) with a max gain of 24 dB, saturation output of 9 dBm, and polarization dependency of 0.6 dBm [134]. The ASE power level was -26 dBm, a slightly higher value when compared with its counterparts made by Thorlabs and InPhenix Inc. (Livermore, CA, USA) when biased at 500 mA [135] [136].

At the start, the SOA gain recovery time was measured using the technique described in [137]. The results are shown in figure 5.2. The shortest measured value 28 ps corresponds to a 250 mA driving current.

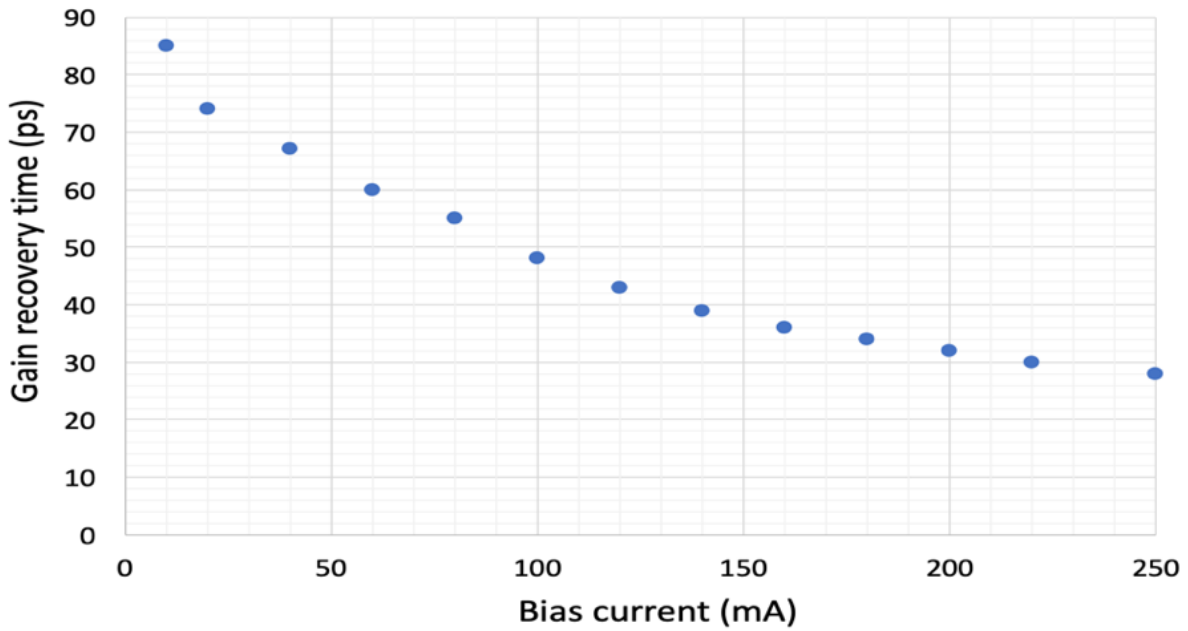


Figure 5. 2. SOA’s gain recovery time against the bias current.

The code integrity was first observed using an optical spectrum analyzer by comparing the code spectrum before and after traveling through a chromatic dispersion compensating fibre link with an SOA device driven at 175 mA (see figure 5.3.). This current level was chosen arbitrarily to illustrate a code carriers’ redshift by comparing figure 5.3a,b. For ease of comparison, the measurements obtained were plotted relative to the signal strength at the SOA input, i.e., a variable optical attenuator (VOA) was used to compensate for the SOA gain. This way, both graphs in figure 5.3 can use an identical Y-scale. Figure 5.3a depicts four wavelength code carriers with 30 ps temporal separation before entering the SOA. The optical average power and carriers’ peak power was 4 mW and 57 mW, respectively. Figure 5.3b shows the impact of the SOA on the code integrity the code carriers are clearly affected by a 0.73 nm wavelength redshift. A carriers’ height variation is also observed. In WDM systems, the effect of non-uniformity of the gain during a stream of pulses passing the SOA is resolved using a Lyot filter [19].

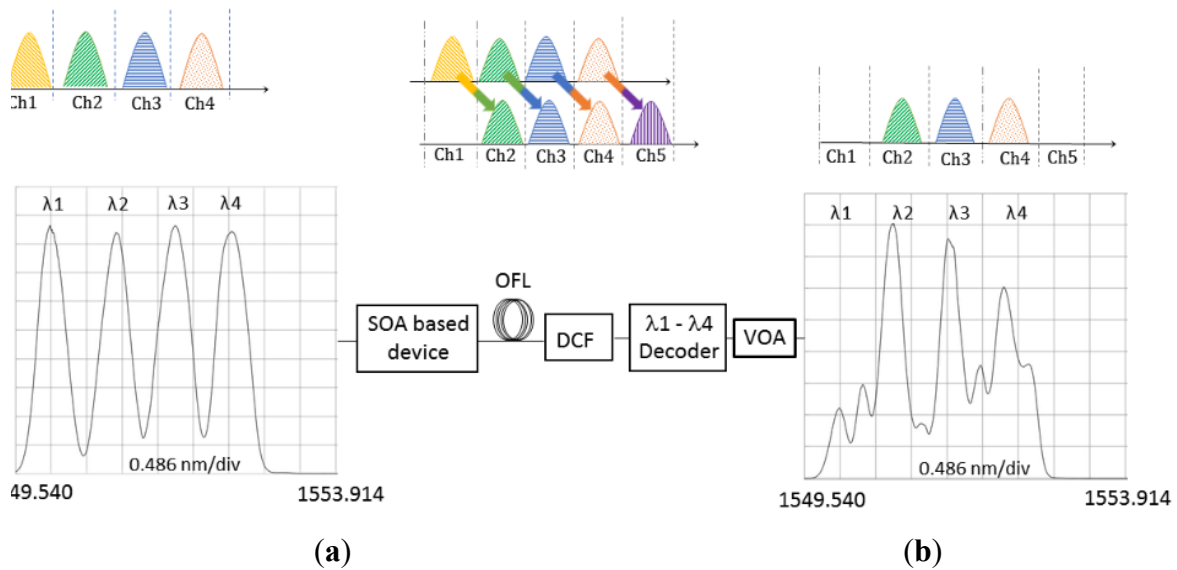


Figure 5. 3. (a) Optical spectrum of the 2D-WH/TS OCDMA code based on four λ_1 to λ_4 multi-wavelength picosecond code carriers before entering the SOA biased at ~ 175 mA; (b) after passing the SOA followed by dispersion compensated fiber link (DCF) and λ_1 – λ_4 decoder. VOA—variable optical attenuator, OFL—optical fiber link.

Contrary to the WDM and its regular bit rate, in 2D-WH/TS OCDMA systems, the 2D-WH/TS OCDMA code formation leads to an uneven temporal multi-wavelength code carrier's separation. Using this solution is thus not feasible. Further analyses of figure 5.3b reveal that the induced wavelength redshift has led to a code carrier 'loss'. This is explained by inspection of figure 5.3. Here, a 2D-WH/TS code composed of four wavelength code carriers is shown before entering the SOA (biased at 175 mA), after the SOA, and then again after passing a λ_1 – λ_4 decoder. After passing the λ_1 – λ_4 decoder with an unmatched channel spacing of 0.8 nm, the code exits distorted and with three code carriers only because of the code carriers' redshift of ~ 0.73 nm. The observed height differences among code carriers results in part from a non-ideal SOA gain flatness in the 1550 nm region.

The impact of the SOA on individual wavelength code carriers will now be investigated under three different SOA driving conditions: 7 mA, 80 mA, and 250 mA, representing an SOA gain of +6 dB, +12 dB, and +24 dB, respectively. The results obtained are shown in figure 5.4. For reference, figure 5.4a shows all four wavelength code carriers at the input of the SOA. To graph the results obtained using an identical Y-axis scale for different SOA gain levels, a VOA was placed after the SOA, but before the OSA. The measurements obtained are shown in red, green, and yellow and represent SOA driving currents of 7 mA, 80 mA, and 250 mA,

respectively. The SOA-induced redshift on individual code carriers λ_1 , λ_2 , λ_3 , and λ_4 is shown in figure 5.2b–d, respectively. Figure 4.4f shows how the entire code spectrum is affected by the SOA biased at 250 mA/24 dB gain (i.e., under the shortest gain recovery time ~ 30 ps (see figure 5.2)).

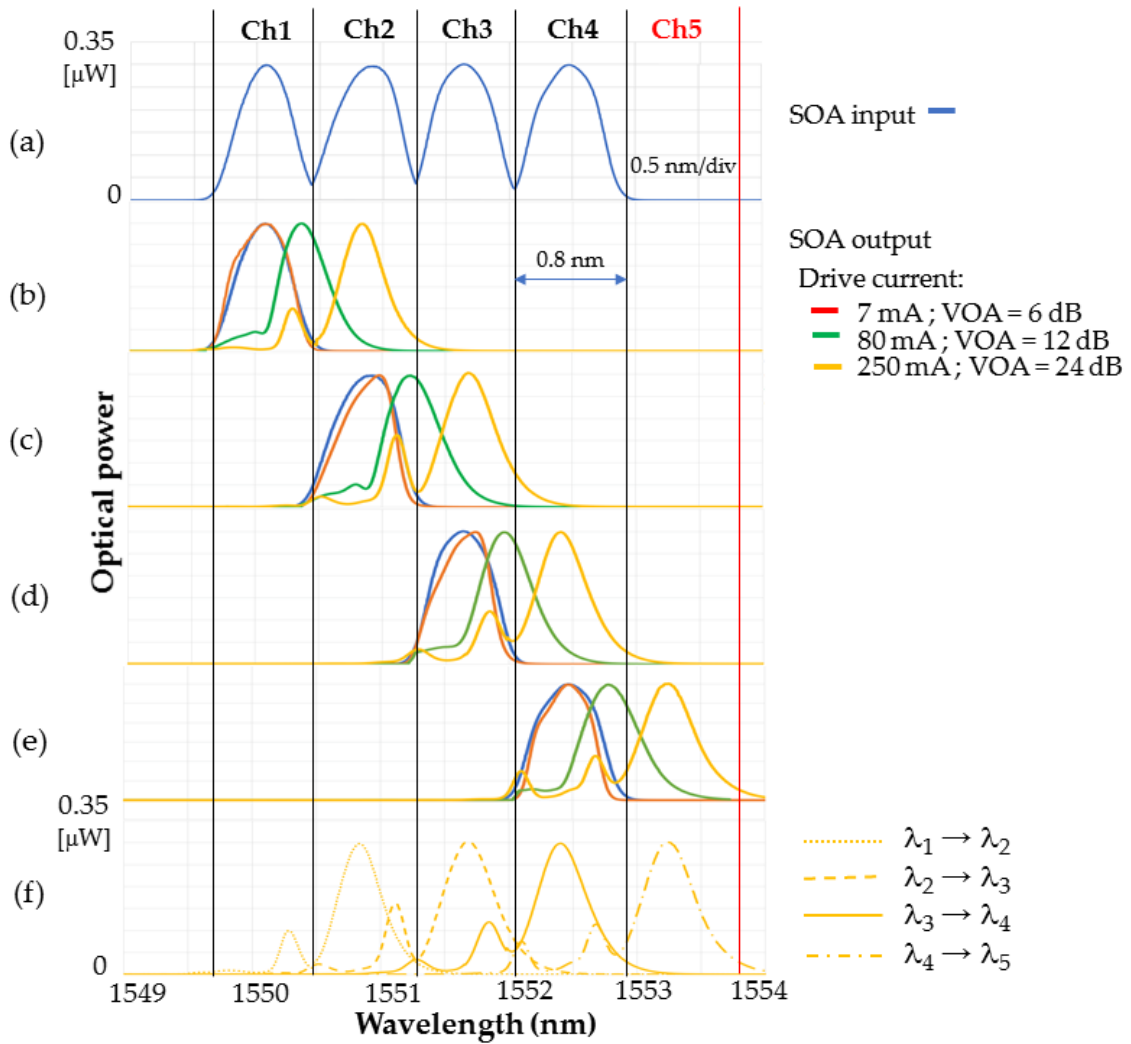


Figure 5. 4. Experimental demonstration of code carriers’ wavelength redshift observed on the optical spectrum analyzer: (a) code carriers at the input of the SOA; (b) effect of SOA on code carrier λ_1 at an SOA current of 7 mA/6dB gain, 80 mA/12 dB gain, and 250 mA/24 dB gain, respectively; (c) similarly for λ_2 ; (d) for λ_3 ; (e) for λ_4 ; (f) illustration of redshift on all four wavelength code carriers for an SOA current of 250 mA/24 dB gain.

5.2.3 Discussion

In the case of 7 mA/6 dB gain, all four code carriers exhibit slight linewidth and spectral shape variations after passing the SOA and the 18.5 km long chromatic dispersion compensated fiber link.

In the case of 80 mA/12 dB gain, the carriers' spectra are affected by self-phase modulation (SPM). Spectral peaks shift towards the longer wavelengths (redshift), leaving a noticeable 'trace' in the original spectral pulse position. The amount of shifting is mainly dominated by the SOA gain and carrier density changes, causing noticeable variations in the refractive index [12]. Consequently, an SPM-induced frequency chirp is imposed on all spectral pulses as they pass the SOA [20]. In the third case of 250 mA/24 dB gain, the SOA is in its highly nonlinear regime and the pulse spectrum shifts further to the red side in addition to one or more new peaks on the red side. These observations agree with [20]. The achieved redshift was ~ 100 GHz/0.8 nm.

As explained before, a matched OCDMA decoder and encoder pair are required to accurately recover the user's data and produce an OCDMA autocorrelation peak. Based on the results in figure 5.4f, this would not be possible. It can be seen that the 100 GHz spectral redshift affected all four wavelength code carriers: λ_1 became λ_2 , $\lambda_2 \rightarrow \lambda_3$, $\lambda_3 \rightarrow \lambda_4$, and $\lambda_4 \rightarrow \lambda_5$. However, the matching 100 GHz lambda DMUX in the OCDMA decoder (see Figure 5.1) was designed to handle only $(\lambda_1, \lambda_2, \lambda_3, \lambda_4)$, thus it cannot recognize the newly 'created' wavelength λ_5 resulting from the $\lambda_4 \rightarrow \lambda_5$ wavelength redshift. As a consequence, the number of wavelengths forming the OCDMA autocorrelation peak at the decoder output will be reduced from four to three.

This will be explained more in the next section. Furthermore, a slightly unequal amount of redshift imposed on individual wavelength code carriers is also observed. This is a result of the fact that the SOA gain is not flat and peaks at around 1550 nm [134]. Thus, multi wavelength code carriers passing the SOA experience slightly different saturation rates. This leads to a slightly different SPM, and thus amount of redshift. This was confirmed by the measurements shown in figure 5.6.

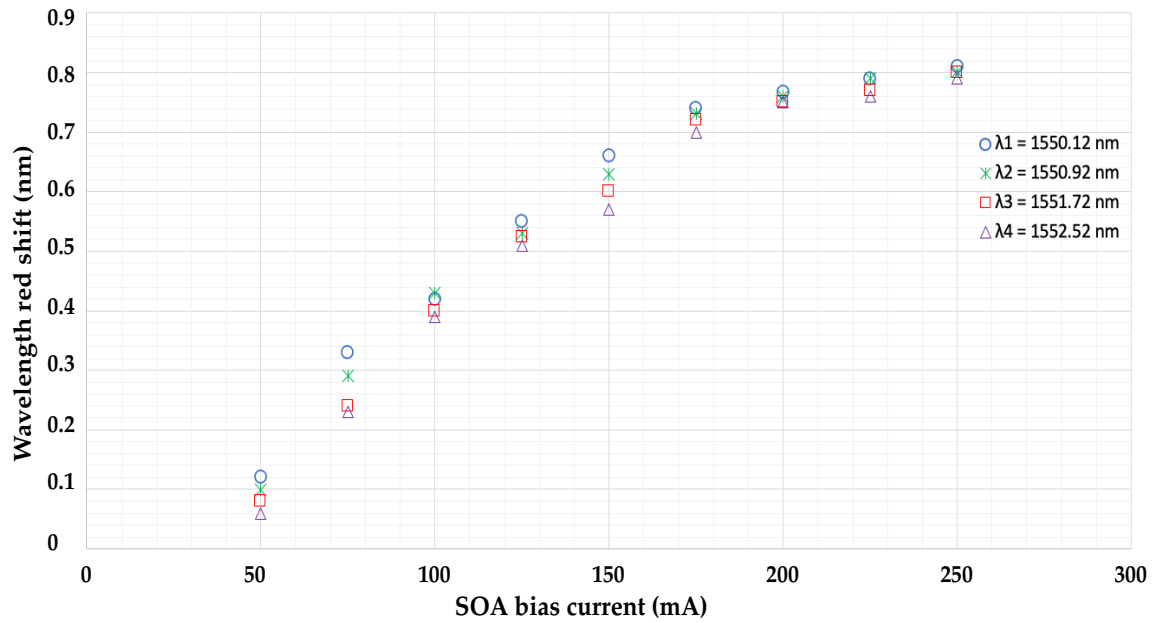


Figure 5. 5. The measured amount of code carriers’ wavelength redshift as a function of the SOA bias current.

The measured amount of the code carriers’ redshift inflicted by the SOA on individual code carriers can be also found theoretically. The nonlinear effect induced by the SOA can be simulated by adopting the model described in [138]. The simulation was designed to mimic to actual WH/Ts code carriers to study the effect of SOA on such a code as shown in figure 5.7.

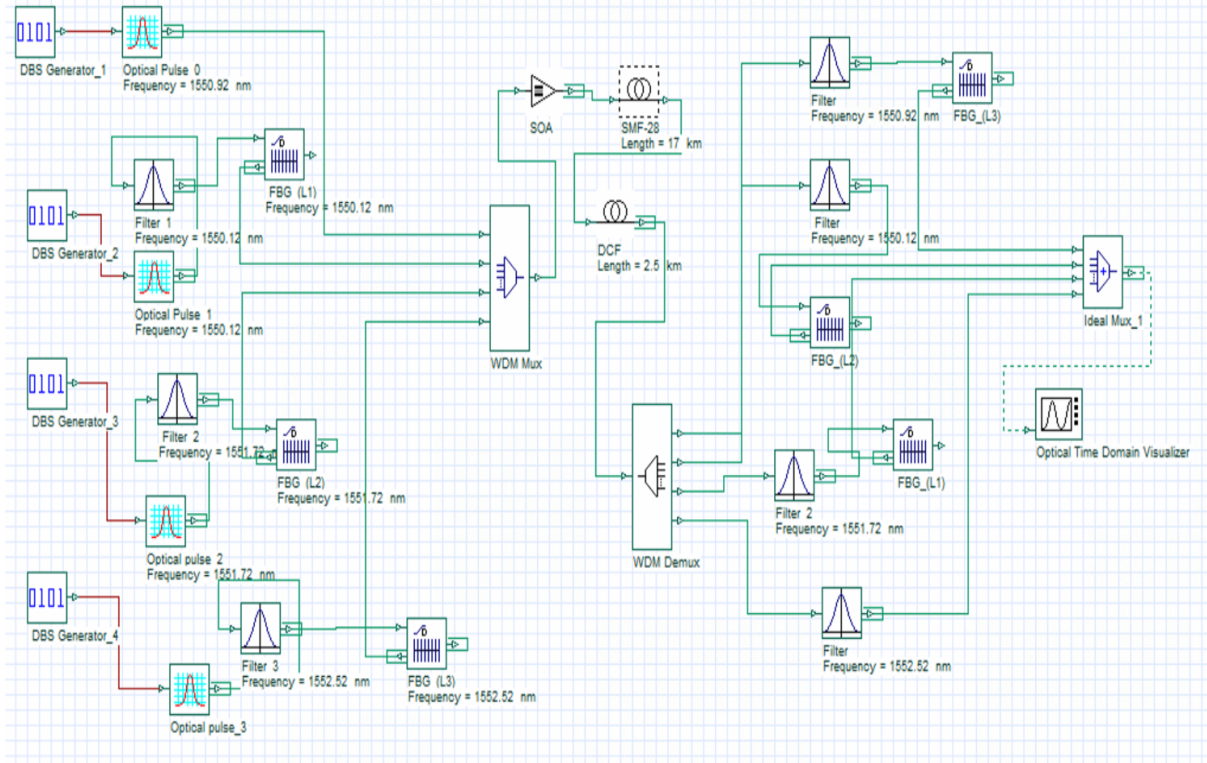


Figure 5. 6. Simulation layout of 2D TS/WH OCDMA transmitter and receiver with SOA in the transmission link.

In the simulation, the multi wavelength code carriers at the input of the SOA were assumed to have a temporal Gaussian shape and measured FWHM of 7 ps ($\tau_0 = 4.2$ ps at 1/e). The model used is applicable if the temporal pulse width of code carriers passing the SOA is ≥ 1 ps. The parameters used in the simulations are given in Table 5.1.

Table 5. 1. Geometrical and material parameters used in the simulation.

<i>Parameter</i>	<i>Description 2</i>	<i>Value</i>
<i>I</i>	<i>Bias current (mA)</i>	250
<i>L</i>	<i>Length (mm)</i>	1 [14]
<i>W</i>	<i>Width (μm)</i>	0.4 [22]
<i>H</i>	<i>Height (μm)</i>	0.4 [22]
α_i	<i>Loss (m^{-1})</i>	3000 [23]
<i>g</i>	<i>Differential gain (m^2)</i>	3×10^{-20} [24]
N_i	<i>Initial carrier density (m^{-3})</i>	3.65×10^{24} [23]
<i>Γ</i>	<i>Optical confinement factor</i>	0.4 [24]

N_0	Carrier density at transparency (m^3)	10^{24} [24]
α	Linewidth enhancement factor	4 [24]
A	Recombination coefficient (s^{-1})	10^8 [23]
B	Recombination coefficient ($m^3 s^{-1}$)	1.5×10^{-16} [23]
C	Recombination coefficient ($m^6 s^{-1}$)	10^{-40} [23]

A great deal of consistency (see figure 5.6) was found between the simulated and measured results. More precise measurements would require a higher resolution OSA than the one available for the experiment, which has a resolution of 0.06 nm. The calculated slope from the measured and simulation values was found to be -0.0083 and -0.0054 . This is shown in figure 5.8, where the dashed line represents the simulation, while the dots are measured values.

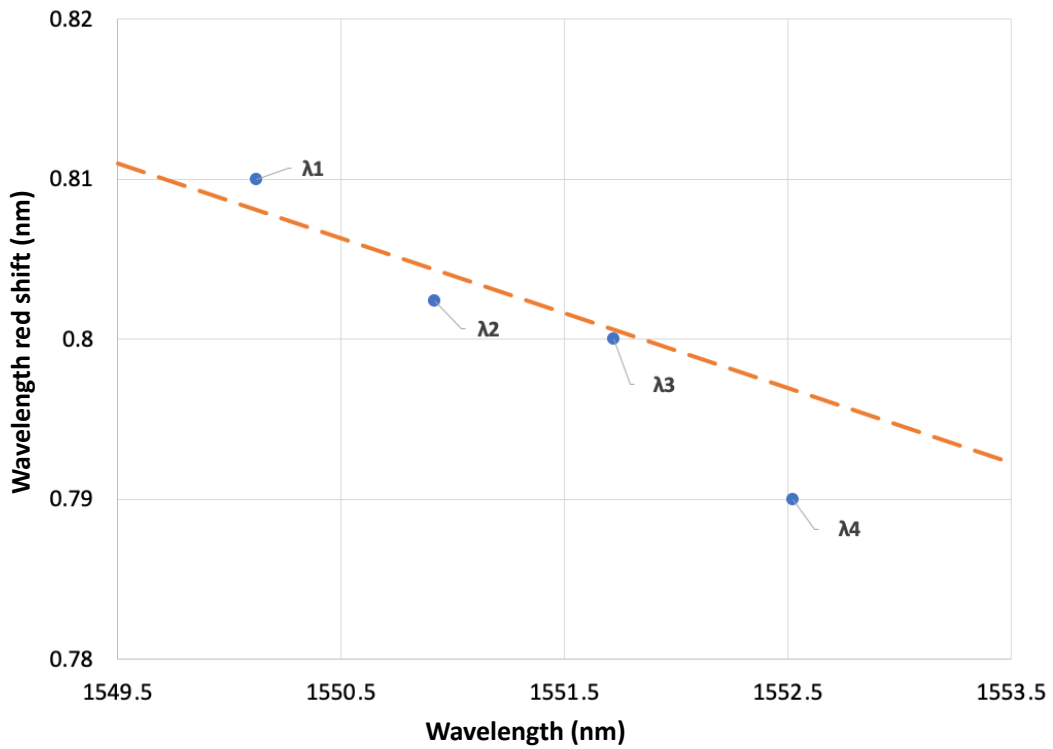


Figure 5. 7. Wavelength red shift for the SOA biased at 250 mA. The dashed line is simulations, and the dots are measured values for $\lambda_1 = 1550.12$ nm, $\lambda_2 = 1550.92$ nm, $\lambda_3 = 1551.72$ nm, and $\lambda_4 = 1552.52$ nm.

5.3 Impact of SOA High Bias Current on 2D-WH/TS OCDMA Prime Code Fidelity

Here, the investigation was repeated by replacing the DWDM-based OCDMA encoder and decoder with a commercial fiber Bragg grating-based encoder and decoder manufactured by OKI, Japan. The implemented 2D-WH/TS OCDMA carrier-hopping prime code (CHPC) [139] is optimized to ensure that the periodic cross correlation function is at most one [139]. This minimizes the multiple-access interference. The encoder/decoder pair uses four wavelength code carriers from a code space $(w, N) = (4, 53)$, where w indicates a number of wavelength code carriers with a channel spacing of 100 GHz and N is the number of chips [132] per bit period. The code signature $(1-\lambda_2, 21-\lambda_4, 27-\lambda_1, 39-\lambda_3)$ guarantees a minimal separation between adjacent code carriers of more than 30 ps. The SOA bias current/gain and code average/code carriers' peak power at the SOA input were 250 mA/24 dB and 4 mW/57 mW, respectively, resulting in a 100 GHz/0.8 nm code carriers' redshift. The results obtained are shown in figure 5.8. Figure 5.8a is the OCDMA code optical spectrum recorded by the OSA without, and figure 5.8b with an SOA being part of the chromatic dispersion compensated transmission link.

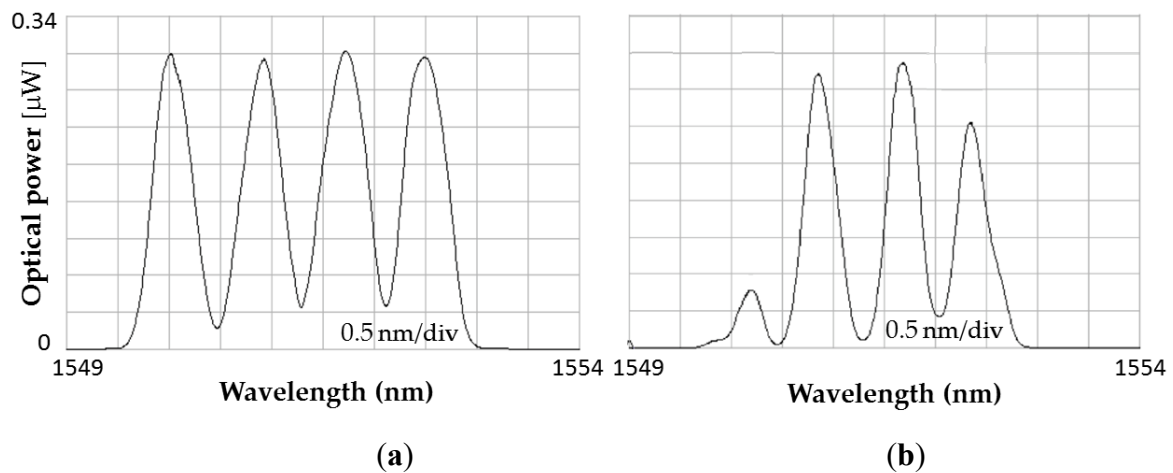


Figure 5. 8. Impact of SOA on 2D-WH/TS code based on four-wavelength code carriers as recorded by an optical spectrum analyzer: (a) without and (b) with the SOA present in the chromatic-dispersion (CD) compensated transmission link.

By comparing both results, it can be observed that wavelength code carriers were red shifted by 100 GHz/ 0.8 nm. As explained in Section 2, because of this redshift, λ_1 became λ_2 , $\lambda_2 \rightarrow \lambda_3$, $\lambda_3 \rightarrow \lambda_4$, and $\lambda_4 \rightarrow \lambda_5$. However, the OCDMA fiber Bragg grating (FBG) decoder

was designed to handle only $(\lambda_1, \lambda_2, \lambda_3, \lambda_4)$. Therefore, the wavelength λ_5 that resulted from the $\lambda_4 \rightarrow \lambda_5$ redshift is ‘missing’ in figure 5.8b.

As a consequence, the resulting OCDMA autocorrelation height will be reduced by one to its new value $w - 1$. This code weight reduction will decrease the signal-to-noise ratio (SNR) and cause deterioration in the OCDMA system bit-error-rate (BER), which in turn reduces the number of simultaneous users. The performance degradation resulting from the code carriers’ red shifting can be theoretically evaluated using equation 5.1 to calculate the probability of error Pe . Equation 5.1 is valid for an OCDMA receiver with hard limiting capabilities [132]. Pe can be used to evaluate the number of simultaneous users (K).

$$Pe = \frac{1}{2} \sum_{i=0}^w (-1)^{w-i} \frac{w!}{[i! (w-i)!]} (q_0 + iq_1 \frac{1}{w})^{k-1} \quad 5.1$$

Here, $q_0 = 1 - q_1$, $q_1 = \frac{w^2}{2NL}$, w is the code weight, L is a number of wavelength code carriers (in this case $w = L$), and N is the number of chips.

The results obtained are shown in figure 5.9. Solid lines show the probability of error of two different 2D-WH/TS OCDMA systems: one that has four wavelength code carriers ($w = 4$) and $N = 53$ chips, denoted by $(w, N) = (4, 53)$, and the second, having $w = 8$ and $N = 53$, denoted by $(8, 53)$. Dashed lines represent calculations of the respective degraded Pe due to the code carrier redshift, which causes autocorrelation peak reduction from w to $w-1$ (i.e., from 4 to 3 and from 8 to 7, respectively).

As illustrated in Figure 5.5, varying the SOA driving current between 50 mA and 250 mA leads to a redshift in 2D-WH/TS code carriers, ranging from 0.08 to 0.8 nm. An analysis of the results presented in Figure 5.5 reveals the effects of the SOA-induced redshift on the OCDMA system's performance and the number of concurrent OCDMA users. Initially, the performance of the $(8, 53)$ OCDMA system was evaluated without the presence of SOA.

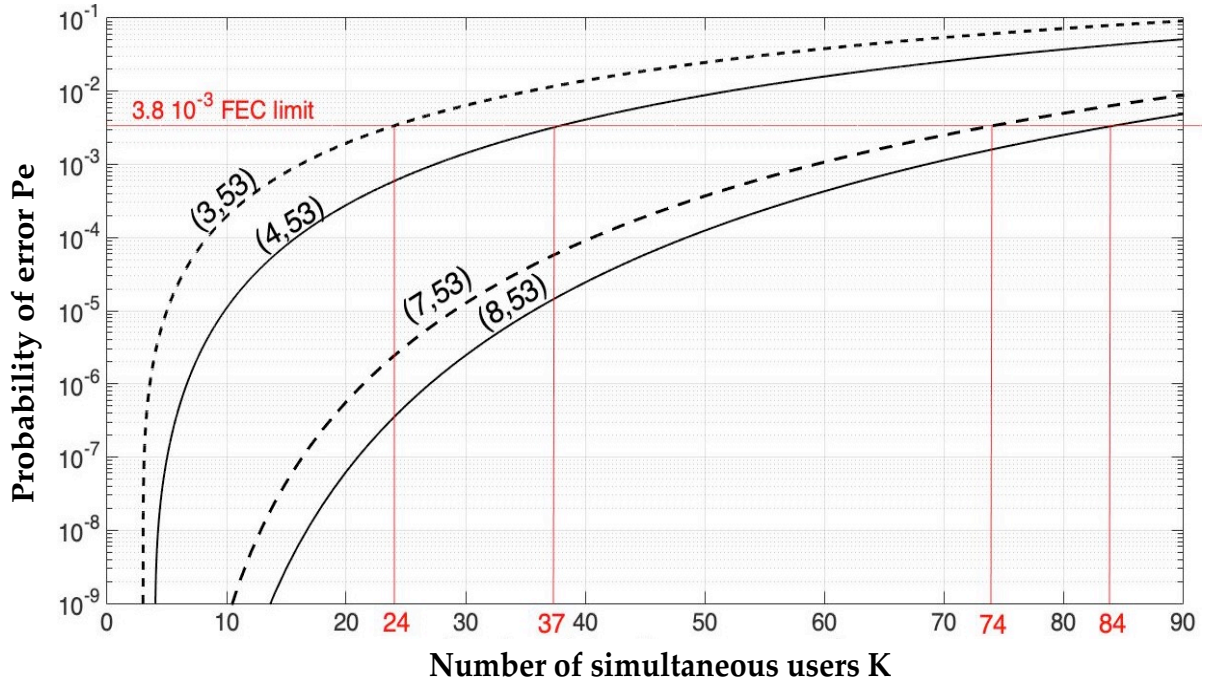


Figure 5. 9. Probability of error as a function of K simultaneous users for a $(4, 53)/(3, 53)$ and $(8, 53)/(7, 53)$ 2D-WH/TS OCDMA system without/with the deployment of an SOA, respectively, the latter causing a one channel code carriers' redshift.

The system supports 14 simultaneous users, each operating at Pe of 10^{-9} . Thanks to OCDMA soft-blocking capabilities, one can readily trade the system's Pe for a number of simultaneous users and then take advantage of the implemented hard-decision forward error correction (HD-FEC) with 7% overhead. By doing so, the number of simultaneous users will be increased (up to 84) by allowing a drop in the Pe to 3.8×10^{-3} and then in turn using FEC to return the Pe back to 10^{-9} (see figure 5.9). However, the SOA present in the transmission link driven at 250 mA leads to the code carriers' redshift of 0.8 nm equal to their channel spacing. As a consequence, the system's OCDMA autocorrelation is reduced by 1 (from 8 to 7) and the $(8, 53)$ -OCDMA system now performs only as $(7, 53)$ -OCDMA. This will result a drop in the number of simultaneous users from 14 to 10 or 84 to 74 with the FEC Pe of 10^{-9} , respectively. Similar performance degradation is demonstrated for a $(4, 53)$ -OCDMA when the system operates under the same experimental conditions. The SOA's 250 mA driving current-induced redshift of 0.8 nm equal to code carriers channel spacing causes a drop in the number of simultaneous users from 4 to 3 or 37 to 24 with the FEC Pe of 10^{-9} , respectively. Thus, the $(4, 53)$ -OCDMA system only performs as $(3, 53)$ -OCDMA to maintain the Pe of 10^{-9} .

5.4 Manipulation of chirp to mitigate SPM effect

When certain devices are used in an optical network, the optical pulse may be subjected to undesirable frequency chirp, which causes pulse broadening and pushes the optical pulse outside of its slot. Prior to transmission, the chirp profile of an optical pulse (pre-chirp) can be changed to significantly minimise or even remove the dispersion penalty [42]. For this purpose, the GVD is precisely adjusted by a straightforward technique that pre-chirps each optical pulse in the opposite direction by the necessary amount, ensuring that the pulse will keep its shape at the fibre output. Pre-chirping is also applied in WAM networks, where it offers a reliable solution to address saturation-induced SPM [122]. The implementation of pre-chirping, however, is complex. For instance, if the optical pulses produced by the transmitter have a positive chirp, the pulse broadens as a result of propagation through a normal dispersion region ($\beta_2 > 0$) because the positive chirp becomes increasingly positive (i.e. the speed of higher frequency components towards the leading edge will be even slower). On the other hand, the positive chirp can be reduced to zero if these optical pulses pass through an area with an anomalous dispersion ($\beta_2 < 0$), which occurs after covering a distance of L_D . This causes the GVD effect to be compensated. Further, as the distance L exceeds length L_D , further propagation in the fibre causes the pulse to broaden as the effect of GVD turns positive [77]. In conclusion, the pulse narrows initially if the product $\beta_2 C < 0$ and the travel distance $L < L_D$, it then broadens as soon as $L > L_D$, until the end of the fibre link. To put it another way, an optical pulse with the chirp parameter C and $\beta_2 C < 0$ initially experiences a narrowing in width before gradually becoming wider. This scenario also applies to optical pulses where the transmitter output features a negative value of C ($C < 0$), where they would propagate in the optical fibre with normal dispersion ($\beta_2 > 0$ and $DCD < 0$), and where the propagation leads to $C\beta_2 < 0$. In general, pulse width widening of up to $\sqrt{2}$ is considered permissible.

Also, pre-chirping technique if it not understood can cause severe changes on the spectral of the input pulses [78]. Therefore, understanding pre-chirp technique and correctly deploy it can increase rapidly the transmission distance for 50% or more. Further explanation on this topic is found in chapter 3.

In this section, the redshift induced chirp caused by the SOA saturation from the section 5.4. is mitigated using two methods. The two methods utilise pre-chirp techniques. The first technique uses lithium-niobate crystal to compensate for the SPM after passing SOA which accompanied all code carries in the 2D WH TS OCDMA system from the previous section in

this chapter. The second technique is utilising anomalous dispersion fibre to counteract larger amount of induced redshift.

5.4.1 Lithium-niobate crystal

In this section the saturation induced SPM imposed on the 2D WHTH OCDMA prime code carriers from previous section will be addressed.

Before we get into why we choose LiNbO_3 modulator to council out the ramification that occurs from deploying SOA in the network, we need to find out, from the point of dispersion penalty, if the additive chirp of the whole setup is a positive or negative chirp. Before adding the LiNbO_3 modulator to the setup shown in figure 5.11 FBG encoders generate 2D-WH/TS OCDMA code with chirp parameter of $C = 0$ as it is demonstrated in chapter 2. The code effected by the SOA nonlinear property (redshift) then passing a fully chromatic dispersion compensated link of total 17 km the decoder at the receiver is supposed to decode the code and retrieve the autocorrelation peak. However, all OCDMA code carriers were redshifted with $100\text{GHz}/0.8\text{nm}$ spectral spacing resulted of mismatching between the encoder and the decoder occur as shown in figure (spectral spectrum). For more information on that see detailed analyses in section 5.5.

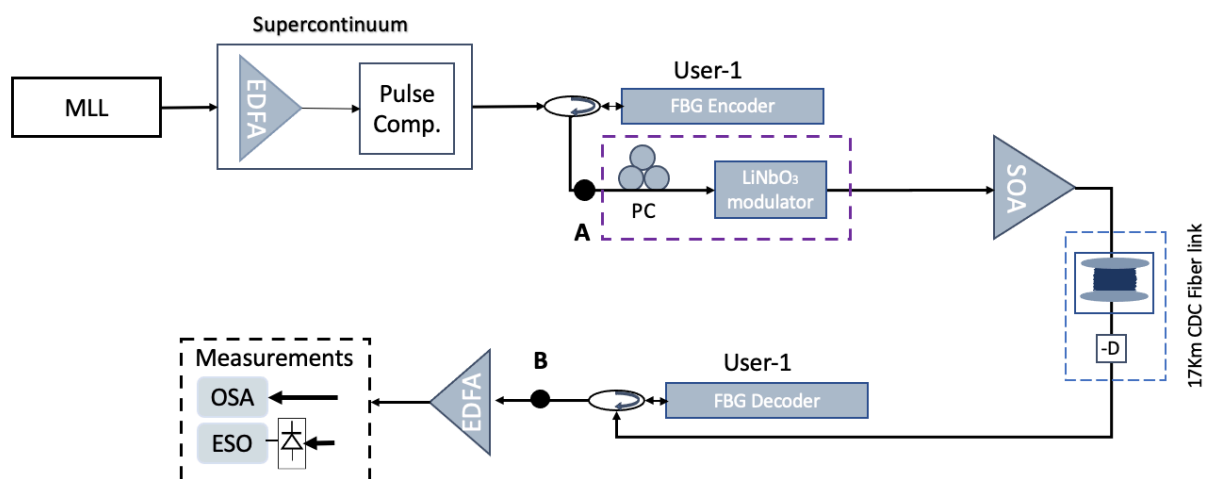


Figure 5. 10. Experimental setup of 2D-WH/TS OCDMA using LiNbO_3 to mitigate SOA induced redshift. Wehere, MLL – mode locked laser, EDFA – erbium doped fibre amplifier, FBG – fibre Bragg grating, SOA – semiconductor optical amplifier, PC – polarisation controller, OSA – optical spectrum analyser, ESO - electrical sampling oscilloscope.

Since the pulse modulates its own phase through gain saturation of the SOA, saturation induced SPM on all code carries can be cancelled out if you select device with reverse effect of the SOA. Our SOA chirp parameter was examined in [79] and is to be $C > 0$ and we used for that LiNbO₃ modulator with chirp parameter of $C < 0$ [140]. The LiNbO₃ modulator was then utilised along with polarisation controller for optimum output. Figure 5.11 illustrates the autocorrelation function of (4, 53) 2D WH TS OCDMA code with 13 ps pulse-width at FWM. In figure 5.12, an autocorrelation peak power of the four wavelength is measured back-to-back.

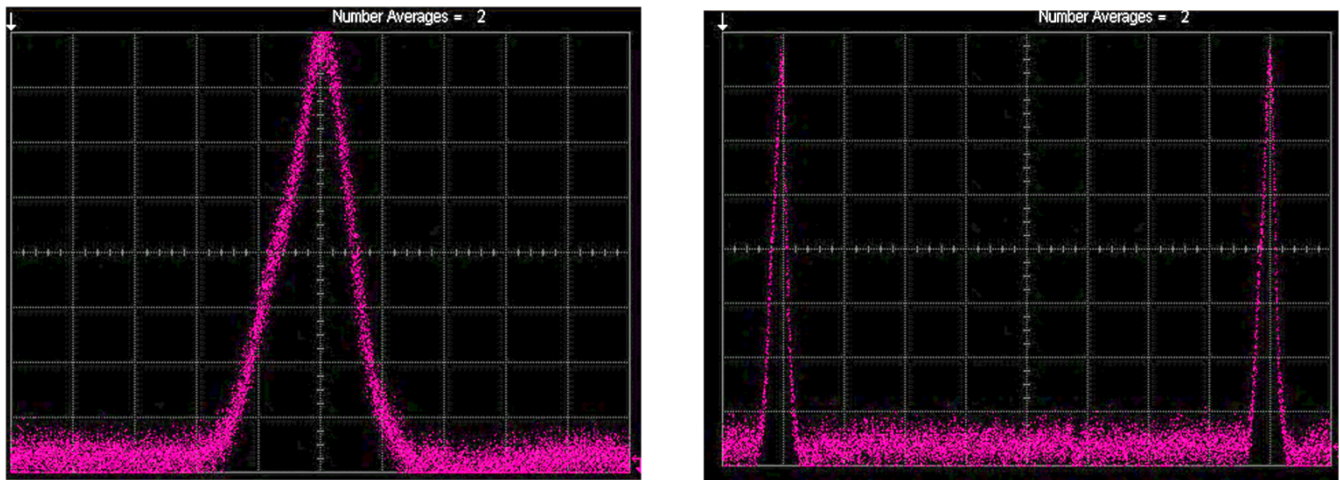


Figure 5. 11. (4, 53) 2D WH TS OCDMA autocorrelation peak as seen on the oscilloscope with back-to-back setup.

After OCDMA code carries passed the SOA with a bias current of 170 mA and transmission line the autocorrelation is completely viciously distorted by additional pulses created by the mismatch encoder and decoder. Moreover, the pulse width of the autocorrelation peak power is measured to be 20 ps as shown in figure 5.13.

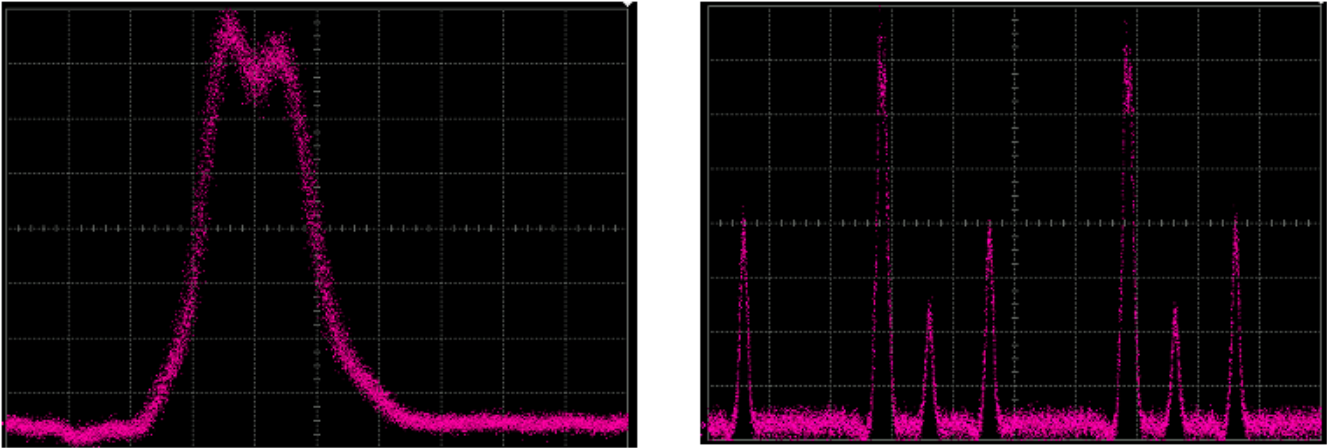


Figure 5.12. Exhibit the effect of SOA redshift at bias current at 170 mA on (4, 53) 2D WH TS OCDMA autocorrelation peak.

When the unit of the PC and LiNbO₃ modulator is added to the setup as shown in figure 5.11 the autocorrelation peak was still very heavy distorted. This is because the imposed chirp by the modulator is not enough to mitigate the full spectral redshift. From the spectrum measurement of the code carries after adding the modulator, the maximum blue shift can be obtained is 0.64 nm when the SOA bias current is 170 mA as it is shown on the autocorrelation peak in figure 5.14. The autocorrelation pulses-width is retrieved as the back-to-back 13 ps.

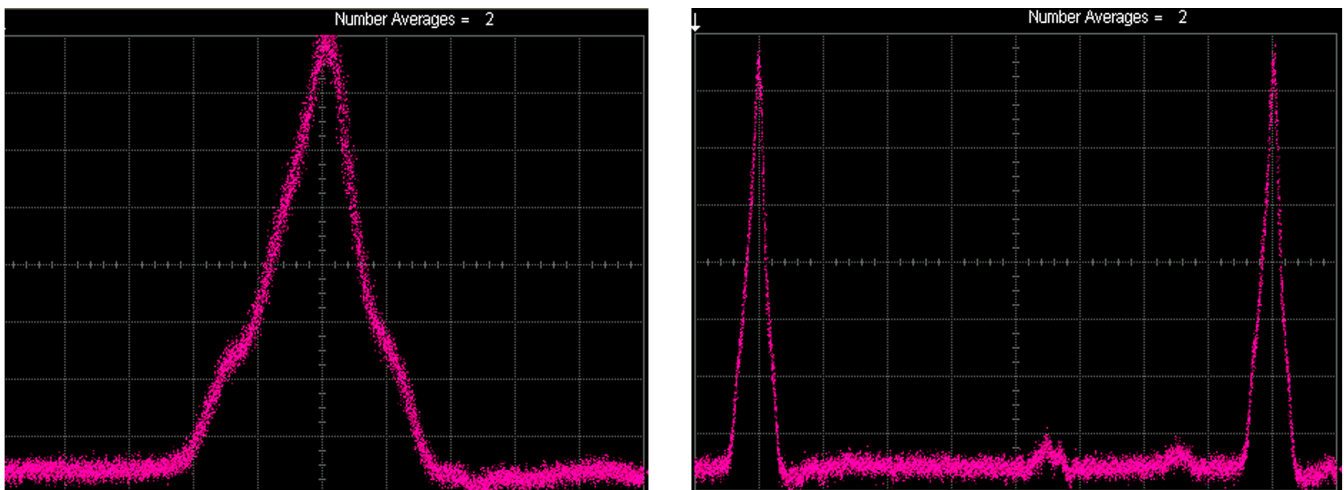


Figure 5.13. Illustrate how negative chirp is imposed on the code after deploying LiNbO₃ modulator mitigates the redshift caused by SOA with bias current of 170 mA.

5.4.2 Anomalous dispersive fibre

The effect of anomalous dispersion fibre is to shift the SPM generated frequencies towards the centre of the pulse. The SPM imposes a frequency chirp [141].

The SPM is a consequence of the gain saturation and variation of the refractive index profile on the leading and tailing of the optical pulse.

As it is shown in figure 5.15, an optical clock of 1547 nm with linewidth of 1.4 nm is generated using erbium doped fiber mode locked laser (FMLL). The optical clock is driven by an RF synthesizer at 2.5 GHz. The optical clock pulses then enter an optical supercontinuum (OS) generator, which consists of a 25 dBm EDFA and an approximately 1 km long dispersion decreasing fiber, thus producing a 3.2 nm wide optical spectrum. A wavelength of $\lambda_1 = 1550.035$ nm is generated by multiplexer (MUX) and enter an anomalous dispersive module of 1300 m with $\beta_2 = -20$ ps²/km. power controller module is used to control the input optical pulse power passing to the SOA. Another anomalous dispersive module of 16 km of SMF-28 is used as a transmission line. This link is fully compensated from chromatic dispersion by adding 2500 m normal dispersion fiber. To measure and monitor accurately, the pulse broadening and SPM Femtochrome optical autocorrelator is used and optical spectrum analyser.

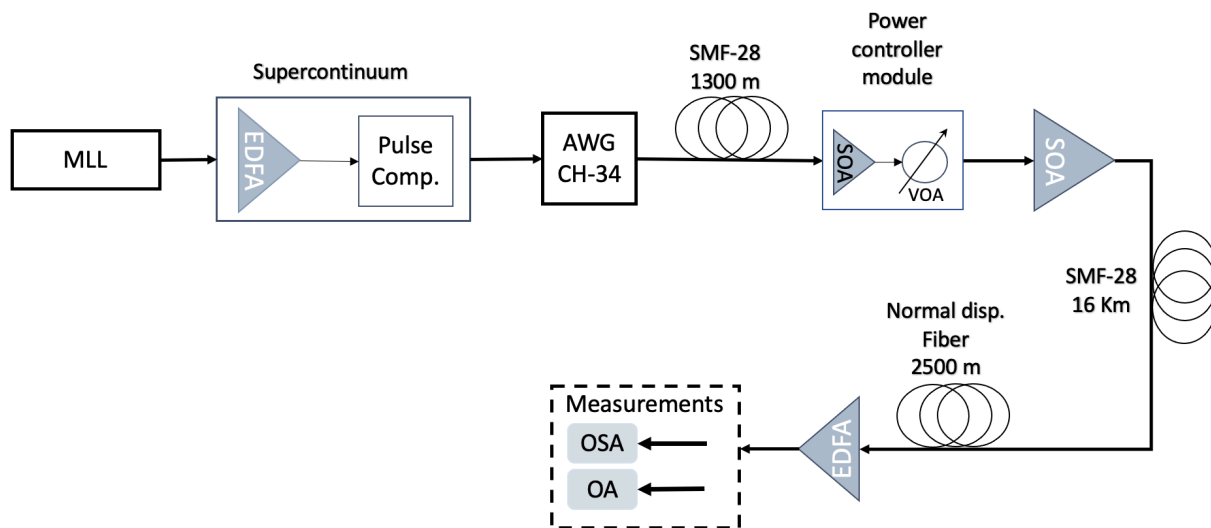


Figure 5. 14. Schematic diagram of the experimental setup. MLL - mode lock laser. EDFA - Erbium doped fibre amplifier. VOA - variable optical attenuator. OSA - optical spectrum analyser. OAC - optical autocorrelator.

This experiment exploits optical fibre with $\beta_2 < 0$ to mitigate the SPM induced on the optical pulse. Anomalous dispersion fibre consists of GVD ($\beta_2 < 0$). The unchirped ($C = 0$) optical pulse can have a reverse effect on the optical pulse passing the SOA. Since the optical pulse is now accompanied with SOA chirp of ($C > 0$) (up-chirp) we can mitigate the saturation induced SPM by choosing the correct length of the additional fibre, as will be shown in this experiment.

For an input pulsed beam, the induced time-dependent phase change is associated with a modification of the optical spectrum, which depends on the initial frequency modulation (chirp) of the pulse electric field. If the pulse is initially Fourier-transform-limited or up-chirped, SPM leads to spectral broadening, whereas an initially down-chirped pulse is spectrally compressed by the effects of SPM. For strong SPM, the optical spectrum can exhibit strong oscillations.

The input pulse is initially Fourier transform limited as it is shown in figure 5.16 the pulse with is 7.6 ps with central wavelength of 1550.035 nm.

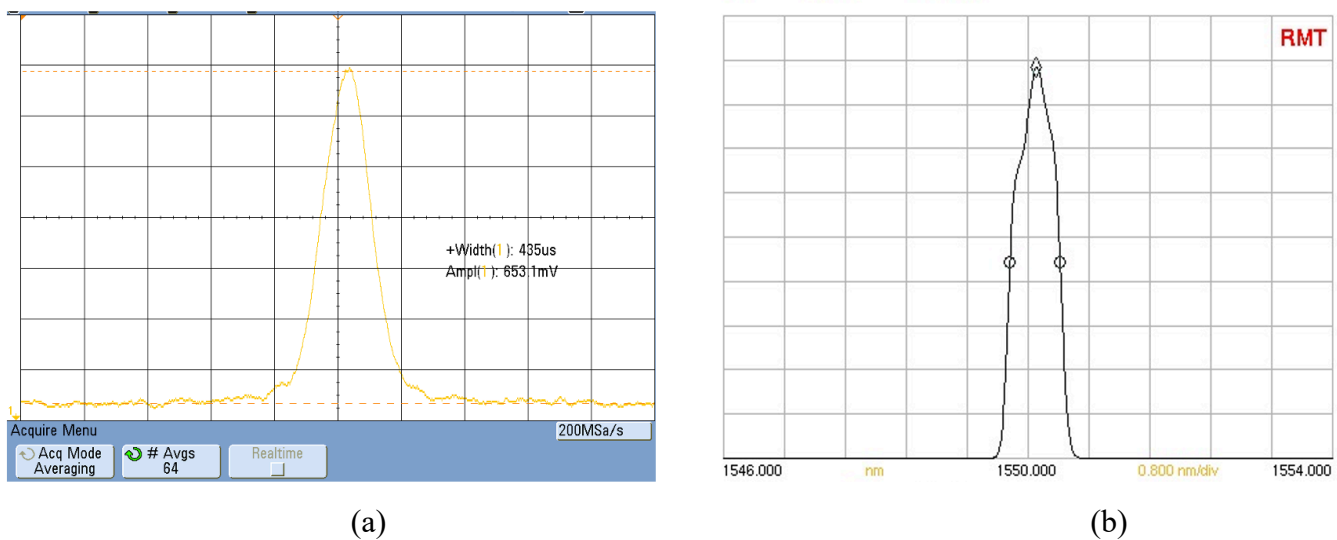


Figure 5.15. Shows, in the right, the optical pulse of $\lambda_1 = 1550.12$ nm with FWHM of 7.6 ps. In the left is the input optical spectral with linewidth of 0.6 nm.

After the wavelength passes the SOA, SPM leads to spectral broadening of the pulse as shown in figure 5.17 strong SPM exhibit strong oscillations and the pulse width becomes 9.4 ps and its frequency spectrum is redshifted 0.84 nm.

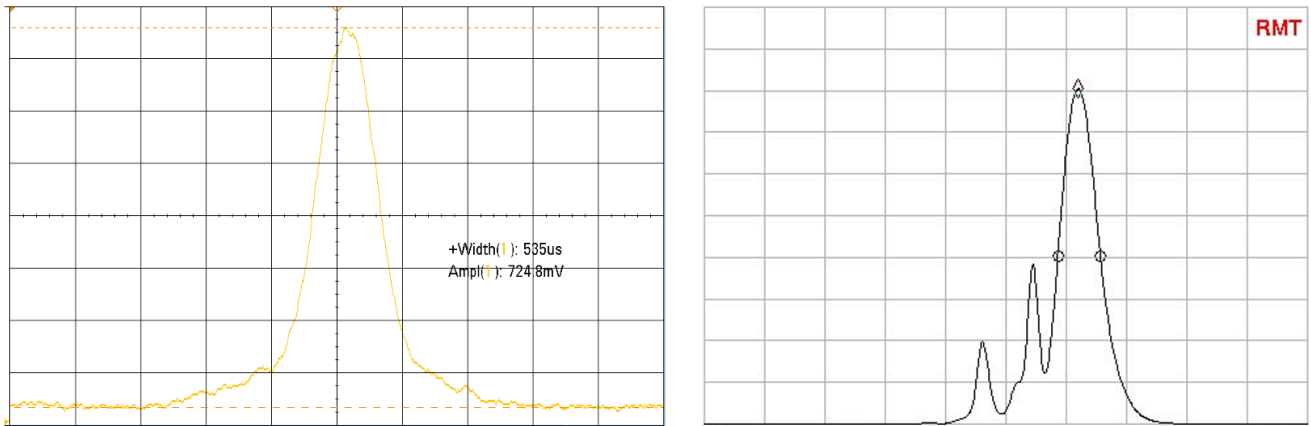


Figure 5.16. Shows, on the right, the redshift of 0.84 nm from the original wavelength $\lambda_1 = 1550.035$ nm. On the left, the optical pulse of 9.4 ps. This figure was captured without the additional 1300 m SMF 28 to the setup.

After adding the 1300 m of anomalous dispersion fiber ($\beta_2 < 0$) to the setup, we could say that the optical pulse is full retrieved from with pulse width of 7.5 ps and central wavelength of 1550.039 nm as shown in figure 5.18.

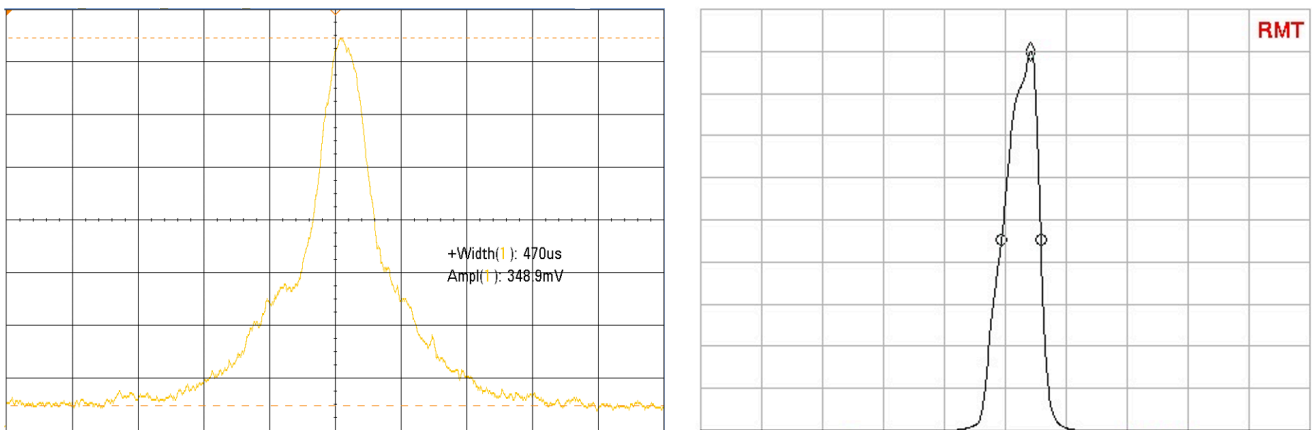


Figure 5.17. On the right, is the measured optical pulse in time domain using optical autocorrelator. The optical pulse at FWM is fully retrieved to 7.6 ps. On the left, the optical spectrum of the output pulse after passing through the EDFA at the receiver side.

Positive chirp: At the leading edge of the optical pulse, absorption drops, and the refractive index decreases. The consequent transient phase variation is traduced by a transient optical

frequency increase (blue shift). Opposite shift occurs at the falling edge of the pulse, leading to a transient optical frequency decrease (red shift). The chirped signal propagating in a standard fiber at 1550 nm is broadened since blue shifted component has a higher group velocity than red shifted component “blue and red chirp”.

When this pulse is transmitted through fiber with anomalous dispersion (positive dispersion coefficient, D), the blue-shifted (shorter wavelength) components of the pulse will travel faster than the red-shifted (longer wavelength) components. This results in the pulse broadening more quickly than if chirp were not present, reducing the maximum possible transmission distance. On the other hand, if the pulse experienced negative chirp or if the fiber was operated in the normal dispersion region, the pulse would initially narrow before broadening. In this manner, system designers can use chirp to their advantage or deliberately.

5.5. Chapter summary

In this chapter, the impact of SOA-induced wavelength redshift on 2D-WH/TS multi wavelength picosecond code carriers was investigated for the first time. For the SOA bias current of 50 to 250 mA, the amount of induced redshift was found to be 0.08 to 0.8 nm. Next, the detrimental effect of 0.8 nm redshift on (8, 53)- and (4, 53)-WH/TS OCDMA systems was investigated. It can be stated that, when the amount of SOA-induced redshift is equal to the code carriers' wavelength channel spacing, then a (w, N) -WH/TS OCDMA system will only perform as a $(w-1, N)$ -WH/TS OCDMA system to maintain the Pe of 10^{-9} .

To mitigate the saturation SPM effect two methods were provided and results were presented and discussed. The first solution used lithium-niobate crystal to compensate for the SPM after passing SOA. In the second solution, an anomalous dispersion fibre is used to counteract larger amount of induced redshift. To the best of my knowledge, this is the first time these pre-chirped techniques have been proposed for mitigating SOA-induced redshift in 2D OCDMA systems.

Chapter 6

Applications of SOA based Devices for Improving 2D - WH/TS OCDMA Network Performance

6.1. Enhancing physical layer communication privacy by using SOAs in OCDMA networks

With a wide range of applications, such as IG, steganography and XOR, the research area of information concealing has garnered a lot of attention recently [142]. In general, there are two types of information concealment techniques: side information and steganography. Side information includes watermarking and various types of cryptography [143]. The implementations typically take place at the higher levels of networks, where side information is digitally processed. The performance of these implementations, however, is somewhat questionable as nearly all digital watermarking methods are vulnerable to cyber-attacks [142]. Therefore, it is advisable to make use of the physical layer [142]. There the operation is not restricted to the field of digital electronics, which gives the physical layer implementation its apparent advantage. In particular, the degree of unknowns for potential security breaches is increased, making it more secure. In addition to being one of the candidates for implementing physical security, OCDMA systems are an emerging research topic for offering flexible access solutions [144] [145].

In the first part of this chapter, I will introduce a new enhanced technique for improving privacy and security in wavelength-hopping/time-spreading incoherent OCDMA communication system (2D WH/TS OCDMA). The proposed technique requires a single semiconductor optical amplifier (SOA) accompanied with a correlated length of a propagation fiber link to adequately stimulate the nonlinear self-phase modulation (SPM) effect in the transmission line leading to wavelength conversions (frequency shift) of the OCDMA code

carriers. At the receiver side, a newly designed 2D-OCDMA decoder based on a matched filter “synchronized” to the resulting new code sequence removes the wavelength translations (shifts) to properly recover the user data.

6.1.1. System setup

Figure 6.1 illustrates the setup to demonstrate -enhanced privacy 2D-WH/TS OCDMA networks by deploying SOA at the transmitter side. Initially, a mode-locked laser is used to generate pulses centred on a wavelength of 1547 nm which are fed into a supercontinuum source with 3.2 nm of linewidth. After, an array waveguide grating (AWG) device is employed in such a wide spectrum to generate four pulses spaced from 0.5 nm wavelength. Consequently, it is created the 2D -WH/TS OCDMA code compatible with the transmission data rate of 2.5 Gb/s related to the SONET OC-48 standard. At the final stage of the transmitter, all of the four wavelengths that compose the 2D-WH/TS OCDMA code pass through an SOA (OPA-20-N-C, Kamelian) device biased with an electrical current of 170 mA to not only amplify the pulse but also stimulate the SPM nonlinear effect. Sequentially, the pulses are propagated by an optical channel 19 km long to the receiver. The optical channel is composed of one segment of 16.5 km of anomalous dispersion fibre and another segment of 2.5 km of normal dispersion fibre to fully compensate for chromatic dispersion. It is worth pointing out that the level of FWM nonlinear effect aggregated through propagation provides wavelength conversions to generate a new 2D-WH/TS OCDMA code at the receiver side. At the receiver side, an EDFA is used to amplify the signals and ensure enough power among all code carriers that compose the new 2D-WH/TS OCDMA code. Finally, a decoder based on the matched filter for the new 2D-WH/TS OCDMA is used to retrieve its autocorrelation peak power by using an oscilloscope with an optical sampling header of 65 GHz.

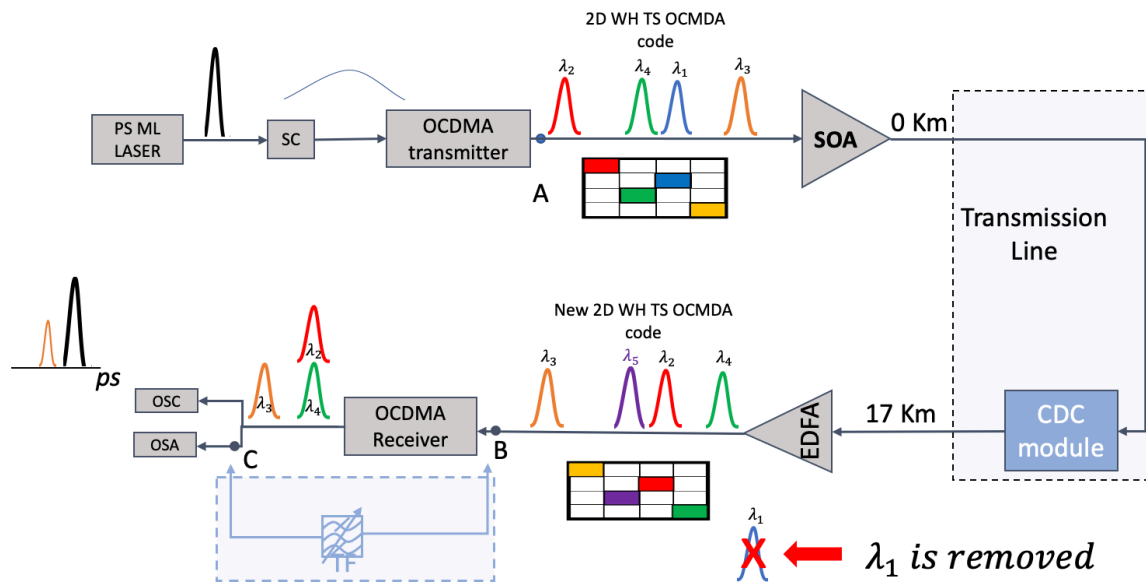


Figure 6. 1. Experimental setup of physical-enhanced secure communication system in 2D WH TS OCDMA system; PS ML – picosecond mode locked laser, EDFA – Erbium doped fibre amplifier, 2D-WH TS OCDMA – wavelength hopping time spreading optical code division multiple access, CDC –chromatic dispersion compensation, SOA – semiconductor optical amplifier, OSC – optical oscilloscope, OSA- Optical spectrum analyser, SC – supercontinuum.

6.1.2. Obtained results and analysis

The physical-enhanced secure 2D-WH/TS OCDMA network described in the previous section is now evaluated. Before starting the network performance analysis, itself, it becomes necessary to define properly the code sequences utilized. The 2D-WH/TS code is denoted as (4,47), where 4 is the code carriers and 47 is the code length (no. time chips). Such code annotation is employed to generate encoded pulses with full width at half maximum (FWHM) of 8 ps within chip times of 8.5 ps. The spectral representation of the encoded pulses is shown in figure 6.2.

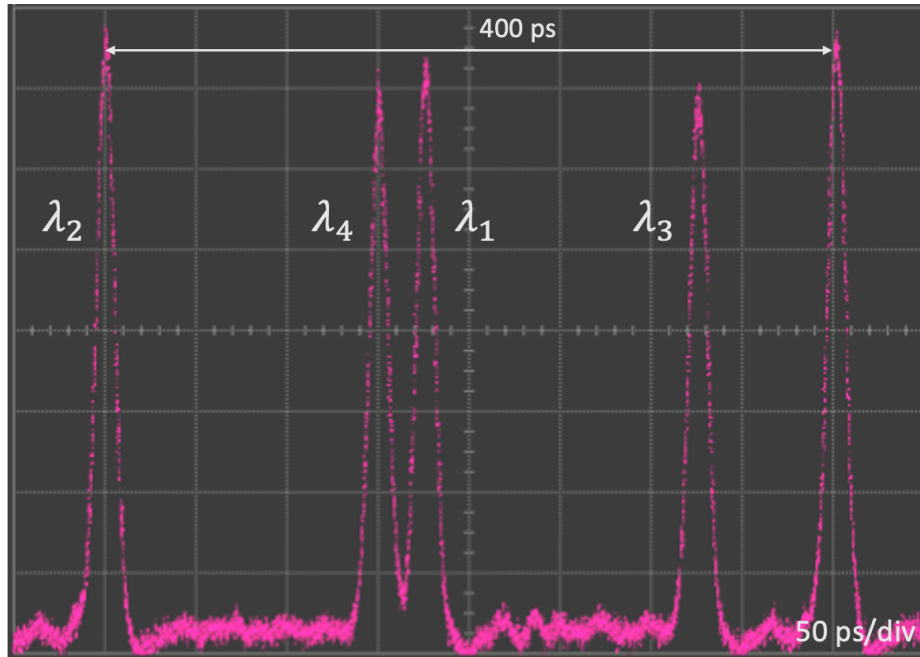


Figure 6. 2. Depicts the 2D WH TS OCDMA code measured by oscilloscope after the encoder.

Let us first describe original OCDMA system without the use of SOA, whereas the proposed physical-enhanced employs a saturated SOA to allow wavelength conversions in the code sequences. Initiating the description with the original system, the pulse generated by the supercontinuum source enters an AWG to perform the DMUX function. After each channel is filtered to pass each wavelength onto a specific channel by the DMUX, each channel passes through optical delay lines (ODL) DL_x which creates time-spreading (TS) in each wavelength, as shown in figure 6.3. In this manner, each wavelength is delayed with a specific displacement of picoseconds order resulting in time spreading sequence. After that, all wavelengths are combined in a single optical fibre to form a specific WH TS encoded signal as shown in figure 6.3.

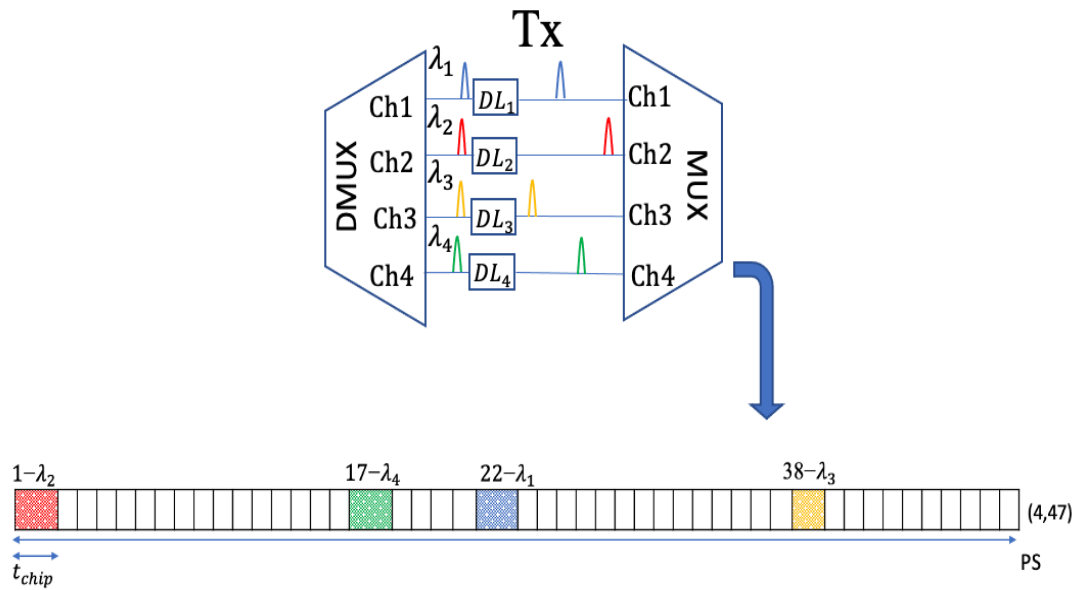


Figure 6.3. Illustration of the structure of the 2D WH TS OCDMA encoder.

At the receiver side, considering the link is fully compensated for skewing and chromatic dispersion, the decoder performs the function of a matched filter to correlate the encoded signal with the impulse response of the encoder. To ensure that all wavelengths arrive within a single window to form the autocorrelation peak, the delay lines (DL_x) at the decoder are arranged in the reverse order compared to those at the encoder. For example, as illustrated in Figure 6.3, at the encoder, λ_1 passes through delay line one, while at the receiver, λ_1 passes through delay line four, as shown in Figure 6.4.

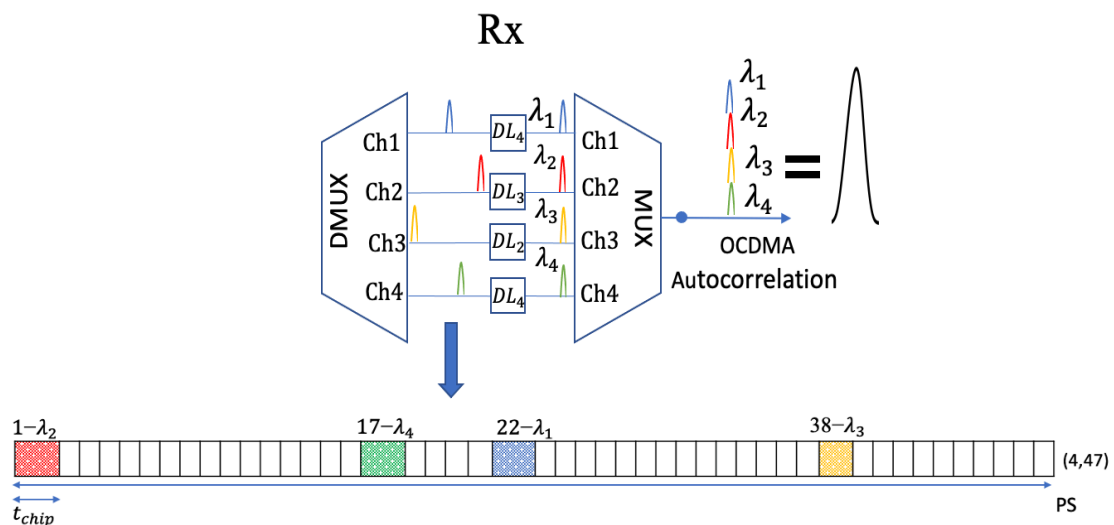


Figure 6. 4. Illustration of the structure of the decoder to retrieve the autocorrelation peak.

I derived an expression of autocorrelation function peak power as a function of delay lines of both the encoder and decoders in a fully compensated link as follows.

$$S(i) = \sum_{i=1}^n DL_i + DL_{(n-i)+1} \quad (6.1)$$

where n is the code weight, DL_i is the delay line for each code carrier in the transmitter, $i = 1, 2, 3, 4, \dots, n$ and $DL_{(n-i)+1}$ is the delay line for each code carrier at the receiver. This expression considers the first wavelength passing to the optical fibre from the transmitter as the reference wavelength. Since the system uses wave hopping technique, it is natural to say that the order of the wavelengths' position is based on the time spreading sequence among the pulses regardless of the code carrier order. Table 6.1 shows that the calculations using such an expression allow predicting adequately that all code carriers arrive at the same time to form the autocorrelation peak power.

λ_i	Chip no	Encoder DL_i ps	Decoder $DL_{(n-i)+1}$ ps	Autocorrelation peak $DL_i + DL_{(n-i)+1}$ ps
λ_1	22	182.75	140.25	323
λ_2	1	4.25	318.75	323
λ_3	38	318.75	4.25	323
λ_4	17	140.25	182.75	323

Table 6. 1. Calculation of the autocorrelation peak of the original decoder designed.

From the table 6.1, the algebraic summation of delay lines in the coder and decoder results in an autocorrelation peak at 323 ps with a window of 8.5 ps.

Now, let us consider the case where a saturated SOA is utilized to generate the new code from the wavelength conversion employed to the original code. In this case, the SPM nonlinear

effect is stimulated by the SOA and amplified through the propagation link to impose light shifts toward longer wavelengths (redshift) for all code carriers. All code carriers that compose the original code ($\lambda_1, \lambda_2, \lambda_3, \lambda_4$) shifted by 0.5 nm to become ($\lambda_2, \lambda_3, \lambda_4, \lambda_5$) when the signals reach the OCDMA decoder at the receiver side. For example, λ_1 at the encoder passed to DL_1 and after is shifted 0.5 nm redshift to become λ_2 while its time still remains associated with original λ_1 delay line (DL_1). Such an effect will impact on both the wavelength hopping pattern and time spreading sequence. The original wavelength hopping pattern was ($\lambda_2, \lambda_4, \lambda_1, \lambda_3$) and at the receiver the code arrives as ($\lambda_{2 \rightarrow 3}, \lambda_{4 \rightarrow 5}, \lambda_{1 \rightarrow 2}, \lambda_{3 \rightarrow 4}$). This conversion is illustrated in the frequency domain (FD) at the top of the figure 6.5.

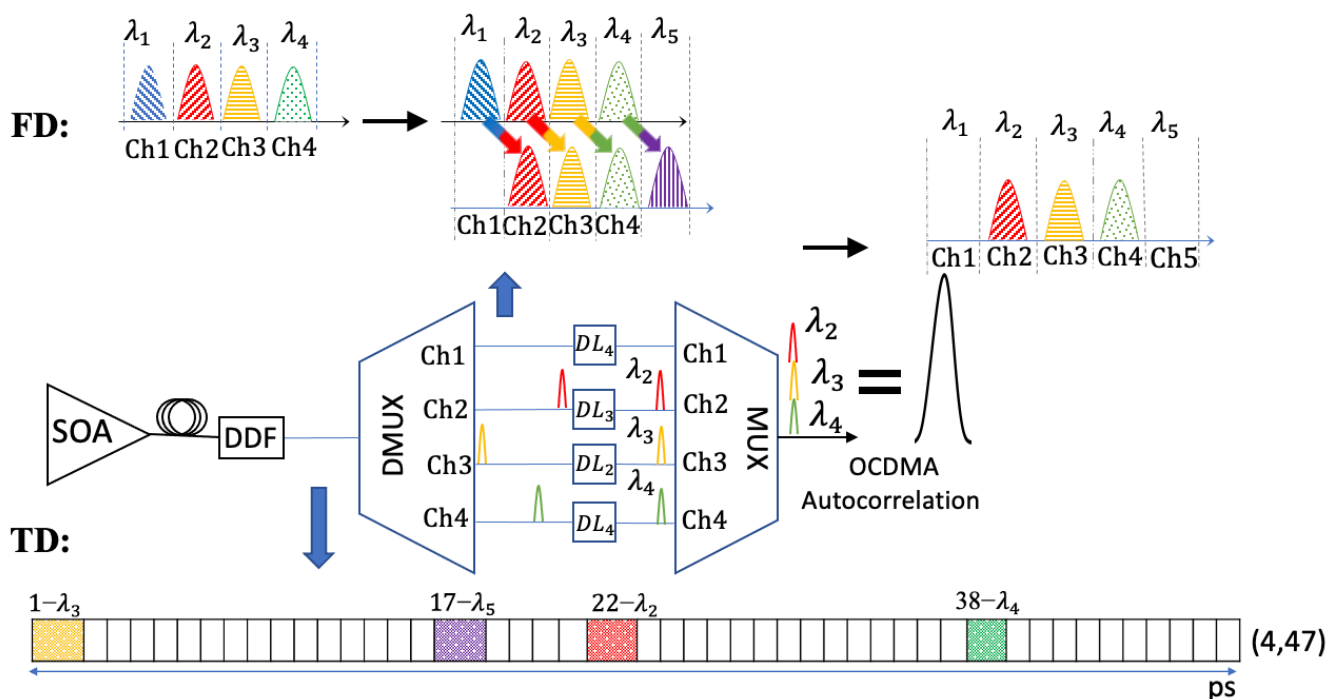


Figure 6. 5. Illustrates the newly formatted 2D WH TS OCDMA code in time and frequency domains imposed by tuning the SOA at the transmitter. Where FD is the frequency domain and TD is the time domain. SOA is the semiconductor amplifier, DDF dispersion compensated fibre

Equally, the time spreading sequence (TS) is impacted by the red shift of the code carriers. This is because the new code is handled by the same delays employed by the ODLs used in the original code. In time domain the TS sequence of the code looks as the original code on the

oscilloscope ($1-\lambda_2, 17-\lambda_4, 22-\lambda_1, 38-\lambda_3$) as shown in figure 6.2. However, this code has completely new TS sequence ($1-\lambda_3, 17-\lambda_5, 22-\lambda_2, 38-\lambda_4$). To verify this newly formatted code shown in figure 5.6. before the decoder, a tuneable optical filter of 0.8nm was connected from point B (figure 6.1) by 50:50 coupler to the OSA and oscilloscope in point C to verify each wavelength position in the time spreading sequence of the code. At this point, it is interesting to see the impact of receiving the new code from the matched filter (decoder) for the original sequence. Moreover, the stimulation of the SPM nonlinear effect combined through the propagation channel causes a significant redshift to all wavelengths resulting in the new code annotation. Consequently, the induced SPM on λ_4 generates the new wavelength λ_5 which cannot be filtered by the original decoder.

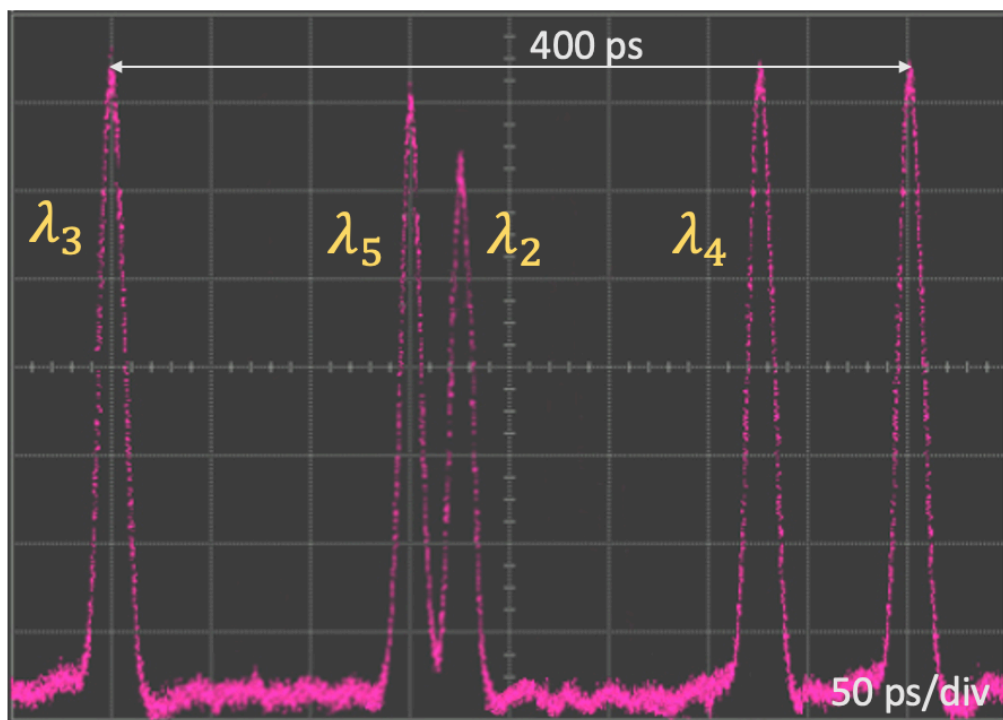


Figure 6. 6. shows the newly formatted 2D-WH/TS OCDMA at point B before the decoder using tuneable filter.

It is possible to predict the expected time the new wavelengths arise at the output of the original receiver. Such information is extremely important to determine the lengths of ODLs (DLx) to be used in designing of the matched filter (decoder) for the new code. If this to be achieved, all new wavelengths are maintained overlapped within the autocorrelation window. The expected autocorrelation function after adding the SOA can be calculated as a function of the delay line for the original annotation of the code by:

$$S(i) = \sum_{i=1}^n DL_i + DL_{n-i} \quad (6.2)$$

Here n is the code weight, DL_i is the delay line for each wavelength in the code in the transmitter, $i = 1, 2, 3, 4, \dots, n$ and DL_{n-i} is the delay line for each wavelength in the code in the receiver. It is important to mention that the decoder used throughout this experiment is designed to match the original code to retrieve the autocorrelation peak. Such decoder helps to evaluate the expression 6.2 of the autocorrelation. To verify this novel derived equation for the prediction of autocorrelation peak at the receiver, the original DLs of the decoder were used in the equation. As shown in table 6.2 and figure 6.6, a great correlation between the practical results and the calculation using equation 6.2 was observed.

λ_i	λ_{i+1}	Chip no	Encoder DL_i ps	Decoder DL_{n-i} ps	Autocorrelation peak $DL_i + DL_{n-i}$ ps
λ_1	none	none	none	none	None
λ_2	λ_2	1	182.75	318.75	501.5
λ_3	λ_3	38	4.25	4.25	8.5
λ_4	λ_4	17	318.75	182.75	501.5
λ_5	none	none	140.25	none	140.25

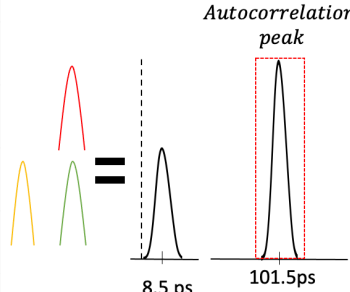


Table 6. 2. Calculation of the 0.5nm redshift induced on all code carriers and its effect on the autocorrelation peak.

As shown in table 6.2, the autocorrelation peak generated by passing the new code through the original decoder was calculated using equation 6.2. In this context, the autocorrelation peak (higher pulse) formed at 501.5 ps consists of only two wavelengths λ_4 and λ_2 instead of four wavelengths. Since the code spreads over 400 ps, the new autocorrelation peak is formed at 101.5 ps ($501.5 \text{ ps} - 400 \text{ ps}$) in the new frame due to code repetition. Also, another peak is formed for wavelength λ_3 (previously λ_2) and is located at 8.5 ps (100 ps far from the autocorrelation). As can be observed from figure 6.7, the autocorrelation peaks at the right and left are formed at 8.5 ps and 101.5 ps, respectively. Therefore, it can be concluded that the calculations proposed are very close to the experimental results obtained.

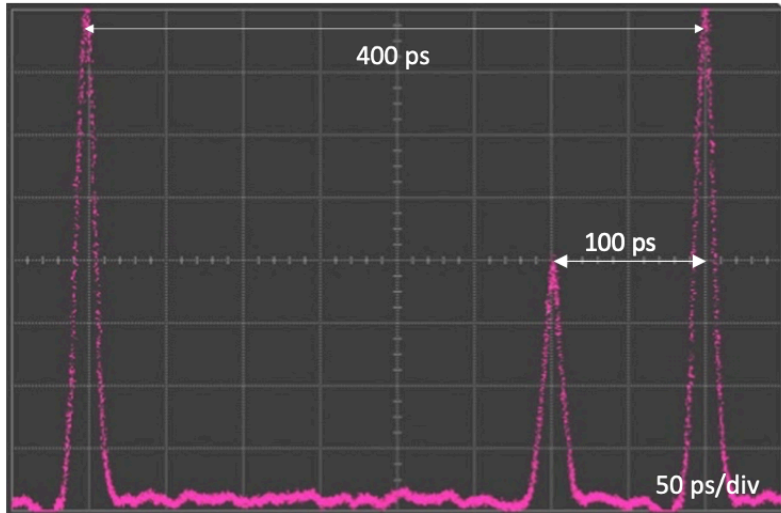


Figure 6. 7. Autocorrelation peak of two perfectly aligned wavelengths with one mismatched wavelength.

In order to successfully implement the proposed privacy enhancement in OCDMA networks the OCDMA decoder design must include two keys features in order to retrieve the autocorrelation peak of the newly created code sequence. Firstly, the newly created wavelength code carrier λ_5 requires addition filter to be added to the decoder. Secondly, in the decoder, the delay lines of λ_3 and λ_5 need adjusted to 497.25 ps and 361.25 ps time delays respectively to properly overlapping all code carriers at 501.5 ps forming the autocorrelation peak. As shown in table 6.3.

λ_i	λ_{i+1}	Chip no	Encoder $DL_{\lambda_{i+1}}$ ps	Decoder DL_{λ_j} ps	$DL_{\lambda_{i+1}} + DL_{\lambda_j}$ ps
λ_1	None	None	None	None	None
λ_2	λ_2	1	182.75	318.75	501.5
λ_3	λ_3	38	4.25	497.25	501.5
λ_4	λ_4	17	318.75	182.75	501.5
λ_5	none	none	140.25	361.25	501.5

Table 6. 3. Calculation of the autocorrelation peak of a new decoder designed considering additional delay lines and new filter for λ_5 .

In figure 6.8, the two different WH/TS code sequences generated by the same OCDMA encoder before and after using the SOA are illustrated. The top part shows the autocorrelation peak generated by the original code without using SOA. The bottom part of the figure represents the autocorrelation peak generated by the new code after implementing the additional filters to the decoder to visualise λ_5 and adjusting the delay lines of λ_3 and λ_5 . The code carriers of both autocorrelation peaks are color-coded to easily visualise the differences between the composition of each autocorrelation peak.

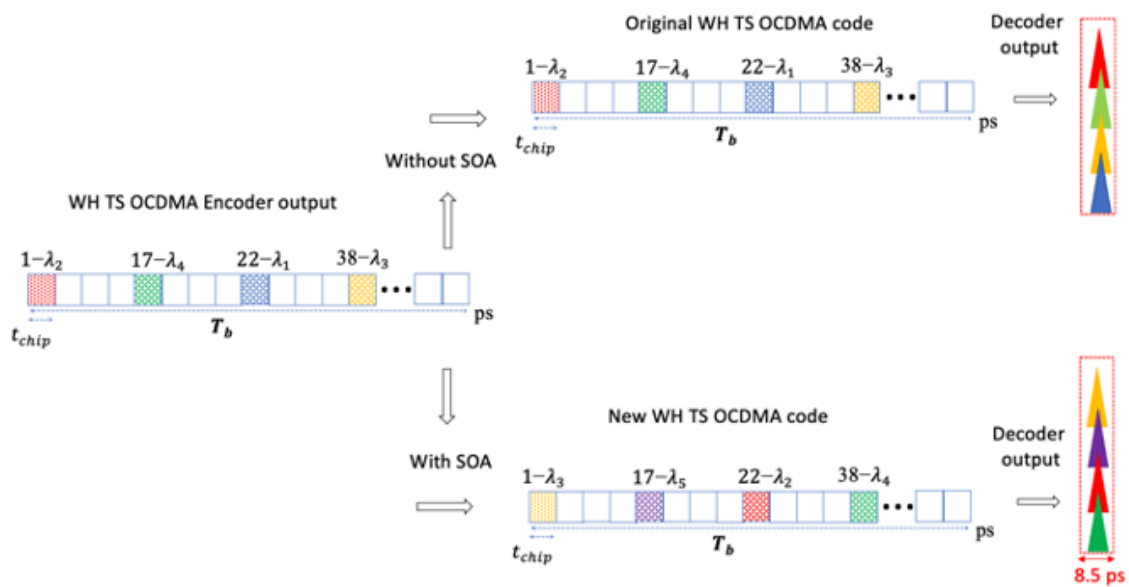


Figure 6. 8. Illustration of the two WH TS code sequences generated by the same OCDMA encoder.

6.1.3. Summary

In this chapter a physical enhanced technique based on a single SOA is proposed and experimentally evaluated. The system relies on 2D-WH/TS OCDMA with multi-colour picoseconds pulses. An equation was derived to predict the autocorrelation peak of the OCDMA system. The experimental results and calculation manifest great correlation and can be used to calculate the delay lines required for the new decoder design.

The technique relies on deploying the SOA induced redshift of 0.5 nm accompanied by the change in the *DLs* at the decoder which are mainly used to complement the *DLs*

implemented in the encoder to generate a new code. The new code carriers generated reaches the OCDMA decoder is the key to the physical-enhanced system with new wavelength hopping sequence. This new code sequence translates each code carrier exactly to its adjacent channel. On the other hand, the time spreading of the code is governed by the delay line of the original wavelengths and generates new time spreading sequence. Then, the novel derived equation is used to predict the autocorrelation peak of the OCDMA system. Finally, all these factors are now used to enhance the communication privacy in the OCDMA network with the implementation of the correct filter to obtain the autocorrelation peak of the newly formatted code.

6.2. A Tuneable Automated System for Temperature Dispersions Mitigation using SOA

The need of an adopting (automated) tuneable dispersion compensating system to correct the distorted width of the OCDMA auto-correlation peak raises from the dynamic nature of the temperature-induced dispersion. It is essential to develop an automation system that can quickly react to real-time events, such as temperature changes, taking the required measures, with the goal of reducing induced dispersion and maintaining the original pulse width of the autocorrelation at the receiver. This is because dispersion sensitivity in fibre-optic transmission systems typically increases with bit rate squared. For a given amount of chromatic dispersion, raising the data rate from 10 to 40 Gb/s, for instance, results in pulses that are four times closer together with four times the frequency content. As a result, pulses spread into each other around 16 times faster at 40 Gb/s than at 10 Gb/s. In 40 Gb/s systems, the permitted net dispersion range is roughly 60 ps/nm [1]. Over a temperature range of 60 °C, the dispersion in a 1000 km link can vary by more than 200 ps/nm. Clearly, a key factor in the design of 40 Gb/s systems is the fluctuation of fibre dispersion with temperature. The most effective dispersion-compensating methods use static targeting of a defined amount of dispersion, such as fibre models of $\beta_2 > 0$ or FBG as discussed in Chapter 3.

The OCDMA auto-correlation function may be impacted by chromatic dispersion or temperature-induced dispersion [111]. This happens as a result of data propagation in optical fibres with different lengths and/or under temperature fluctuations that have an adverse effect on the characteristics of the optical fibre. The initially fully compensated fibre link becomes overcompensated as the temperature of the fibre is raised or its length is shortened. It will become under-compensated if the fibre temperature drops or if its length increases. For

instance, in [111] [79], it was discovered that removing/adding around 80 m of SMF-28 from the original length of the fibre link would be necessary in order to make it properly dispersion adjusted again at 5/45 °C, respectively. This enables the modification of a fully compensated fibre link to replicate the behaviour of induced temperature dispersion in order to replace the effect of temperature dispersion. Instead of using temperature dispersion as discussed in [111], chromatic dispersion compensation is employed in the second part of this chapter.

In the past, the chromatic dispersion compensation of a data transmission technology employing a single wavelength as the data carrier was examined using a semiconductor optical amplifier (SOA) [10]. In the collaborative research work, it was shown that an SOA can be successfully used as a tuneable compensation device for a chromatic or temperature induced dispersion, both affecting OCDMA auto-correlation function and can mitigate the system performance degradations.

The idea behind employing a SOA for distorted OCDMA auto-correlation width adjustment is based on the fact that gain variations in a biased SOA depend on the characteristics of the refractive index medium. The SOA bias current can be changed, the SOA gain can be depleted, an optical continuous wave containing a data signal can be injected at the SOA input, or an optical pulse stream can be used to induce these changes in the SOA refractive index [120].

In order to reduce induced temperature dispersion or chromatic dispersion in an incoherent OCDMA system by utilising the tunability feature of the SOA, an autonomous dispersion management system is built and proposed for implementation in this section. The system is controlled by a software simulation (LabVIEW) that is connected to a data acquisition (DAQ) module and consists of a processing unit that is primarily fed by pre-set knowledge. Through a DC motor attached to mechanical arrangement, this unit attenuates the SOA using the information obtained from the two-dimensional wavelength-hopping time spreading (2D-WH/TS) autocorrelation shown in the oscilloscope. By adjusting the bias current to introduce the necessary changes in the refractive index of the SOA, this proposed unmanned system, with all the in situ developed and 3D printed components, manipulates the chirp of OCDMA code carriers to limit chromatic dispersion or induced temperature dispersion.

6.2.1. Description of Experimental Setup

A Mode-Locked Laser (MLL) produces optical pulses with a centre wavelength of 1545 nm and a linewidth of 2.6 nm, as shown in figure 6.9. The optical supercontinuum is then

created using the Supercontinuum Generator (SCL), which has a linewidth of 3.2 nm and a centre wavelength of 1550 nm. Four optical poles are created (carved from the supercontinuum) by utilising a Fiber Bragg Grating (FBG) OCDMA encoder (OKI Industries, Japan): $\lambda_1=1550.92$ nm, $\lambda_2=1550.12$ nm, $\lambda_3=1551.72$ nm, and $\lambda_4=1552.52$ nm. The linewidth of each wavelength pulse is 0.8 nm. A 19.5 km long SMF-28 optical fibre spool is used to convey the OCDMA code. Using a commercial Dispersion Compensated Fibre (DCF), the fibre link is fully compensated for chromatic dispersion. The 2D-WH/TS OCDMA code is amplified at the receiver via EDFA. Using the FBG decoder, the autocorrelation peak is obtained. In order to handle the code chirp, a SOA is implemented. An Agilent Oscilloscope (86100C) with an optical sampling head and a 65 GHz bandwidth was used to record the measurements.

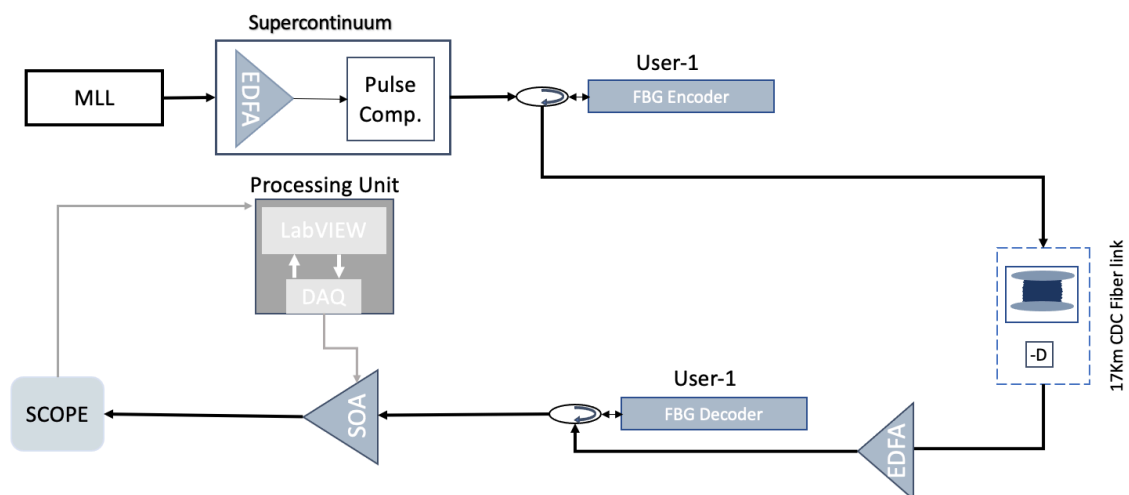


Figure 6. 9. Experimental setup of an automated system to compensate for chromatic dispersion effect on OCDMA system; MLL -mode locked laser, EDFA – Erbium doped fibre amplifier, FBG – fibre Bragg grating, CDC –chromatic dispersion compensation, SOA – semiconductor optical amplifier, DAQ – data acquisition.

The dynamic changes of temperature-induced dispersion by adding/removing 66 m of SMF to the transmission link create scenarios of autocorrelation broadening and shrinking at the receiver of 4 ps and 2 ps from the actual autocorrelation width (12 ps) respectively.

The testbed of the system was installed as depicted in figure 6.10. The SOA bias current was controlled by a potentiometer and a mechanical device was developed and employed that rotates the potentiometer in either a clockwise or anti clockwise direction, changing the current

accordingly. In this configuration the DC motor is controlled by LabVIEW through DAC. The findings and analysis section discusses the entire LabVIEW code.

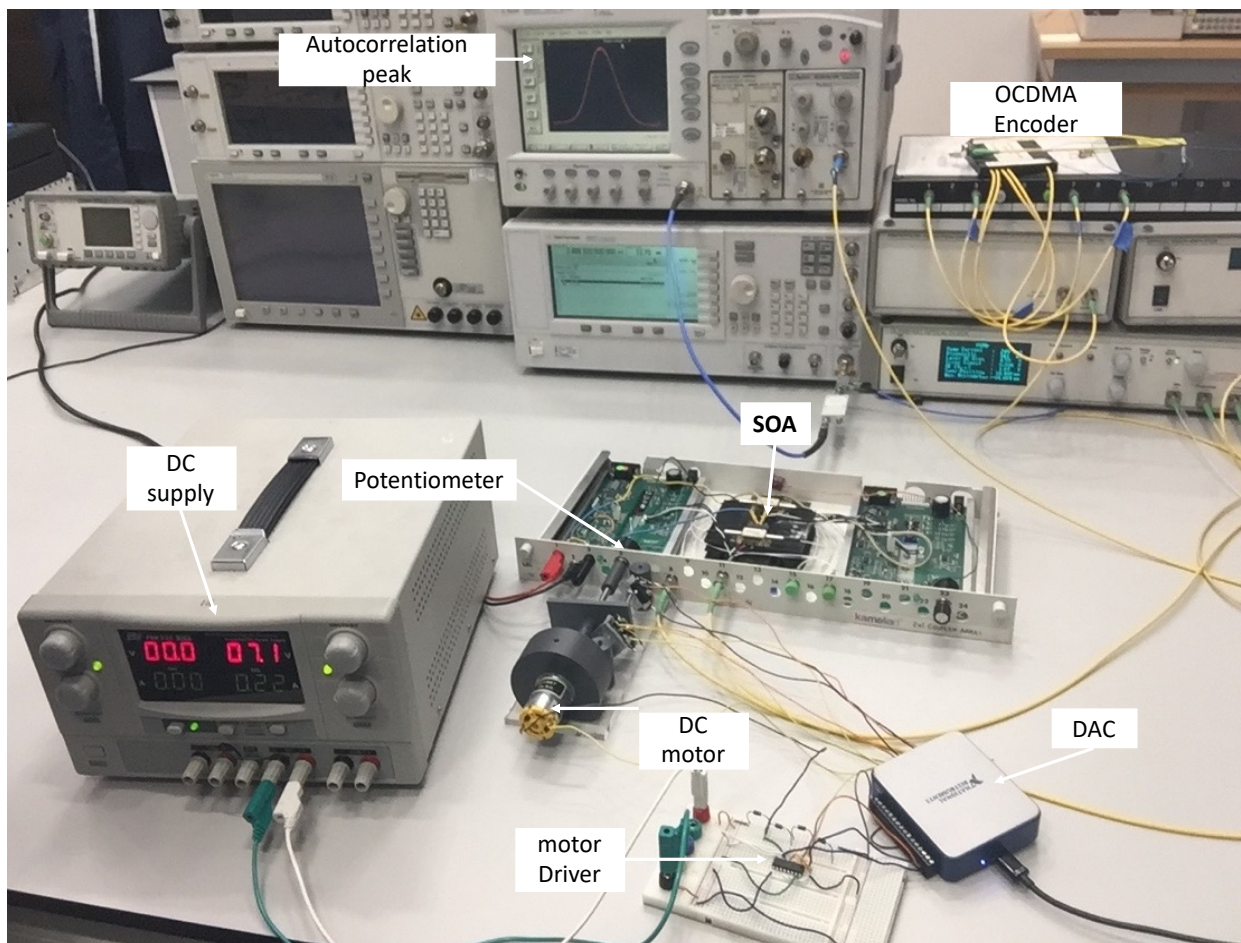


Figure 6. 10. Picture of the components of the automated tuneable system setup

The plate shown in figure 6.11 moves forward or backward when the DAC supplies the DC motor with the rotation direction and duration, thereby regulating the potentiometer, changing the current, and hence adjusting the autocorrelation width. The DC motor and potentiometer were mounted at either end of a threaded rod. To prevent the potentiometer from overturning, a rectangular plate was attached to the rod. Two switches, switch 1 (SW1) and switch 2, placed at predetermined intervals before and after the plate, allow for this mechanism. When the DC motor rotates in a clockwise direction, the plate moves forward according to the protective mechanism. The DC motor will stop when the plate presses SW1. The same applies to the anticlockwise rotation.

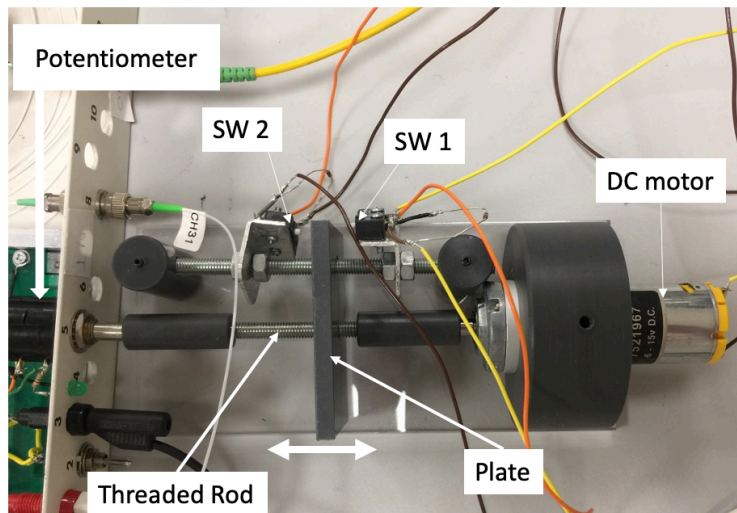


Figure 6. 11. Picture of 3D printed mechanical device to control the SOA bias current.

6.2.2. Results and analyses

The aforementioned automated adjustable testbed was successfully used in two separate instances to obtain the original autocorrelation width of 12 ps. In these scenarios, the chromatic dispersion mismatch induced by adding/removing 66 m of SMF to the transmission link, leads to a broadened and a shrunk autocorrelation peak of 16 ps and 10 ps, respectively, as shown in figure 6.12.

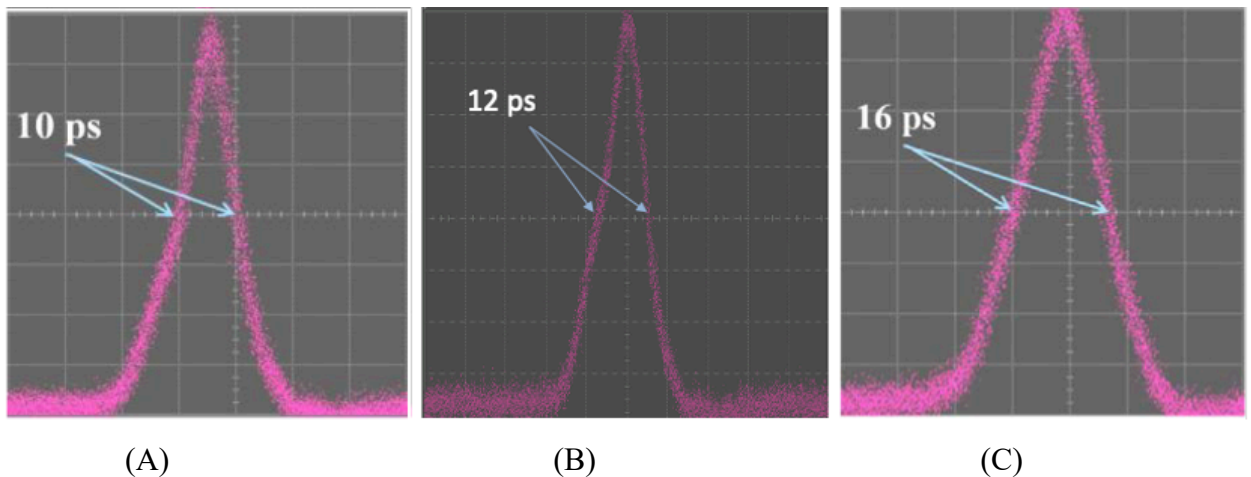


Figure 6. 12. Autocorrelation peak at the receiver before and after adding and removing 66 m of SMF: (A) shrinking of 2 ps from the original autocorrelation width,(B) back-to-back autocorrelation width, (C) broadening of 4 ps from the original autocorrelation width.

The system in the aforementioned configuration is LabVIEW-programmed. An algorithm is used to analyse the continuous oscilloscope autocorrelation peak data and compute the direction and duration of the motor. In this study a virtual instrument (VI) was employed within LabVIEW. This VI manages the interaction with the measuring device (Agilent 86100), broken down in multiple communication elements. Figure 6.13 illustrates how string format directives are sent to the oscilloscope using VISA Read and Write blocks. Firstly, the waveform source and data format are chosen. On the front panel, there is a control for choosing the source. The control provides the index of the item that was chosen, and using this information, a row from a constant string array containing the available commands is chosen.

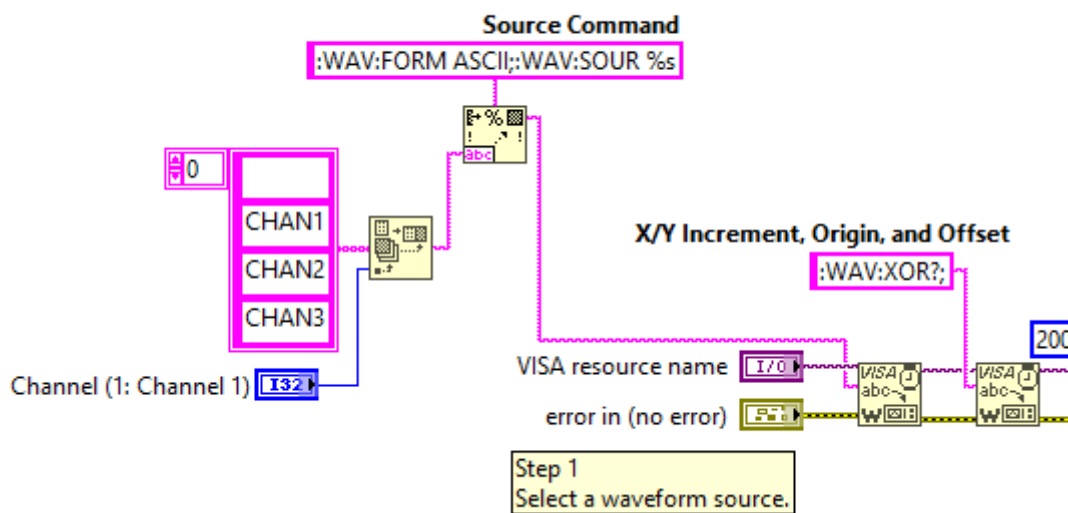


Figure 6. 13. Screenshot of selecting the waveform source for VI in LabVIEW.

Secondly, the software then transfers all the required waveform data from the oscilloscope, as depicted in figure 6.14. The parameters are contained in the response message of the instrument according to the following commands:

- XOR: start time of the measurement (t_0).
- XINC: time increment between the measured values (dt).
- YOR: Y axis offset.
- YINC: Y axis increment.
- YREF: Y axis offset is measured from this level.
- POIN: the number of measurement points.
- DATA: measurement data.

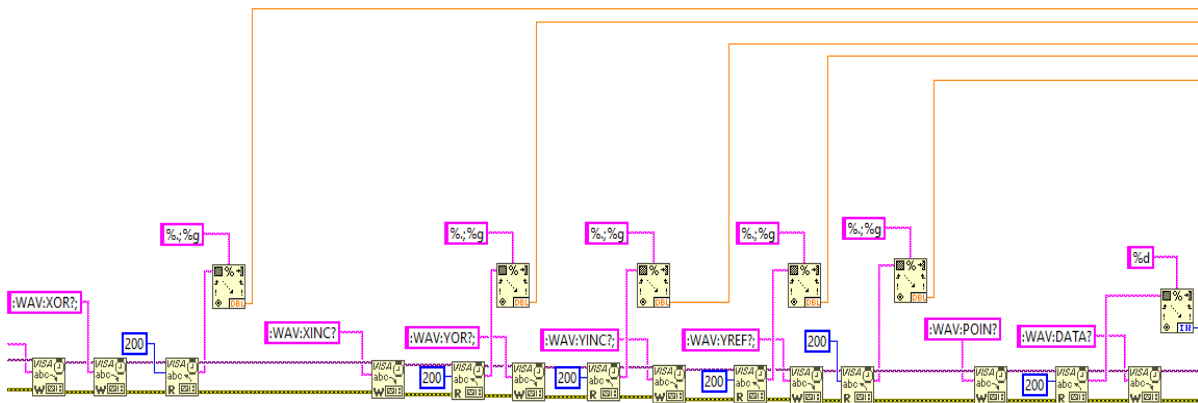


Figure 6. 14. Screenshot of the transfer of waveform parameters in VI (VISA).

Thirdly, as depicted in figure 6.15, a While loop is used to read the waveform data from the scope. A VISA Read block gets the data, which is in string format, with commas separating the values. Subsequently, a Spreadsheet String to Array block is used to extract the numerical values from this string. In addition to the string input, this block requires the format of the value (currently a floating-point number) and a separating character (.). This block produces a two-dimensional array as its output. The first row of the two-dimensional array has to be selected, as the instrument only provides one-dimensional waveform information.

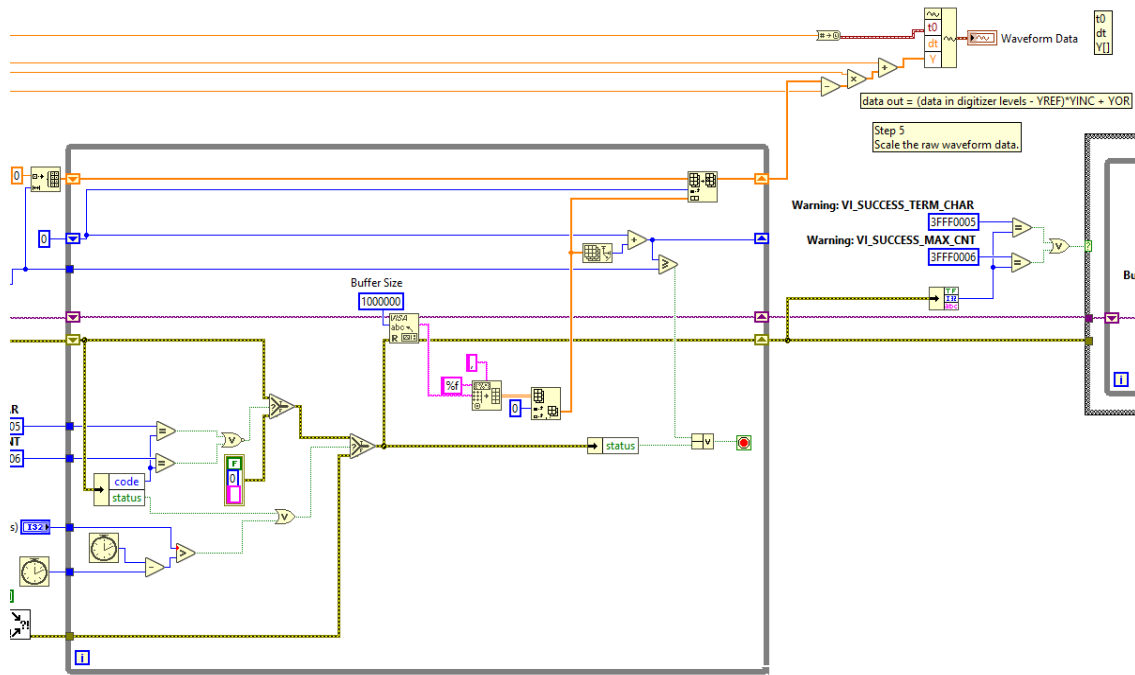


Figure 6. 15. Screenshot of extraction of waveform information from the instrument response (Oscilloscope 86100C).

The While loop is terminated once all defined values have been obtained. Two Shift Registers, one for counting the number of received values and the other for storing the data in an array, are located at the start of the cycle. The size of the Shift Register array is established at the beginning of the cycle, therefore the new values are added using Replace Array Subset. Once a sufficient number of values have been obtained the cycle is terminated, and the values are processed to produce the desired waveform (Step 5).

The final phase, Step 4, clears the instrument buffer, as necessary. To clear the buffer, a While loop reads 1000 bytes from the buffer in every cycle, until it becomes empty.

The VI generates the final waveform data from the raw data and waveform parameters in Step 5. The formula calculates the actual measurement (dataout) as follows:

$$dataout = (data \in digitizerlevels - YREF) * YINC + YOR \quad (6.3)$$

Where data is the received data from the digitizer or oscilloscope, which is the raw measurement that needs to be converted into actual values. YREF is the Y-axis reference, which is the level from which the Y-axis offset is measured. It is used to adjust the data for any offset or baseline differences in the measurement system. YINC is the Y-axis increment, a

scaling factor that determines the relationship between the received data and the actual measurement units. It is used to convert the data into the desired measurement units. YOR is the Y-axis origin or offset, a constant value added to the scaled data to account for any additional offset in the measurement system.

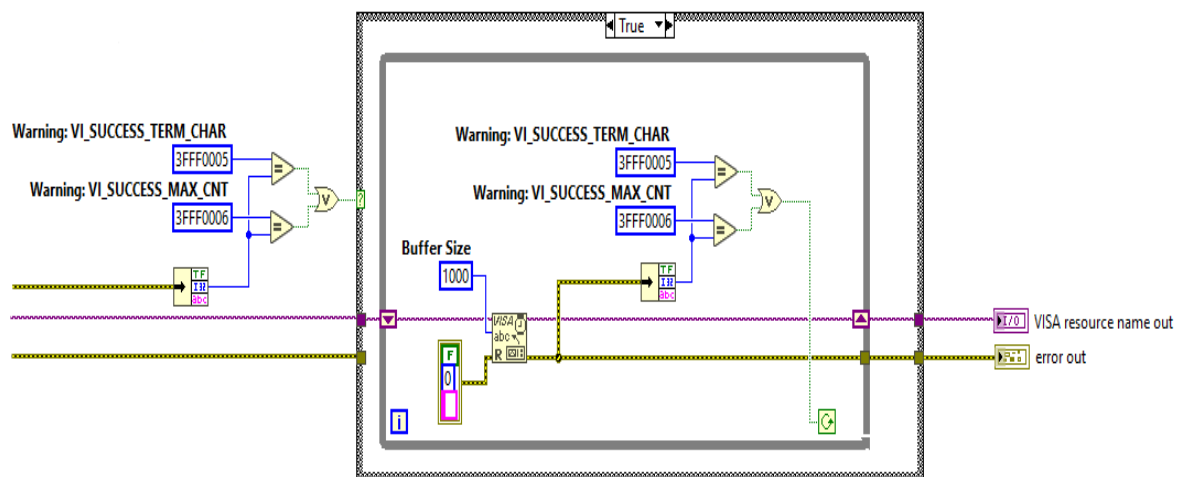


Figure 6. 16. Capture of clearing of the instrument buffer.

6.2.2.1. Calculation of the Full Width at Half Maximum

The FWHM (Full Width at Half Maximum) value is computed in the VI. The waveform signal originates from Fetch Waveform (Scope) in the VI, as previously described. The half-maximum value is obtained using the following equation.

$$halfmaximumvalue = min + \frac{max - min}{2} \quad (6.4)$$

The Array Max & Min block is used to determine the maximum and minimum values. The indices of the respective minimum/maximum values are also provided by this block, so that they can be used as the starting index with the highest value for the search in both directions. Two parallel while cycles that check whether the currently selected element is smaller than the half maximum are used to conduct the search. If the index is discovered, the cycle comes to an end, and the difference between the two indexes is determined by subtracting them. Since the time difference in addition to the distance in terms of the number of samplings

is required, the result is multiplied by the time interval between the samples (dt), as seen in figure 6.17.

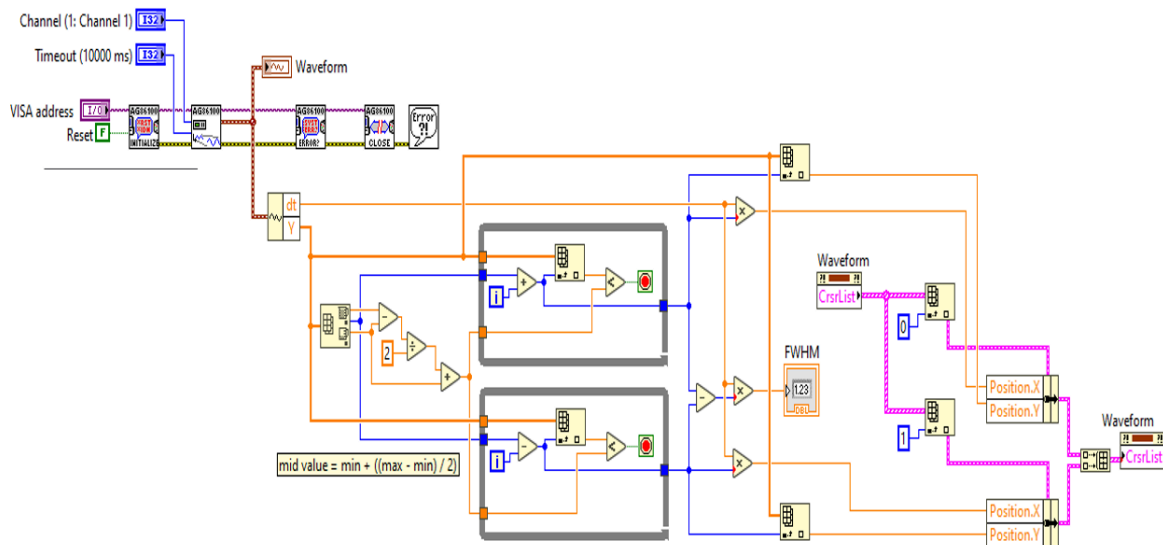


Figure 6. 17. Capture of the calculation of the FWHM (Full Width at Half Maximum).

See figure 6.18, which shows the calculation visually with two cursors on the graph.

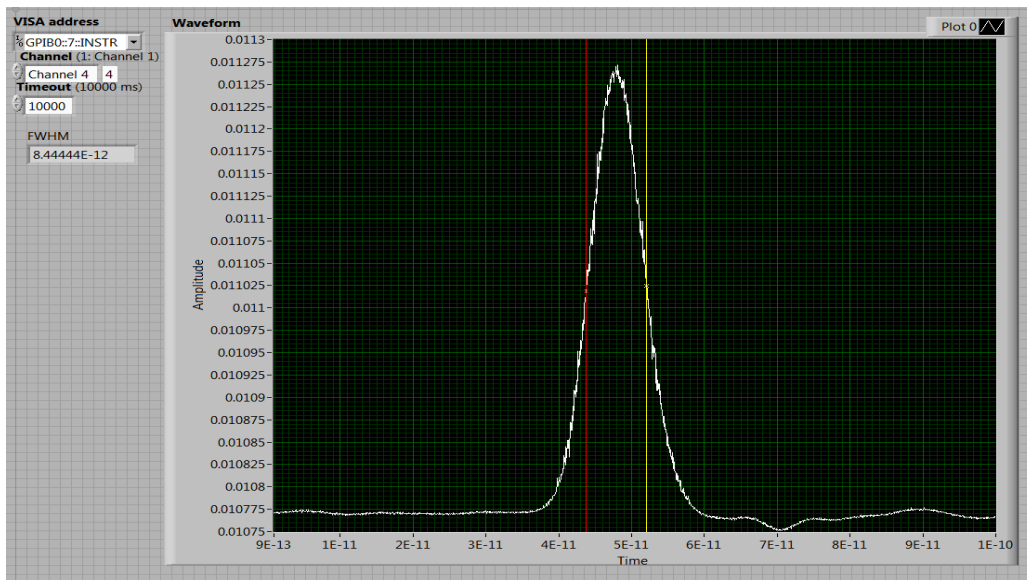


Figure 6. 18. Virtual scope VI displays the autocorrelation peak with two curses denoting the FWHM.

The X and Y axis positions can be used to control the position of the cursor. The index of the element, which must be multiplied by sampling time (dt), can be used to determine the X location. The value of the function at the indexed point is the Y position. These settings can be realised with the aid of a Waveform Graph Property Node, used to obtain a collection of graph-related cursors. The parameters are assigned, an array is created out of them, which is then written back to the cursor list after using Bundle by Name to choose the appropriate parameters from the cursor cluster.

Now that the OCDMA autocorrelation peak is located, the FWHM can also be recorded. The effect of over and under compensated link on the autocorrelation pulse width is monitored using the FWHM parameter, and the bias current of the SOA is controlled accordingly. The details are discussed in the following section.

6.2.2.2. Automated system

Prior to the experiment, it was determined that an SOA bias current of $I = 45 \text{ mA}$ corresponds to an SOA gain of 0 dB while a bias current of $I = 125 \text{ mA}$ causes SOA gain saturation. When the autocorrelation width changes, it is shown by the ratio $\frac{\tau}{\tau_0}$, whereas $\frac{\tau}{\tau_0} = 1$ indicates that the pulse width does not vary.

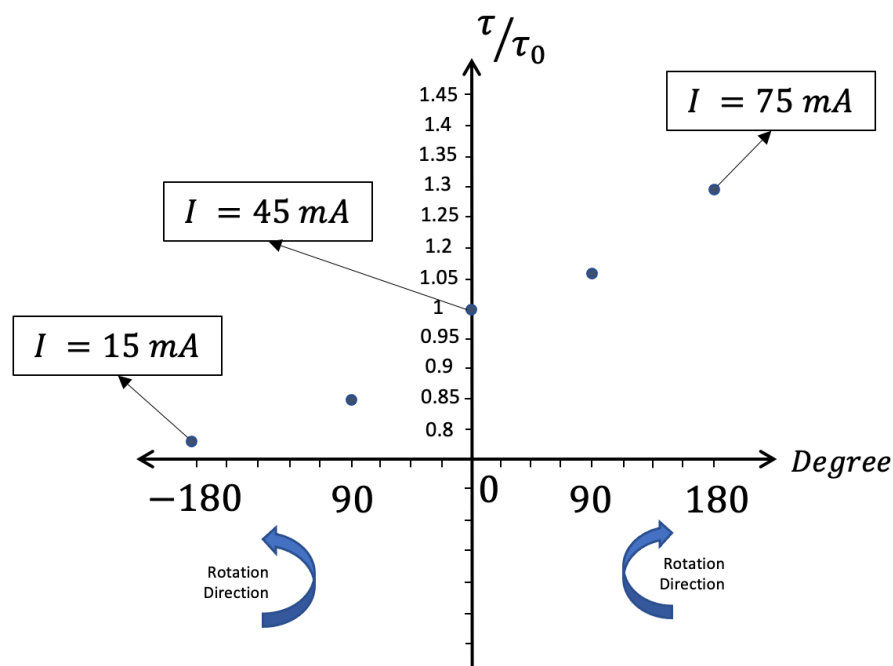


Figure 6. 19. Illustrates the ratio (τ/τ_0) of the autocorrelation width (Y axis) and the corresponding change on the rotation direction of the DC motor (X axis) by adjusting the bias current of the SOA.

As a result of the chromatic dispersion mismatch induced by adding/removing 66m of SMF to the transmission link, as shown in figure 6.19, the ratio (τ/τ_0) of the autocorrelation width widened or contracted in the experiment. The tuneability of the SOA was used to take advantage of the chromatic dispersion mismatch and compensate for the mismatched length of the transmission link. The potentiometer is rotated by the motor via a treaded rod within a range of $-180^\circ + 180^\circ$ (See figure 6.11). The ratio (τ/τ_0) = 1 and the SOA bias current $I = 45mA$ are the norm state described by the 0° . In the first situation, the transmission link becomes undercompensated as a result of the addition of 66 m of SMF, resulting in a chromatic dispersion mismatch of (τ/τ_0) > 1. As a result, the potentiometer will turn clockwise with the motor, changing the SOA bias current. The VI will then get the updated autocorrelation FWHM and compare it to the old one. The degree of rotation and direction of the motor are depicted in figure 6.19.

The SMF transmission connection would become overcompensated if 66m were removed, which would lead to a chromatic dispersion mismatch of (τ/τ_0) < 1. As a result, the FWHM of the autocorrelation is decreased. The motor will rotate the potentiometer counter-clockwise for a range between 0° and 180° and modify the SOA bias current until the original FWHM width is retrieved after the LabVIEW code has compared the FWHM to the original.

It is important to keep in mind that the autocorrelation width is slightly variable depending on whether the transmission connection is overcompensating or undercompensating (by $\pm 66m$). The autocorrelation widens by 4 ps when 66m SMF is removed from the transmission connection while it narrows by 2 ps when 66m of the SMF is added to the transmission link, according to figure 6.12.

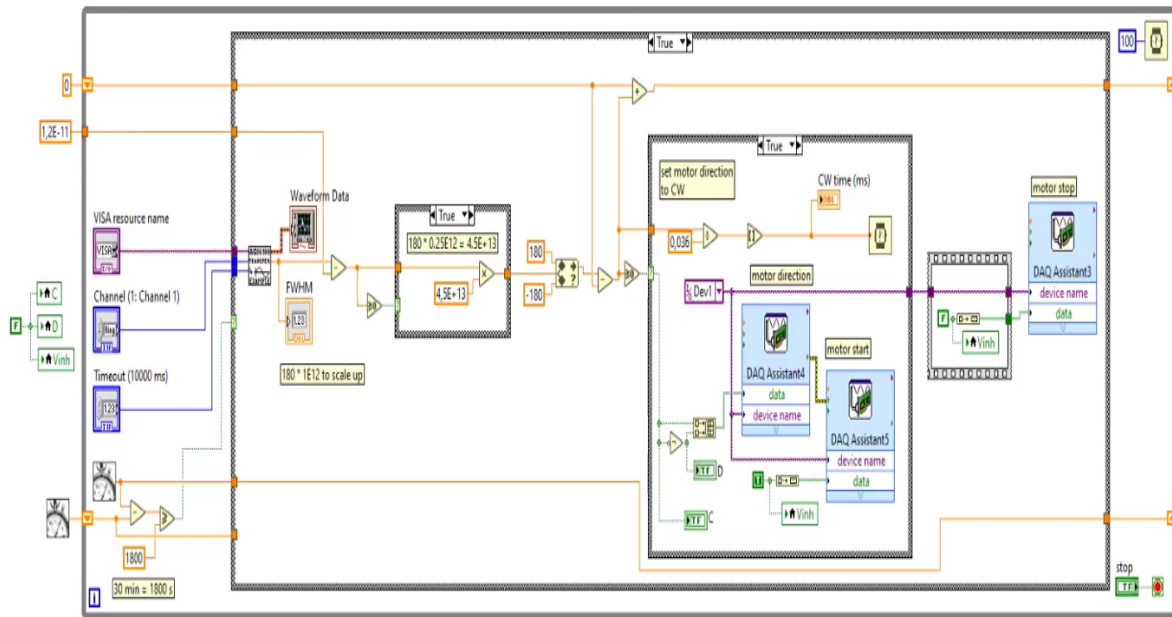


Figure 6. 20. Illustration of the VI in the motor controller when the system exhibits under-compensation.

Figure 6.20 and figure 6.21 depict the VI of the motor controller when the system exhibit under/over compensation. Here, the while cycle must continue until the stop button is pressed, but only once per 30 minutes should be used for the measurement. The High Resolution Relative Seconds block is utilised, which provides the relative current time in seconds, to calculate the amount of time that has passed. The elapsed seconds can be calculated as the difference of the two values with two successive calls to this block. The programme will do a measurement and based on the outcome, manage the motor when the discrepancy is greater than 30 minutes (1800 seconds). The FWHM nominal value is 8.5×10^{-12} . The difference from this nominal value has to be scaled to that range to facilitate the regulation of the motor in the range of $\pm 180^\circ$. Since the rate of change in the pulse width in case of over compensated and under compensated link are not the same, these both cases are processed separately as shown in figure 6.20 and figure 6.21.

The difference from this value must be scaled to the specified range to enable motor regulation within the $\pm 180^\circ$ range. Since the rate of change in pulse width varies for overcompensated and undercompensated links, both cases are processed separately, as demonstrated in Figure 6.20 and Figure 6.21.

In the case of under compensation, $(\tau/\tau_0) > 1$, the autocorrelation widens by 4 ps when 66m SMF is removed from the transmission connection. For the angle range, the maximum FWHM difference is $+ 4 \times 10^{-12}$. With these values, scaling is performed by multiplying the FWHM difference by $180 \times \frac{1}{4} \times 10^{-13}$. The difference is manipulated such that it fits into the range if it is outside of it (from 0° to $+180^\circ$), preventing the motor from rotating more than is necessary. In case of overcompensation, $(\tau/\tau_0) < 1$, the autocorrelation narrows by 2 ps when 66m SMF is added to the original length of the transmission line. All calculations are shown in figure 6.21 for the angle range, the maximum FWHM difference is $- 2 \times 10^{-12}$. With these values, scaling is performed by multiplying the FWHM difference by $180 \times \frac{1}{2} \times 10^{-13}$. The difference is manipulated such that it fits into the range if it is outside of it (from -180° to 0°), preventing the motor from rotating more than is necessary. In order to prevent the motor from rotating again if the difference is still the same between cycles, the real angle of the motor is saved in a shift register.

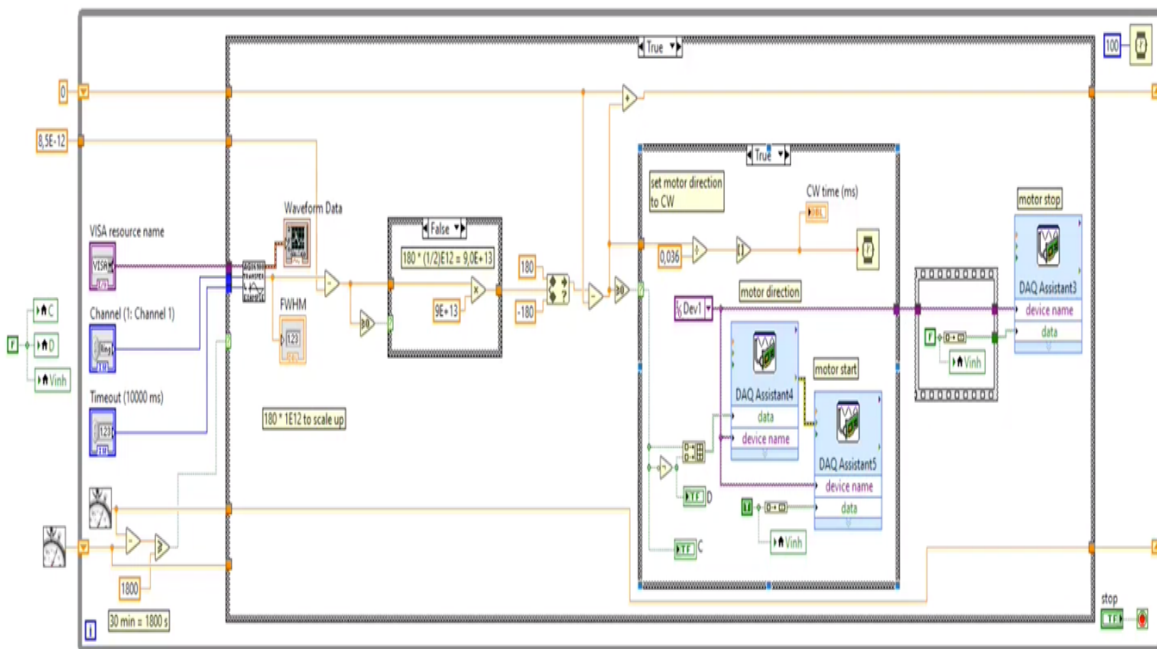


Figure 6. 21. Illustration of the VI in the motor controller when the system exhibits overcompensation.

Before the programme begins, the motor should be set to 0° for the proper angle positions. If the angle between the new and actual values is greater than zero, the motor will rotate

clockwise. Conversely, if the angle is less than zero, the motor will rotate in an anticlockwise direction.

Given that the motor rotates 360 degrees every 10 seconds at a steady speed, only the determination of the rotation time from the angle difference data is required. For this purpose, the angle is divided by 0.036 to get the time in milliseconds.

$$Time(ms) = \frac{\theta}{\frac{360^\circ}{10s}} * 1000 \quad (6.5)$$

An L293B chip was used to drive the motor, which has three inputs: C, D, and Vinh, to control the motor. Vinh turns on the motor rotation, while the C and D inputs select the direction of the motor. With the DAQ Assistant blocks, the NI USB 6002 DAQ is configured to produce these three signals. The C and D signals must be combined into an array because the input of the block is an array, and it can set multiple outputs simultaneously. The enable signal could be transmitted along with the other two, but it is preferable to select the direction of the motor before turning it on. Another DAQ Assistant output write stops the motor once the calculated rotation time has passed.

6.2.3. Summary

Temperature-induced dispersion is dynamic in nature. Therefore, a flexible compensation system is required to correct the distorted width of the OCDMA auto-correlation peak. This system has to be able to quickly react to real-time events, such as temperature changes. Furthermore, dispersion sensitivity in fibre-optic transmission systems typically increases with bit rate squared. Therefore, the function of the compensation system is the reduction of induced dispersion and the preservation of the original pulse width of the autocorrelation at the receiver. In this chapter the design and implementation of an autonomous dispersion management system in a WH/TS incoherent OCDMA system was described. The system proposed herein, manipulates the chirp of OCDMA code carriers to limit chromatic dispersion detrimental effect on Transmission systems using 2D OCDMA coding scheme. It was shown how the tuneability of the SOA is exploited to reduce chromatic dispersion. In particular, the bias current is adjusted to introduce the necessary changes in the refractive index of the SOA.

It was shown how the changes of the SOA chirp by adjusting its driving current could be used to reduce the impact of chromatic dispersion on the networks using 2D-WH TS OCDMA based communication system.

Chapter 7

Conclusion & Future Work

7.1 Conclusion

In this thesis, a wave hopping time spreading code based on picosecond optical pulses has been used to explore incoherent OCDMA systems, primarily considering prime codes. The main focus was directed at investigating different aspects of an incoherent OCDMA system including the impact of SOA-devices in OCDMA systems, the influence of self-phase modulation as well as chromatic dispersion, and the effect of ambient temperature fluctuations on data transmission over a 17-km bidirectional fibre link between Strathclyde and Glasgow University.

Chapter 2 presents a thorough examination of the core OCDMA ideas, with a particular focus on 2D-WH/TS with picosecond code carriers and code generating methods.

Chapter 3 considers the transmission impairments, especially chromatic dispersion (broadening and time skewing) and self-phase modulation due to GVD effects. The chapter concludes with a discussion of dispersion compensation techniques.

In **Chapter 4**, the temperature induced dispersion coefficient on 2D WH/TS incoherent OCDMA system was experimentally investigated as a function of different wavelengths. This was let to study the ramification of thermal dispersion skewing on OCDMA code carriers and evaluate the conventional equation that was predominantly used to predict the impact of the temperature induced dispersion. The obtained results showed great correlation with the value found in the literature for a narrow spectral spacing between wavelengths. While using a wider spectral region of wavelengths led to change in the dispersion slope indicating that temperature induced dispersion is wavelength dependent. Hence, the conventional expression was modified to suit wider spectrum enabling the prediction of the temporal coefficient of multi-wavelength picosecond code carriers from a wider than a few nanometres spectral range. In addition, a common approach (pulse broadening) for measuring the temperature-induced dispersion was investigated and a novel straightforward and cost-effective configuration for precise

measurement of the temperature dispersion coefficient in 2D WH/TS incoherent OCDMA system was implemented.

In **Chapter 5**, the impact of SOA-device on 2D OCDMA code carriers is evaluated under different bias conditions. Since the investigation is on deploying SOA on WH/TS OCDMA with multi-wavelength code carriers, this evaluation addressed the potential challenges and ramifications of the gain recovery time of SOA and its wavelength dependency with respect to gain ratio and self-phase modulation (SPM). Firstly, the OCDMA code was built using multiplexers and delay lines to create 2D OCDMA code to allow studying the impact of deploying a SOA under different conditions on each wavelength. Secondly, the foundation from part one was used as a ground for investigating SOA's impact on a 2D-WH/TS OCDMA prime code under high bias current/gain conditions. Thirdly, the overall performance (the probability of error and the maximum number of simultaneous users) of two different 2D-WH/TS OCDMA systems deploying the SOA was calculated. It was observed that redshift SPM induced by the SOA distorts the code and shifts wavelengths to the neighbouring channels. Two novel solutions utilising pre-chirp techniques were then proposed and analysed for mitigating the redshift induced chirp caused by the SOA saturation in 2D OCDMA code. The first solution used lithium-niobate crystal to compensate for the SPM after passing SOA. In the second solution, an anomalous dispersion fibre is used to counteract larger amount of induced redshift. To the best of my knowledge, this is the first time these pre-chirped techniques has been proposed for mitigating SOA-induced redshift in 2D OCDMA systems.

For the first time to the best of my knowledge, a proof-of-concept experiment which verified the possibility of improving the privacy and security in 2D WH/TS incoherent OCDMA communication system was conducted and proposed in **Chapter 6**. The proposed technique requires a single semiconductor optical amplifier accompanied with a correlated length of a propagation fiber link to adequately stimulate the nonlinear self-phase modulation effect in the transmission line leading to wavelength conversions (frequency shift) of the OCDMA code carriers. At the receiver side, a newly designed 2D-OCDMA decoder based on a matched filter "synchronized" to the resulting new code sequence removes the wavelength translations (shifts) to properly recover the user data.

In the second part of Chapter 6, the design and implementation of an autonomous dispersion management system in a WH/TS incoherent OCDMA system was described. The system proposed manipulates the chirp of OCDMA code carriers to limit chromatic dispersion

detrimental effect on transmission systems. It was shown how the changes of the SOA chirp by adjusting its driving current could be used to reduce the impact of chromatic dispersion on 2D WH TS OCDMA based communication system.

7.2 Future work

The security of optical code-division multiple access (OCDMA) systems is a critical consideration in their design and operation. In order to enhance the security of OCDMA systems, it is important to incorporate various strategies that can make it difficult for potential eavesdroppers to intercept and decipher the transmitted signal. One approach that can be used is the incorporation of multiple decoders, which can help to increase the complexity of the system and make it more difficult for unauthorized users to intercept the signal. By using a pseudorandom sequence to switch between the different decoders, the security of the system can be further enhanced, as it becomes more challenging for attackers to predict and intercept the signal.

Another approach that can be used to enhance the security of OCDMA systems is the use of multiple channels. By transmitting data over two or more channels, each with its own unique characteristics, the system can provide an additional layer of redundancy and make it more difficult for attackers to interfere with the transmission. One way to implement this is by using one channel with a semiconductor optical amplifier (SOA) and another channel without a SOA. By switching between the two channels using a pseudorandom sequence, the system can provide additional security against potential attackers.

In the context of using a SOA as an optical amplifier in a WH/TS OCDMA network, there are several areas of research that may be worth exploring in the future. One potential area of interest is the use of a phase modulator to manipulate the chirp of the optical pulse using an electrical signal. This approach can help to mitigate the effects of self-phase modulation (SPM)-induced redshift, which can be a significant problem in OCDMA systems. By manipulating the chirp of the optical pulse, it may be possible to compensate for the redshift induced by SPM, which can help to improve the overall performance of the system.

There are several potential benefits to using a phase modulator to manipulate the chirp of the optical pulse. One advantage is that it provides a means of compensating for the SPM-induced redshift without the need for additional optical components, which can help to simplify the system and reduce its complexity. Additionally, this approach can provide a means of

achieving higher spectral efficiency, which is an important consideration in many OCDMA systems. By optimizing the modulation scheme used in the phase modulator, it may be possible to achieve greater spectral efficiency and improve the overall performance of the system.

However, further research is needed to determine the optimal approach for using a phase modulator to manipulate the chirp of the optical pulse. This may involve studying the effects of different modulation schemes and optimizing the parameters used in the modulation process. Additionally, it may be necessary to investigate the trade-offs between performance and complexity when using a phase modulator in an OCDMA system. Despite these challenges, the use of a phase modulator to compensate for SPM-induced redshift shows promise as a potential area of research for improving the performance of SOA-based optical amplifiers in WH/TS OCDMA networks.

Automated tunable induced temperature dispersion compensation is an important area of research in the field of optical communication systems. In order to investigate this further, it may be worthwhile to implement temperature chambers to simulate real-world scenarios and study the effects of temperature on the system. By using a temperature chamber, it is possible to create a controlled environment that can be used to study the impact of temperature on the performance of the system. This can help to identify potential areas of improvement and optimize the performance of the system.

In addition to investigating temperature dispersion compensation, it is also important to explore other methods of managing dispersion in optical communication systems. One potential approach is to use all-optical tunable dispersion management, which involves using a semiconductor optical amplifier (SOA) to control dispersion in the system. This approach can be particularly effective in systems that use 2-D wavelength-time codes, such as carrier-hopping prime codes (CHPCs). By using an SOA to manage dispersion in the system, it may be possible to achieve higher performance and improved reliability, even in the presence of temperature-induced dispersion.

References

- [1] P. Z. Dashti, C. F. Lam, R. Urata, H. Liu and . M. Medin, "Optoelectronic integration for broadband optical access networks," in *IEEE Photonics Conference (IPC)*, 2012.
- [2] Z. Drago, K. Visnja and G. Kresimir, "Business case assessments of fixed and mobile broadband access networks deployments," in *20th International Conference on Software, Telecommunications and Computer Networks (SoftCOM)*, 2012.
- [3] G. Kramer, M. D. Andrade, R. Roy and P. Chowdhury, "Evolution of Optical Access Networks: Architectures and Capacity Upgrades," in *2012, Proceedings of the IEEE*.
- [4] S. Kartalopoulos, "Understanding SONET/SDH and ATM: Communications Networks for the Next Mellennium," in *Wiley-IEEE Press*,, 1999.
- [5] I. Andonovic and L. Tancevski, "Incoherent optical code division multiple access systems," in *Proceedings of IEEE 4th International Symposium on Spread Spectrum Techniques and Applications*, 1996.
- [6] I. Glesk, P. R. Prucnal and I. Andonovic, "Incoherent ultrafast OCDMA receiver design with a 2 ps all-optical time gate to supress multiple access interference," *IEEE Journal of Selected Topics in Quantum Electronics*, vol. 14, no. 3, pp. 861-867, 2008.
- [7] G. C. Yang and W. C. Kwong, Prime codes with applications to cdma optical and wireless networks, Boston: Artech House, 2002.
- [8] R. S. Tucker, G. Eisenstein and S. K. Korotky, "Optical time-division multiplexing for very high bit-rate transmission," *J. Lightwave Technol*, vol. 6, no. 11, pp. 1737-1749, Nov. 1998.
- [9] V. Baby, D. Rand, C. X. Brès, L. Xu , I. Glesk and P. R. Prucnal., "Incoherent Optical CDMA Systems," in *Optical code division multiple access: fundamentals and applications*, Boca Raton, CRC press, 2006, pp. 199-240.
- [10] I. Glesk, I. Andonovic and P. R. Prucnal, "Design and demonstration of OCDMA system with superior scalability," *Photonics, Devices, and Systems IV*, vol. 7138, p. 71381P, Nov 2008.
- [11] A. B. Dar and R. K. Jha, "Chromatic dispersion compensation techniques and characterization of fiber Bragg grating for dispersion compensation," *Optical and Quantum Electronics*, vol. 49, no. 3, pp. 1-35, 2017.
- [12] Z. Pan, C. Yu and A. E. Willner, "Optical performance monitoring for the next generation optical communication networks," *Optical Fibre Technology*, vol. 16, no. 1, pp. 20-45, 2010.
- [13] A. Sahin and A. E. Willner, "System limitations due to chromatic dispersion and receiver bandwidth for 2-D time-wavelength OCDMA systems," in *The 16th Annual Meeting of the IEEE Lasers and Electro-Optics Society (LEOS)* , 2003.

- [14] T. B. Osadola, S. K. Idris, I. Glesk and W. C. Kwong, "Effect of variations in environmental temperature on 2DWH/TS OCDMA code performance," *Journal of Optical Communications and Networking*, vol. 5, no. 1, p. 68–73, 2013.
- [15] N. A. n. d., "Didn't know what is CDMA: Now you will know," [Online]. Available: URL: <http://www.mgovworld.org/techbytes/didn-t-know-what-is-cdma-now-you-will-know;> [Accessed 2 2022].
- [16] G. P. n. d, "Optical CDMA," University at Buffalo, [Online]. Available: URL: http://www.ee.buffalo.edu/faculty/paololiu/566/op_cdma.ppt.
- [17] n. d. S. J. Ben Yoo, "Optical CDMA Technology," [Online]. Available: URL:http://www.citris-uc.org/research/projects/optical_cdma_technology.
- [18] Karbassian and M. Massoud, "Optical CDMA Networks," University of Birmingham, [Online]. Available: http://postgrad.eee.bham.ac.uk/karbassm/OCDMA_Concept.pdf.
- [19] J. Edwards, *Telecosmos: The Next Great Telecom Revolution*, John Wiley and Sons, 2005.
- [20] K. -L. Deng, R. J. Runser, P. Toliver, C. Coldwell, D. Zhou, I. Glesk and P. R. Prucnal, "Demonstration of a Highly Scalable 100-Gbs OTDM Computer Interconnect with Rapid Inter-channel Switching Capability," in *Optical Fiber Communication Conference and the International Conference on Integrated Optics and Optical Fiber Communication, OSA Technical Digest*, Optical Society of America, Washington DC, 1999.
- [21] V. Baby, C. -S. Brès, L. Xu, I. Glesk and P. R. Prucnal, "Demonstration of differentiated service provisioning with 4-node 253 Gchip/s fast frequency hopping time-spreading OCDMA," *Electronics Letter*, vol. 18, no. 6, pp. 385-387, 2004.
- [22] E. Forestieri, in *Optical Communication Theory and Techniques*, Springer Nature, 2005, p. 104.
- [23] C. -S. Brès, Y. -K. Huang, . D. Rand, I. Glesk, P. R. Prucnal, T. Bazan, C. Michie, D. Harle and I. Andonovic, "On the Experimental Characterization of Beat Noise in 2-D Time-Spreading Wavelength-Hopping OCDMA Systems," *IEEE Photonics Technology Letters*, vol. 18, no. 21, pp. 2314-2316, 2006.
- [24] N. D. G. n. d, "Optical CDMA-An Introduction," [Online]. Available: http://www.honet.niit.edu.pk/presentations/Session6/Dr%20Gohar/Optical%20CDMA-An%20Introduction_nD_gohar.pdf.
- [25] H. Fathallah and K. Fouli, "Enhanced optical fast frequency hopping-CDMA by means of over-spreading and interleaving". United states of America Patent 10/529,229, 8 June 2006.
- [26] Y. K. Huang, V. Baby, I. Glesk, C. S. Bres, C. M. Greiner , D. Iazikov , T. W. Mossberg and P. R. Prucnal, "Novel Multicode-Processing Platform for Wavelength-Hopping Time Spreading Optical CDMA: A Path to Device Miniaturization and Enhanced Network Functionality," *IEEE Journal of Selected Topics in Quantum Electronics*, vol. 13, no. 5, pp. 1471-1479, 2007.
- [27] H. Yin and D. J. Richardson, in *Optical Code Division Multiple Access Communication Networks*, Beijing & New York, Tsinghua University Press & Springer Berlin Heidelberg, 2008, p. 382.

- [28] D. Sarwate, "Reed-Solomon Codes and the Design of Sequences for Spread Spectrum Multiple access Communications," in *Reed-Solomon Codes and their Applications*, NJ, IEEE Press, 1994.
- [29] T. Conway, "Galois field arithmetic over GF(pm) for high-speed/lowpower error-control applications," *IEEE Transactions on Circuits and Systems I: Regular Papers*, vol. 51, no. 4, pp. 709-717, 2004.
- [30] J. -H. Tien, G. -C. Yang, C. -Y. Chang and W. C. Kwong, "Design and Analysis of 2-D Codes With the Maximum Cross-Correlation Value of Two for Optical CDMA," *Journal of Lightwave Technology*, vol. 26, no. 22, pp. 3632-3639, 2008.
- [31] G. C. Yang and W. C. Kwong, "Performance analysis of optical CDMA with prime codes," *Electronics Letters*, vol. 31, no. 7, pp. 569-570, 1995.
- [32] K. S. M, K. O. J, A. S. R and K. L. B, *Spread Spectrum Communications Handbook*, New York: McGraw-Hill, 2002.
- [33] J. V. A, *CDMA: Principles of Spread Spectrum Communication*, Reading, MA: Addison-Wesley, 1995.
- [34] D. V. Sarwate and M. B. Pursley, "Crosscorrelation properties of pseudorandom and related sequences," *Proceedings of the IEEE*, vol. 68, no. 5, pp. 593 - 619, 1980.
- [35] A. C. Chen, "Overview of code division multiple access technology for wireless communications," in *Proceedings of the 24th Annual Conference of the IEEE Industrial Electronics Society*, 1998.
- [36] J. G. Zhang, W. C. Kwong and S. Mann, "Construction of $2n$ extended prime codes with cross-correlation constraint of one," *IEE Proceedings on Communications*, vol. 145, no. 5, pp. 297-303, 1998.
- [37] W. C. Kwong and G. C. Yang, "Construction of $2n$ prime-sequence codes for optical code division multiple access," *IEE Proceedings*, vol. 142, no. 2, pp. 141-150, 1995.
- [38] M. Medard and S. Lumetta, "Architectural Issues for Robust Optical Access," *IEEE Communications Magazine*, vol. 39, no. 7, pp. 116-122, 2001.
- [39] Y. K. Huang, K. Kravtsov, I. Glesk, P. R. Prucnal, C. M. Greiner , D. Iazikov and T. W. Mossberg, "Integration of DualCode Optial CDMA Encoder and Decoder by Holographic Bragg Reflectors," in *Optical Fiber Communication Conference (p. JThA28)*, 2007.
- [40] Y. Zhang, H. Chen, Z. Si , H. Ji and S. Xie, "Design of FBG En / Decoders in Coherent 2-D Time-Wavelength OCDMA Systems," *IEEE Photonic Technol. Letter*, vol. 20, no. 11, p. 891-893, 2008.
- [41] I. Glesk, V. Baby, C. S. Bres, Y. K. Huang and P. R. Prucnal, "Performance enhancement of optical CDMA systems using ultrafast all-optical sampling," in *IEEE Conference Avionics Fiber-Optics and Photonics*, 2005.

- [42] G. P. Agrawal, in *Fiber optic communication systems, 3rd ed.*, Hoboken, NJ, USA, John Wiley & Sons, 2010.
- [43] M. K. Smit and C. V. Dam, "PHASAR-Based WDM-Devices," *IEEE Journal of selected topics in quantum electronics*, vol. 2, no. 2, pp. 236-250, 1996.
- [44] C. Dragone, "Efficient Techniques for Widening the Passband of a Wavelength Router," *Journal of lightwave technology*, vol. 16, no. 10, pp. 1895-1906, 1998.
- [45] S. V. Kartalopoulos, "Introduction to DWDM Technology : Data in a rainbow," in *SPIE Optical Engineering Press & IEEE Press*, Piscataway, New Jersey, 2000.
- [46] S. Yegnanarayanan, A. S. Bhushan and B. Jalali, "Fast Wavelength-Hopping Time-Spreading Encoding / Decoding for Optical CDMA," *IEEE Photonic Technology Letter*, vol. 12, no. 5, pp. 573-575, 2000.
- [47] Z. Knittl, in *Optics of Thin Films*, Prague, Czechoslovakia, John Wiley & Sons, 1976, p. 551.
- [48] H. A. Macleod, in *Thin-Film Optical Filters, 3rd ed*, Bristol, UK: Institute of Physics Publishing Bristo; and Philadelphia, 2001, p. 667.
- [49] S. Sumriddetchkajorn and K. Chaitavon, "A reconfigurable thin film filterbased 2x2 add-drop fiber-optic switch structure," *IEEE Photonic Technology Letter*, vol. 15, no. 7, pp. 930-932, 2003.
- [50] L. H. Domash, in *Thin Films Sing a New Tune (Photonics Spectra Features)*, Photonic spectra, 2004, pp. 70-74.
- [51] V. Baby, I. Glesk, R. J. Runser, R. Fischer, Y. Huang, C. Bres, W. C. Kwong, T. H. Curtis and P. R. Prucnal, "Experimental Demonstration and Scalability Analysis of a Four-Node 102-Gchip/s Fast Frequency-Hopping TimeSpreading Optical CDMA Network," *IEEE Photonics Technology Letter*, vol. 17, no. 1, pp. 253-255, 2005.
- [52] K. O. Hill and G. Meltz, "Fiber Bragg grating technology fundamentals and overview," *Journal of Lightwave Technology*, vol. 15, no. 8, p. 1263–1276, 1997.
- [53] R. Kashyap, in *Fibre Bragg Gratings, 2nd editio*, Montreal Canada, Academic Press, 2009, p. 614.
- [54] J. Magné, D. Wei, S. Ayotte, L. A. Rusch and S. Larochelle, "Experimental Demonstration of Frequency-Encoded Optical CDMA using Superimposed Fiber Bragg Gratings," in *Bragg Gratings, Photosensitivity, and Poling in Glass Waveguides (p. WD4)*. *Optical Society of America.*, Bragg Gratings, Photosensitivity, and Poling in Glass Waveguides, 2003.
- [55] A. Grunnet-Jepsen, A. E. Johnson, E. S. Maniloff, T. W. Mossberg, M. J. Munroe and J. N. Sweetser, "Fibre Bragg grating based spectral encoder/ decoder for lightwave CDMA," *Electronics Letter*, vol. 35, no. 13, p. 1096– 1097, 1999.
- [56] J. H. Lee, P. C. Teh, P. Petropoulos, M. Ibsen and D. J. Richardsn, "A Grating-Based OCDMA Coding – Decoding System Incorporating a Nonlinear Optical Loop Mirror for Improved Code

Recognition and Noise Reduction," *IEEE Journal of Lightwave Technology*, vol. 20, no. 1, pp. 36-46, 2002.

- [57] L. R. Chen, "flexible fiber bragg grating encoder/ decoder for hybrid wavelength-time optical CDMA," *photonic Technology Letter*, vol. 13, no. 11, p. 1233–1235, 2001.
- [58] N. Minato, S. Kutsuzawa, K. Sasaki, S. Kobayashi, A. Nishiki, T. Ushikubo, T. Kamijoh, Y. Kamio, N. Wada and F. Kubota, "Field trial of time-spreading and wavelength- hopping OCDM transmission using FBG en / decoders," *Optics Express*, vol. 14, no. 13, pp. 5853-5859, 2006
N. Minato, S. Kutsuzawa, K. Sasaki, S. Kobayashi, A. Nishiki, T. Ushikubo, T. Kamijoh, Y. Kamio, N. Wada, and F. Kubota,.
- [59] L. R. Chen, "Optical Code-Division Multiple-Access Enabled by Fiber Bragg Grating Technology," in *optical code division multiple access : fundamental and applications, 1st ed.*, P. R. Prucnal and B. Raton, Eds., CRC Press, 2006, p. 111–164.
- [60] N. Minato, H. Tamai, A. Iwamura, K. Satoko, S. Kobayashi, K. Sasaki and A. Nishiki, "Demonstration of 10 Gbit/s-Based Time-Spreading and WavelengthHopping Optical-Code-Division-Multiplexing Using Fiber-Bragg-Grating En/Decoder," *IEICE Trans Commun*, Vols. E88-B, no. 10, pp. 3848-3854, 2005.
- [61] H. B. Jaafar, S. LaRochelle, P. Y. Cortes and H. Fathallah, "1.25 Gbit / s transmission of optical FFH-OCDMA signals over 80 km with 16 users," in *Optical Fiber Communication Conference (OFC)*, 2001.
- [62] N. Wada, H. Sotobayashi and K. Kitayama, "2.5 Gbit/s timespread/wavelength-hop Optical Code Division Multiplexing Using fiber Bragg grating with supercontinuum light source," *Electronics Letter*, vol. 36, no. 9, p. 2000, 815–817.
- [63] L. R. Chen and P. W. Smith, "Demonstration of Incoherent wavelengthencoding/time-spreading optical CDMA using chirped Moire gratings," *IEEE Photonic Technology Letter*, vol. 12, no. 9, p. 1281–1283, 2000.
- [64] T. B. Osadola, S. K. Idris, I. Glesk, K. Sasaki and G. C. Gupta, "In Situ Method for Power Re-Equalization of Wavelength Pulses Inside of OCDMA Codes," *IEEE Journal of Quantum Electronics*, vol. 47, no. 8, p. 1053–1058, 2011.
- [65] A. Scherer, O. Painter, J. Vuckovic, M. Loncar and T. Yoshie, "Photonic Crystals for Confining , Guiding , and Emitting Light," *IEEE Transactions Nanotechnology*, vol. 1, no. 1, pp. 4-11, 2002.
- [66] T. W. Mossberg, "Planar holographic optical processing devices," *Optical Letter*, vol. 26, no. 7, p. 414–416, 2001.
- [67] C. Greiner, D. Iazikov and T. W. Mossberg, "Lithographically Fabricated Planar Holographic Bragg Reflectors," *Journal of Lightwave Technology*, vol. 22, no. 1, p. 136–145, 2004.
- [68] Y. K. Huang, I. Glesk, C. M. Greiner, D. Iazkov, . T. W. Mossberg, T. Wang and P. R. Prucnal, "Single integrated device for optical CDMA code processing in dual-code environment," *Optics Express*, vol. 15, no. 12, p. 7327–7334, 2007.

- [69] M. Gagnaire and S. Zahr, "Impairment-aware routing and wavelength assignment in translucent networks: State of the art," *IEEE Communications Magazine*, vol. 47, no. 5, pp. 55-61, 2009.
- [70] M. Yannuzzi, E. Marin-Tordera, R. Serral-Gracia, X. Masiip-Bruin, O. González, J. Jiménez and D. Verchere, "Modeling Physical-Layer Impairments in Multi-domain Optical Networks," in *15th International Conference on Optical Network Design and Modeling (ONDM)*, 2011.
- [71] C. V. Saradhi, S. Subramaniam and S. Member, "Physical Layer Impairment Aware Routing (PLIAR) In WDM Optical Networks : Issues and Challenges," *IEEE Communications Surveys & Tutorials*, vol. 11, no. 4, pp. 109-130, 2009.
- [72] B. Mukherjee, "All-Optical Impairment-Aware Routing," in *Optical Network series: Optical WDM Networks*, United States of America, Springer , 2006, p. 723–749.
- [73] G. Keiser, in *Optical communication essentials*, McGraw-Hill Education, 2003, p. 372.
- [74] J. Liu, in *Photonic devices*, Cambridge University Press, 2005, p. 1052.
- [75] T. M. Jeong and J. Lee, "Generation of High-Intensity Laser Pulses and their Applications," in *High Energy and Short Pulse Lasers* , London, IntechOpen, 2016, pp. 10-12.
- [76] F. Mitschke, *Fiber Optics: Physics and Technology* second edition, Berlin Heidelberg: Springer, 2016.
- [77] E. G. Neumann, *Single-mode fibers: fundamentals (Vol. 57)*, Verlag, Berlin : Springer, 2013.
- [78] G. P. Agrawal, *Nonlinear fibre optics*, Academic press , 2007.
- [79] S. M. Ahmed and I. Glesk, , "Management of OCDMA Auto-Correlation Width by Chirp Manipulation Using SOA," *IEEE Photonics Technology Letter*, vol. 30, no. 9, p. 785–788, 2018.
- [80] R. Bonk, T. Vallaitis, W. Freude, J. Leuthold, R. Penty, A. Borghesani and I. F. Lealman, "Linear semiconductor optical amplifiers," in *Fibre Optic Communication*, Berlin, Heidelberg, Springer, 2012.
- [81] C. H. Henry, R. A. Logan, and K. A. Bertness, "Spectral dependence of the change in refractive index due to carrier injection in GaAs lasers," *Journal of Applied Physics*, vol. 52, no. 7, pp. 4457-4461, 1981.
- [82] J. Wang, A. Maitra, C. G. Poulton, W. Freude and J. Leuthold, "Temporal dynamics of the alpha factor in semiconductor optical amplifiers," *Journal of Lightwave Technology*, vol. 25, no. 3, pp. 891-900, 2007.
- [83] M. N. Ngo, H. T. Nguyen, C. Gosset, D. Erasme, Q. Deniel and N. Genay, "Transmission performance of chirp-controlled signal emitted by electroabsorption modulator laser integrated with a semiconductor optical amplifier," in *Optical Fibre Communication Conference, Optical Society of America*, 2012.

- [84] A. H. Gnauck, S. K. Korotky, J. J. Veselka, J. Nagel, C. T. Kemmerer, W. J. Minford and D. T. Moser, "Dispersion penalty reduction using an optical modulator with adjustable chirp," *IEEE Photonics Technology Letters*, vol. 3, no. 10, pp. 916-918, 1991.
- [85] O. P. software, "Effects of Group Velocity Dispersion (GVD) on Gaussian Pulse Propagation," Optisystem, [Online]. Available: <https://optiwave.com/resources/applications-resources/optical-system-effects-of-group-velocity-dispersion-gvd-on-gaussian-pulse-propagation/>. [Accessed 30 09 2022].
- [86] N. T. Dang, A. T. Pham and Z. Cheng,, "Impact of GVD on the Performance of 2-D WH/TS OCDMA Systems Using Heterodyne Detection Receiver," *IEICE Transactions on Fundamentals of Electronics, Communications and Computer Sciences*, Vols. E92-A, no. 4, p. 1182-1191, 2009.
- [87] X. Y. Yao, J. Feinberg, R. Logan and L. Maleki, "Limitations on Peak Pulse Power , Pulse Width , and Coding Mask Misalignment in a Fiber-optic Code-Division Multiple-Access System," *Journal of Lightwave Technology*, vol. 11, no. 5/6, p. 836-846, 1993.
- [88] T. Pfeiffer, M. Witte and B. Deppisch, "High-speed transmission of broadband thermal light pulses over dispersive fibers," *IEEE Photonics Technology Letter*, vol. 11, no. 3, p. 385-387, 1993.
- [89] H. P. Sardesai and A. M. Weiner, "A Femtosecond Code-Division Multiple Access," *Journal of Lightwave Technology*, vol. 16, no. 11, pp. 1953-1964, 1998.
- [90] L. Grüner-nielsen, M. Wandel, P. Kristensen, C. Jørgensen, L. V. Jørgensen, B. Edvold, B. Pálsdóttir and D. Jakobsen, "Dispersion-Compensating Fibers," *Journal of Lightwave Technology*, vol. 23, no. 11, pp. 3566-3579,, 2005.
- [91] E. A. Sharma, E. S. Singh and E. B. Sharma, "Dispersion Compensation In Optical Communication - A Review," *International Journal of Computing and Technology*, vol. 4, no. 3, p. 742-754, 2013.
- [92] R. L. Lachance, Y. Painchaud and A. Doyle,, "Fiber Bragg Gratings and Chromatic Dispersion," *Proc. SPIE 4833, Applications of Photonic Technology 5*, vol. 4833, no. 418, pp. 1-8, 2003.
- [93] B. Chomycz, *Planning Fibre Optic Networks*, New York: McGrawHill, 2009.
- [94] S. Spolitis, V. Bobrovs and G. Ivanovs, "Realization of combined chromatic dispersion compensation methods in high speed WDM optical transmission systems," *Electrical and Electronics Engineering* , vol. 10, no. 116, pp. 33-38, 2001.
- [95] Y. Danziger and D. Askegard, "High-order-mode fiber- an innovative approach to chromatic dispersion management that enables optical networking in longhaul high-speed transmission systems," in *Optical Networks Magazine*, 2001, p. 40-50.
- [96] S. L. Jansen, D. van den Borne, P. M. Krummrich, . S. Spalter, G. D. Khoe, and H. de Waardt, "Long-haul DWDM transmission systems employing optical phase conjugation," *IEEE Journal of Selected Topics in Quantum Electronics*, vol. 12, no. 4, p. 505-520, 2006.

- [97] M. J. Li and D. A. Nolan, "Optical Transmission Fiber Design Evolution," *Journal of Lightwave Technology*, vol. 26, no. 9, p. 1079–1092, 2008.
- [98] S. K. Idris, T. B. Osadola and I. Glesk, "Investigation of all-optical switching OCDMA testbed under the influence of chromatic dispersion and timing jitter," *Journal of Engineering Technology*, vol. 4, no. 1, pp. 51-65, 2013.
- [99] J. Vojtech, M. Karasek and J. Radil, "Comparison of an Unconventional All-Optical Chromatic Dispersion Compensation Techniques in Nonlinear Line Scenarios with Emphasis to Tunability," in *9th international Conference on Transparent Optical Networks ICTON'07*, 2007.
- [100] B. J. Eggleton, A. Ahuja, P. S. Westbrook, J. A. Rogers, P. Kuo, T. N. Nielsen and B. Mikkelsen, "Integrated tunable fibre gratings for dispersion management in high-bit rate systems," *Journal of Lightwave Technology*, vol. 18, no. 10, pp. 1418-1432, 2000.
- [101] K. Tanizawa and A. Hirose, "Adaptive control of tunable dispersion compensator that minimizes time-domain waveform error by steepest descent method," *IEEE photonic Technology Letters*, vol. 18, no. 13, pp. 1466-1468., 2006.
- [102] A. Sano, T. Kataoka, M. Tomizawa, K. Hagimoto, K. Sato, K. Wakita and K. Kato, "Automatic dispersion equalization by monitoring extracted-clock power level in a 40-Gbit/s, 200-km transmission line," in *Proceedings of European Conference on Optical Communication*, 1996.
- [103] Z. Pan, Y. W. Song, C. Yu, Y. Wang, Q. Yu, J. Popelek and A. E. Willner, "Tunable chromatic dispersion compensation in 40-Gb/s systems using nonlinearly chirped fiber Bragg gratings," *Journal of lightwave technology*, vol. 20, no. 12, pp. 2239-2246, 2002.
- [104] K. Takiguchi, K. Okamoto and K. Moriwaki, "Planar lightwave circuit dispersion equalizer," *Journal of Lightwave Technology*, vol. 14, no. 9, pp. 2003-2011, 1996.
- [105] G. H. Lee, S. Xiao and A. M. Weiner, "Optical dispersion compensator with >4000-ps/nm tuning range using (VIPA) and spatial light modulator (SLM)," *IEEE Photonics Technology Letters*, vol. 18, no. 17, pp. 1816-1829, 2006.
- [106] P. S. André and A. N. Pinto, "Chromatic dispersion fluctuations in optical fibers due to temperature and its effects in high-speed optical communication systems," *Optics Communications*, vol. 246, no. 4-6, pp. 303-311, 2005.
- [107] H. C. Ji, J. H. Lee and Y. C. Chung, "Evaluation on system outage probability due to temperature variation and statistically distributed chromatic dispersion of optical fiber," *Journal of lightwave technology*, vol. 22, no. 8, pp. 1893-1898, 2004.
- [108] G. Ghosh, M. Endo and T. Iwasaki, "Temperature-Dependent Sellmeier Coefficients and Chromatic Dispersions for Some Optical Fiber Glasses," *Journal Lightwave Technology*, vol. 12, no. 8, p. 1338–1342, 1994.
- [109] A. Walter and G. S. Schaefer, "Chromatic dispersion variations in ultra-long-haul transmission systems arising from seasonal soil temperature variations," *Proc. Optical Fiber Conference*, pp. 332- 333, 2002.

- [110] M. Abuhelala, S. M. Ahmad, M. Ibrahim and I. Glesk,, "Investigation on temporal skewing among O-CDMA code carriers under fiber temperature variations," in *2017 25th Telecommunication Forum (TELFOR). IEEE.*, 2017.
- [111] M. S. Ahmed, M. Abuhelala and I. Glesk, "Management of OCDMA auto-correlation function distorted by dispersion effects," in *19th International Conference on Transparent Optical Networks (ICTON)*, Girona, Spain, 2017.
- [112] M. J. Hamp, J. Wright, M. Hubbard and B. Brimacombe, "Investigation into the Temperature Dependence of Chromatic Dispersion in Optical Fiber," *IEEE PHOTONICS TECHNOLOGY LETTERS*, vol. 14, no. 11, pp. 1524-1526, 2002.
- [113] C. H. Hsieh, G. C. Yang, C. Y. Chang and W. C. Kwong, "Multilevel prime codes for optical CDMA systems," *Journal of Optical Communications and Networking*, vol. 1, no. 7, pp. 600-607, 2009.
- [114] X. Wang and K. Kitayama, "Analysis of beat noise in coherent and incoherent time-spreading OCDMA," *Journal of Lightwave Technology*, vol. 22, no. 10, pp. 2226-2235, 2004.
- [115] V. Baby, C. S. Bres, I. Glesk, L. Xu and P. R. Prucnal, "Wavelength aware receiver for enhanced 2D OCDMA system performance," *Electronics Letters*, vol. 40, no. 6, pp. 385-387, 2004.
- [116] T. Kato , Y. Koyano and M. Nishimura, "Temperature dependence of chromatic dispersion in various types of optical fiber," *Optics Letter*, vol. 25, no. 16, p. 1156–1158, 2000.
- [117] K. S. Kim and M. E. Lines, "Temperature dependence dispersion in dispersion-shifted fibers: Experiment and analysis," *Journal of Applied Physics*, vol. 73, no. 5, p. 2069–2074, 1993.
- [118] C.-Y. Tsai, G.-C. Yang, J.-S. Lin, C.-Y. Chang, I. Glesk and W. C. Kwong, "Pulse-power-detection analysis of incoherent O-CDMA systems under the influence of fiber temperature fluctuations," *Journal of Lightwave Technology*, vol. 35, no. 12, pp. 2366-2379., 2017.
- [119] . P. S. André, A. N. Pinto and J. L. Pinto, "Effect of temperature on the single mode fibers chromatic dispersion," *Journal of Microwaves, Optoelectronics and Electromagnetic Applications (JM0e)*, vol. 3, no. 5, pp. 64-70, 2004.
- [120] S. M. Ahmed and I. Glesk, "Mitigation of Temperature Induced Dispersion in Optical Fiber on OCDMA Auto-correlation," *IEEE Photonics Technology Letters*, vol. 29, no. 22, pp. 1979-1982, 2017.
- [121] M. Abuhelala, U. A. Korai , A. L. Sanches, W. C. Kwong and I. Glesk, "Investigation of 2D-WH/TS OCDMA Code Stability in Systems with SOA-Based Device," *Applied Sciences*, vol. 10, no. 21, pp. 7943-7954, 2020.
- [122] Y. Khorrami, V. Ahmadi, M. Razaghi and N. Das, "Picosecond and femtosecond asymmetric switching using a semiconductor optical amplifier-based Mach–Zehnder interferometer," *Applied Optics*, vol. 57, no. 7, pp. 1634-1639, 2018.
- [123] J. C. Palais, *Fiber optic communications*, NJ: Pearson, 2005.

- [124] Kamelian, "Semiconductor Optical Amplifiers (SOAs) as Pre-Amplifiers," Kamelian, 0002 datasheet, 2012.
- [125] T. Watanabe, N. Sakaida, H. Yasaka, F. Kano and M. Koga, "Transmission performance of chirp-controlled signal by using semiconductor optical amplifier," *Journal of lightwave technology*, vol. 18, no. 8, p. 1069, 2000.
- [126] R. Stabile, A. Albores-Meija, A. Rohit and K. A. William, "Integrated optical switch matrices for packet data networks," *Microsyst. Nanoeng.*, vol. 2, no. 1, pp. 1-10, 2016.
- [127] I. Glesk, J. Sokoloff and P. R. Prucnal, "Demonstration of all-optical demultiplexing of TDM data at 250 Gbit/s," *Electron. Lett.*, vol. 30, no. 4, p. 339–341, 1994.
- [128] L. Xu, D. Rand, V. Baby, I. Glesk and P. R. Prucnal, "Suppression of beating noise of narrow linewidth Erbium doped fiber ring lasers using Semiconductor Optical Amplifier," *Optics Letters*, vol. 28, no. 10, pp. 780-782, 2003.
- [129] M. Xia, H. Ghafouri-Shiraz, L. Hou and E. A. Kelly, "High-speed pulse train amplification in semiconductor optical amplifiers with optimized bias current," *Appl. Opt.*, vol. 56, no. 4, p. 1079–1086, 2017.
- [130] P. P. Baveja, D. N. Maywar, A. M. Kaplan and P. G. Agrawal, "Self-Phase modulation in semiconductor optical amplifiers: Impact of amplified spontaneous emission," *IEEE Journal of Quantum Electronics*, vol. 46, no. 9, p. 1396–1403, 2010.
- [131] D. A. McCoy, M. Ibsen, P. Horak, C. B. Thomsen and J. D. Richardson, "Feasibility study of SOA-based noise suppression for spectral amplitude coded OCDMA," *Journal Lightwave Technology*, vol. 25, no. 1, p. 394–401, 2007.
- [132] C. W. Kwong and C. G. Yang, *Optical Coding Theory with Prime*, New York: CRC Press, 2013.
- [133] K. Lee, H. J. Lee and B. S. Lee, "Tunable photonic microwave notch filter using SOA-based single-longitudinal mode dual-wavelength laser," *Optics Express*, vol. 17, no. 15, p. 13216–13221, 2009.
- [134] OPA-20-N-C-FA, "1550 nm Nonlinear SOA From Kamelian," [Online]. Available: http://www.kamelian.com/data/opa_15_ds.pdf. [Accessed 28 4 2019].
- [135] M. A. Umyy, S. Bikorimana, N. Madamopoulos and R. Dorsinville, "Combining of SOA-Based Bidirectional Tunable Fiber Nested Ring Lasers With Continuous Tunability Over the C-band at Room Temperature," *Journal of Lightwave Technology*, vol. 34, no. 16, p. 3703–3710, 2016.
- [136] Thorlabs. [Online]. Available: https://www.thorlabs.com/newgrouppage9.cfm?objectgroup_id=3901. [Accessed 1 05 2020].
- [137] Y. Liu, E. Tangdionga, Z. Li, S. Zhang, H. de Waardt, G. D. Khoe and H. J. Dorren, "Error-free all-optical wavelength conversion at 160 gb/s using a semiconductor optical amplifier and an optical bandpass filter," *Journal of Lightwave Technology*, vol. 24, no. 1, p. 230–236, 2006.

- [138] G. p. Agrawal and N. A. Olsson, "Self-phase modulation and spectral broadening of optical pulses I semiconductor laser amplifiers," *IEEE Journal of Quantum Electron.*, vol. 25, no. 11, p. 2297–2306, 1989.
- [139] R. Yadav and G. Kaur, "Design and performance analysis of 1D, 2D and 3D prime sequence code family for optical CDMA network," *Journal of Optics*, vol. 45, no. 4, p. 343–356, 2016.
- [140] E. L. Wooten, k. M. Kissa, A. Yi-Yan, E. J. Murphy, D. A. Lafaw, P. F. Hallemeier, D. Maack, D. V. Attanasio, D. J. Fritz, G. J. McBrien and D. E. Bossi, "A review of lithium niobate modulators for fiber-optic communications systems," *IEEE Journal of selected topics in Quantum Electronics*, vol. 6, no. 1, pp. 69-82, 2000.
- [141] J. W. Choi , E. Sahin , B. U. Sohn , G. F. Chen , D. K. Ng , A. M. Agarwal, L. C. Kimerling and D. T. Tan , "High spectro-temporal compression on a nonlinear CMOS-chip," *Light: Science & Applications*, vol. 10, no. 1, pp. 1-15, 2021.
- [142] P. Moulin and J. a. O'Sullivan, "Information-theoretic analysis of information hiding," *IEEE Transactions on information theory*, vol. 49, no. 3, p. 2003, 563-593.
- [143] R. F. Fischer, R. Tzschoppe and R. Bäuml, "Lattice cost schemes using subspace projection for digital watermarking," *European transactions on telecommunications*, vol. 15, no. 4, pp. 351-361, 2004.
- [144] Y. K. Huang, B. Wu, I. Glesk, K. Kravtsov , E. E. Narimanov, P. R. Prucnal and T. Wang, "Achieving physical layer security/privacy with self-wrapped OCDM transmission," in *MILCOM 2007-IEEE Military Communications Conference*, 2007.
- [145] D. Zhou, K. I. Kang, I. Glesk and P. R. Prucnal, "An Analysis on Signal-to-Noise Ratio and Design Parameters of a Terahertz Optical Asymmetric Demultiplexer," *Journal of Lightwave Technology*, vol. 17, no. 2, p. 298, 1999.
- [146] N. Tarhuni, N. M. Elmusrati and T. Korhonen , "Polarized optical orthogonal code for optical division multiple access systems," *Progress in Electromagnetic Research (PIER)*, vol. 65, no. 2, pp. 125-136, 2006.
- [147] A. Othonos and K. Kalli, in *Fiber Bragg Gratings: fundamentals and applications in telecommunications and sensing.*, 1st ed., Norwood: Artech House, 1999, p. 422.
- [148] "What is frequency chirp in an optical Pulse? (VIDEO)," Fiber Optics for sale co, [Online]. Available: <https://www.fiberoptics4sale.com/blogs/wave-optics/what-is-frequency-chirp-in-an-optical-pulse-video>. [Accessed 18 09 2021].
- [149] W. H. Hatton and M. Nishimura, "Temperature Dependence of Chromatic dispersion in Single Mode Fibers," *Journal of Lightwave Technology*, Vols. LT-4, no. 10, p. 1552–1555, 1988.
- [150] A. Wonfor, H. Wang, R. V. Penty and I. H. White, "Large port count high-speed optical switch fabric for use within datacentres," *Journal of Optical Communications and Networking*, vol. 3, no. 8, p. A32–A39, 2011.

- [151] S. Singh , A. Singh and R. S. Kaler, "Performance evaluation of EDFA, RAMAN and SOA optical amplifier for WDM systems," *Optik*, vol. 124, no. 2, pp. 95-101, 2013.
- [152] J. Dong, X. Zhang, F. Wang, W. Hong and D. Huang, "Experimental study of SOA-based NRZ-to-PRZ conversion and distortion elimination of amplified NRZ signal using spectral filtering," *Optics Communications*, vol. 281, no. 22, p. 5618–5624, 2008.
- [153] L. A. Coldren, S. W. Corzine and M. L. Mashanovitch, *Diode Lasers and Photonic Integrated Circuits*, 2nd Edition, New jersey : John Wiley & Sons, 2012.